BONNER METEOROLOGISCHE ABHANDLUNGEN

Heft 67 (2015) (ISSN 0006-7156)
Herausgeber: Andreas Hense

Elham Rahmani

THE EFFECT OF CLIMATE VARIABILITY ON WHEAT IN IRAN

BONNER METEOROLOGISCHE ABHANDLUNGEN

Heft 67 (2015) (ISSN 0006-7156)
Herausgeber: Andreas Hense

Elham Rahmani

THE EFFECT OF CLIMATE VARIABILITY ON WHEAT IN IRAN

The effect of climate variability on wheat in Iran

Dissertation
zur
Erlangung des Doktorgrades (Dr. rer. nat.)
der
Mathematisch-Naturwissenschaftlichen Fakultät
der
Rheinischen Friedrich-Wilhelms-Universität Bonn

vorgelegt von
MSc. Agrarmeteorologin Elham Rahmani
aus
Karaj - Iran

Bonn
September 2014

Diese Arbeit ist die ungekürzte Fassung einer der Mathematisch-Naturwissenschaftlichen Fakultät der Rheinischen Friedrich-Wilhelms-Universität Bonn im Jahr 2014 vorgelegten Dissertation von Elham Rahmani aus Karaj - Iran.

This paper is the unabridged version of a dissertation thesis submitted by Elham Rahmani born in Karaj - Iran to the Faculty of Mathematical and Natural Sciences of the Rheinische Friedrich-Wilhelms-Universität Bonn in 2014.

Anschrift des Verfassers: Address of the author:

Elham Rahmani
Meteorologisches Institut der
Universität Bonn
Auf dem Hügel 20
D-53121 Bonn

1. Gutachter: **Prof. Dr. Andreas Hense**, Rheinische Friedrich-Wilhelms-Universität Bonn
2. Gutachter: **Prof. Dr. Clemens Simmer**, Rheinische Friedrich-Wilhelms-Universität Bonn

Tag der Promotion: 16. Dezember 2014
Erscheinungsjahr: 2015

Dedication

I dedicate my dissertation to my lovely family,

to

Mohammad Reza

Mani

Makan

my loving parents

and give special thanks to them. May they also reach their dreams...

Zusammenfassung

In dieser Arbeit werden die Auswirkungen von Temperaturschwankungen auf die Weizen Phänologie im Iran untersucht. Grund dafür ist, dass die Temperatur dort die wichtigste Klimavariable für den Anbau von Weizen unter Bewässerung ist.

Dafür wird zunächst eine effektive und potenziell skalierbare statistische Downscaling Methode für Temperatur und growing degree-days (GDD) von Weizen entwickelt. Statistisches Downscaling ist eine Modellformulierung, die quantitative statistische Verbindungen zwischen lokalen oder regionalen Klimadatensätzen und großskaligen Reanalyse- oder Klimamodelldaten herstellt. GDD ist ein Stellvertreter Variabele für die Energie, die eine Pflanze braucht, um phänologischen Phasen wie die Erntephase zu erreichen. Die GDD Werte werden während der Vegetationsperiode mit phänologischen Daten und täglichen mittleren Temperaturen aus Beobachtungen und Reanalyse bestimmt.

Die zugrunde liegende Datenbasis umfasst die ERA-40 Reanalyse für die globale Skala und Beobachtungen der lokalen Tagestemperatur und Jahreswerte des GDD von Weizen an 16 synoptischen Stationen für den Zeitraum 1961-2001 für die regionale Skala. Die Analyse wird mittels zweier verschiedener Ansätze durchgeführt: Das erste ist ein lineares Regressionsmodell (LR), der zweite Ansatz basiert auf linearer multipler Regression (MR). Das LR wird mit Hilfe des Fingerabdrück-Verfahrens umgesetzt. Diese werden durch die Korrelationskoeffizienten zwischen den Variablen an ERA-40 Gitterpunkte und jede Station festgelegt. Die MR Technik berücksichtigt die Reanalysegitterpunkte aus der direkten Nachbarschaft der synoptischen Station in den Berechnungen. Als Erweiterung des üblichen Downscalings, wird ein Wettergenerator (WG) implementiert, welcher die Temperaturbeobachtungen mit gaußsche Zufallsstörungen mit Erwartungswert 0 und Varianz der Differenz zwischen Beobachtungen und den LR/MR-Erwartungswerte versieht.

Die Temperaturen aus der ERA-40 Reanalyse passen sehr gut zu den Beobachtungen der Station Temperatur. Auch die aus den Modelldaten berechneten GDD-Werte und deren Variabilität stimmen gut mit den beobachteten Daten überein. Für die 2m-Temperatur sind die FPs im Sommer stärker lokalisiert als in der kalten Jahreszeit. Statistisches Downscaling mit FP funktioniert besonders gut für das jährliche GDD. Es erscheint, dass FP besser für Jahres-GDD ist, während MR bessere Ergebnisse für die Temperatur liefert. Desweiteren wird die Qualität des WGs mit Hilfe des probabilistischen kontinuierliche Scores, CRPS, untersucht. Es zeigt sich, dass die Anwendung des WGs deutlich bessere Ergebnisse für die lokale Temperatur ergeben als ein deterministisches Downscaling.

Im zweiten Schritt wird ein probabilistisches Weizen Modell entwickelt. Dieses repräsentiert die probabilistische Beziehung zwischen dem phänologischen- und dem Klimaparameter. Ein geeignetes probabilistisches Modell für die Wachstumsphase von Weizen wird aus der Schätzung und Interpretation der Survival Funktion basierend auf einer Normalverteilung abgeleitet.

Das probabilistische phänologische Modell wird durch die Survivalanalyse (SA) unter Berücksichtigung des Risikos in der Reifezeit des Weizens angepasst. SA ist eine statistische Methode, die das Auftreten eines Ereignisses, wie Z.B. die Reifezeit von Weizen als Zufallsvariable interpretiert und analysiert.

Zusammenfassend ergibt sich aus der vorliegenden Arbeit, dass probabilistische phänologische Modelle durchaus das Potential besitzen, die Verwundbarkeit von landwirtschaftlichen Produktionssystem durch den Klimawandel zu reduzieren und dadurch die Lebensmittelsicherheit in die Region zu verbessern.

Abstract

In this study, we investigated the impact of temperature variability on wheat phenology in Iran. Temperature is the most appropriate climate variable affecting wheat production wheat in cultivation under irrigation in Iran.

To that aim, an effective and potentially scalable statistical downscaling method is developed for temperature and growing degree days (GDD) of wheat. Statistical downscaling quantitatively establishes statistical links between the large-scale reanalysis or climate model and regional climate data. GDD is the atmospheric energy that a plant utilizes to grow over the phenological phases until the harvesting stage. The GDD values are calculated during the growth period from the phenological dates and the daily mean temperature data of observations and reanalysis.

The underlying database in downscaling comprises the ERA-40 reanalysis for the global scale and observations of local daily temperature and annual GDD of wheat at 16 synoptic stations for the period 1961-2001 for the regional scale. For the quantitative analysis of the statistical downscaling, we used the linear regression model (LR) and multiple regression model (MR). The LR is implemented using the ERA-40 fingerprints (FP) of local variability by squared correlation coefficients between the variable at ERA-40 grid points and each station. The MR technique is performed to relate the large-scale information at the neighboring grid points to the stations data. Extending the usual downscaling, we implement a weather generator (WG) providing realizations of the local temperatures and GDD by adding Gaussian random noise with expectation zero and the variance between the downscaled values and the observations.

ERA-40 reanalysis well represents the local daily temperature and the annual GDD. From the analysis of 2m temperature, FPs are more localized in warm seasons than cold seasons. FP statistical downscaling seems to perform best for annual GDD and it is particularly beneficial for the annual GDD. Whereas, the MR calculated robust results for daily mean temperature time series. The quality of the WGs is assessed along with verification score such as the continuous ranked probability score, CRPS. The local temperature time series through WGs are more realistic and well represented than the deterministic downscaling.

As a next step, the probabilistic wheat model is developed. It represents the probabilistic relations between the phenological and climate parameters. The basic idea of the model is to interpret a survival function which is based on the normal distribution, on a time scale which is defined by lifetime or growth duration for wheat. The probabilistic phenological model is adjusted by the survival analysis (SA) considering the risk in interpreting the maturity time of wheat. SA is a statistical method to study the occurrence and timing of event which here is the ripening time of wheat from the random variable of ripening dates.

In summary, we believe that the probabilistic phenological model have the potential to reduce the vulnerability of agricultural production system and can increase the food security in the region.

Contents

List of Figures and Tables

List of Figures

List of Tables

1. Introduction

During the recent decades, climate change has gradually been recognized as a factor which, together with other external constraints, will have a significant impact on agricultural crop productivity.

Many previous agro-meteorological studies concentrated on agricultural climate change impacts. They investigated long-term changes under different climate change scenarios on reducing the yield of crop production (Schär et al., 2004; Challinor et al., 2005)and wheat as a strategic crop in particular (Batts et al., 1997; Tsvetsinskaya et al., 2003; Semenov and Stratonovitch, 2010). If it could be proven that climate predictions have significant skill in contrast to the well known scenario descriptions, then using them to predict crop productivity on a regional scale will become important.

Many studies have been made in different regions on different crops which we discuss some of them in this chapter.

Luo et al. (2013) conducted similar research and assessed two downscaling techniques: statistical and dynamical downscaling and compared the differences in their future projection of climate change impact on wheat crop yields for three locations across New South Wales in Australia. Statistical downscaling produced better results for reproducing the past climate and for future projection the two methods show significant differences.

McMaster and Wilhelm (1998) studied the effect of soil and air temperature for predicting winter Wheat phenology in the central USA. For predicting winter wheat phenology, they mentioned that using soil temperature did not show any more significant advantage than air temperature.

Mozny et al. (2009) assessed the vulnerability of Saaz hops crops to climate change with the crop model CORAC for a 52 year period under current and future climate conditions.

Van Ittersum et al. (2003) researched the effects of changes in CO_2 concentration, temperature and precipitation on the wheat crop system in a Mediterranean climate with the Agricultural Production System Simulator (APSIM)-N wheat model.

The results are presented by Chavas et al. (2009) on the effects of climate change on agricultural productivity in China. They assessed that the productivity of corn (18.6%) and winter wheat (24.9%) increase significantly in the north of China determined by the EPIC agroecosystem simulation model for far future (2071-2100). A similar study was made in the U.S. with three atmospheric general circulation models (GCMs), which illustrates that increasing global mean temperature causes a reduction in corn and wheat production (Brown and Rosenberg, 1999).

The impact of climate change on wheat as a strategic crop in dry southern Israel and cotton as a major crop in the humid climate of northern Israel was made by Haim et al. (2008). They assessed the research with the outputs of model HadCM3 projected for 2070-2100 for the A2 and B2 scenarios.

Niu et al. (2009) simulated the yield of grain sorghum by the EPIC model and examined its reliability in the U.S. under different climate scenarios with normal or extreme temperature and precipitation.

A case study in Sistan and Baluchestan in the south east of Iran was made of the impacts of climate change on wheat (Valizadeh et al., 2013). They simulated the future effects on wheat yield and biomass, the maturity period and leaf area index (LAI). They applied HadCM3 and IPCM4 models under A1B, B1 and A2 scenarios for time periods 2020, 2050 and 2080. For simulating climatic parameters and wheat growth, they used LARS-WG and CERES-Wheat models.

In Iran's Zayandeh-Rud River Basin, Gohari et al. (2013) investigated the Multi-model ensemble scenarios considering uncertainties in climate change projections for the study period (2015-2044). They assessed that out of wheat, barley, rice and sweet corn, the latter two showed more sensitivity to climate change because of their high irrigation water requirement. Overall, increasing temperature causes a short crop growth period and reduction in crop productivity due to lower precipitation and higher water demands.

Specially in Iran, such studies for a large area with different climatic conditions is unique and has not been done before. This is the first study of which we know that presents a probabilistic phenological model instead of a common deterministic prediction.

Winter wheat (Triticum aestivum L.) (Özgen et al., 1998) or bread wheat is the most widely grown food crop in the world (Röder et al., 1998). It is also the oldest and most extensively grown crop in Iran (Deihimfard et al., 2007) and the most important winter cereal grown in this country (Zand et al., 2007). Wheat is grown mostly under irrigated conditions in this region. For that reason, temperature is the most important climatic parameter in wheat production. Precipitation is not considered in this study, since due to the predominant use of irrigation in wheat cultivation in Iran, precipitation is of minor importance for wheat development and yields.

According to the statistics of the Ministry of Jihad-e-Agriculture in Iran[1] (Figure 1.1), the yield of irrigated wheat has increased from 1710 to 3745 kg per hectare, and the yield of non-irrigated wheat has increased from 598 to 1085 kg per hectare during the period from 1982 to 2006. In the year 2005-2006 an area of about 8478250 hectares were cultivated with wheat, barley and other grains in Iran. About 81% of this area was dedicated to irrigated wheat production. This indicates the outstanding importance of wheat for the Iranian agricultural system.

Figure 1.1 presents the cultivated area (ha) of wheat, barely and other grains under irrigated condition in Iran and also the yield (kg/ha) of irrigated and non-irrigated wheat during 1980 to 2005. This graph shows that wheat is a strategic crop in Iran compared with the other grains.

The aim of our research is to investigate the impact of temperature variability on wheat production in Iran. To that end, we developed a simple, effective and easy to use statistical downscaling model for local climate conditions that is relevant in crop productivity under irrigated conditions. It relates local temperature variability to the large-scale ERA-40 reanalysis (S.M. Uppala et al., 2005) and introduced a probabilistic wheat model based on survival analysis theory.

Our study domain is Iran which is located in southwestern of Asia, Iran is bordered by the Persian Gulf, the Gulf of Oman and the Caspian Sea. Its topography is characterized by rugged mountainous rims enclosing interior high-elevation basins. Two highest mountain ranges divide the country in separate landscapes with different climate regimes. The Zagros

[1] The wheat statistics was retrieved from the website of the Ministry of Jihad-e-Agriculture in Iran (www.maj.ir) checked in January 2009.

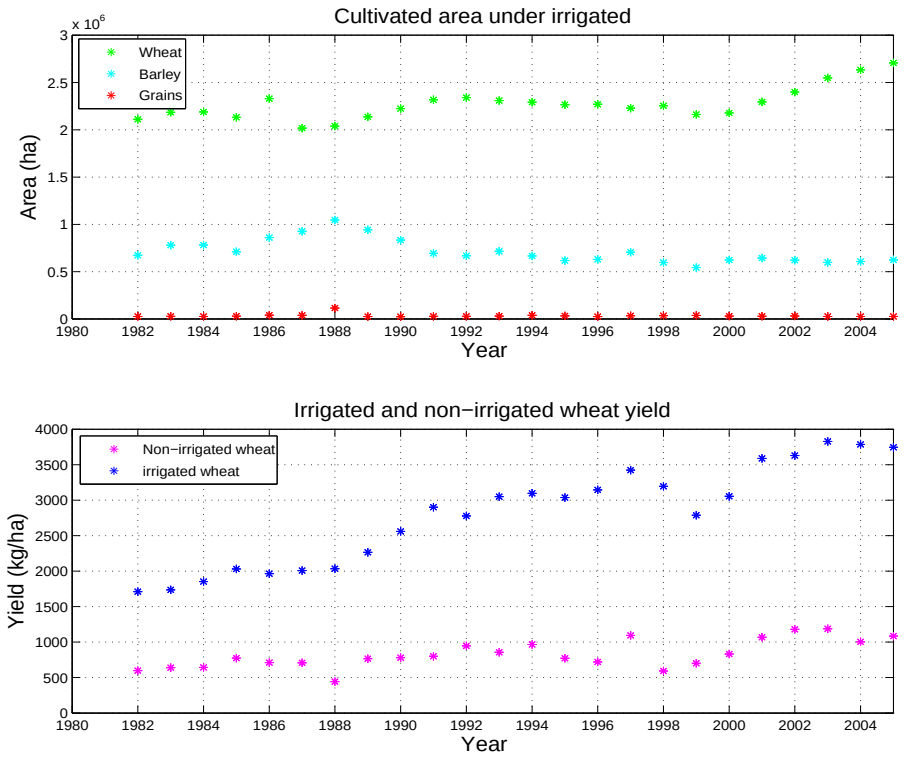

Figure 1.1.: The upper panel shows the cultivated area under irrigation in Iran for wheat, barley and other grains for the period 1982-2005. The lower panel shows the yield per hectare for irrigated and non-irrigated wheat for the same period

Mountains in southern Iran follow a northwest-southeast direction parallel to the border to Iraq and the Persian Gulf. The Albroz mountain range stretches across the northern part of Iran from Azerbaijan and Armenia to the borders of Turkmenistan and Afghanistan following the southern coast of the Caspian sea with Mount Damavand, the highest mountain in the Middle East (5,610 meters), being located at its center (Badripour, 2004).

The general climate of Iran is arid. Based on a cluster analysis of rainfall in Iran, Modarres and Sarhadi (2011) have identified eight climatic zones. They can be combined to three major zones (Figure 1.2) namely the Caspian mild and wet climate (green area), the arid and semi-arid climate (yellow area) in the central Iranian plateau that covers nearly 2/3 parts of the country, and finally the high mountainous area (brown color) which dominates the northwestern and northeastern part of Iran.

1.1. State of the art

1.1.1. Pragmatic temperature and growing-degree-days (GDD) downscaling

In developing countries, applying effective and computationally efficient downscaling methods in agro meteorological studies, has great advantage for strategic crops such as wheat and rice.

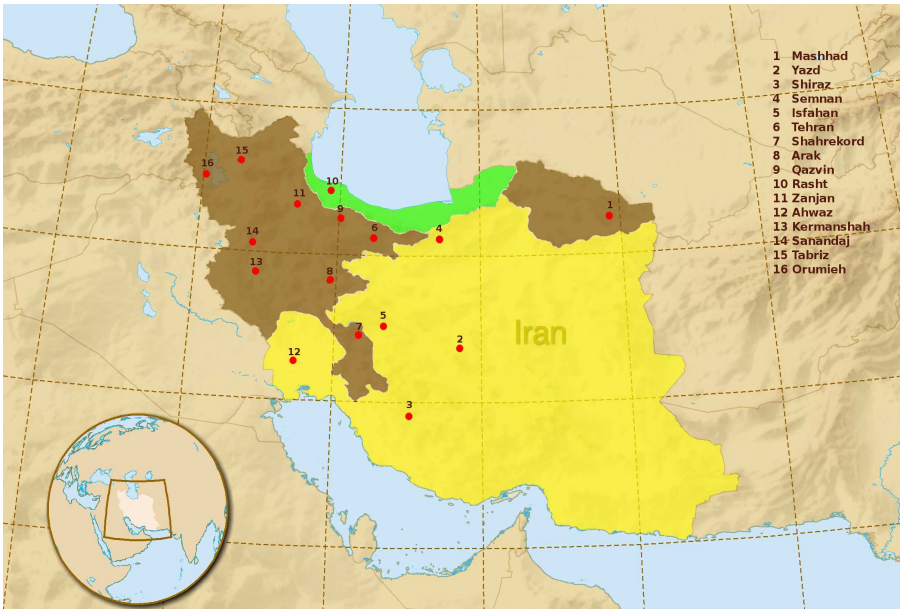

Figure 1.2.: Climate zones based on rainfall in Iran and location of stations (red dots) with three-hourly temperature observations for the period 1961to 2005

The downscaling model should determine the local climatic variability on time scales from days to years and should be conditioned on large-scale climatic information from global or regional earth system models or reanalysis (e.g, ERA-40 (S.M. Uppala et al., 2005)).

In general, downscaling refers to approaches that relate local or regional climate information to large-scale global climate model output (Hewitson and Crane, 1996). One method is the statistical approach. Statistical downscaling involves a statistical model formulation that quantitatively establishes statistical links between the large(r)-scale and the observed local-scale weather (R. Wilby et al., 2004; R. L. Wilby and Fowler, 2010; Maraun et al., 2010).

Huth (2002) examined three linear methods of statistical downscaling with daily mean temperature data and evaluated them within the cross-validation framework. In another study, statistical downscaling by means of three linear models for daily maximum and minimum temperature and one non-linear model (ANN) was examined at 25 stations in 5 different Canadian provinces (Jeong et al., 2012).

For a comprehensive overview of downscaling methods, applications and evaluation techniques, the reader is referred to Murphy (1999) and Teutschbein et al. (2011) who concentrate on hydrological impacts of climate change, and to Maraun et al. (2010) who focus on precipitation.

In this study, we utilized a very pragmatic downscaling method to adjust temperature variability of ERA-40 to the local variability and climate model. We named it as fingerprint (FP) downscalling method because it is based on the obtained fingerprints of squared correlation coefficients and field of weights on each ERA-40 grid provided by the regression analysis. The verified FP models for temperature and GDD represent very comparable results to the standard multivariate regression downscaling method with very small differences. The fingerprint method makes use of the fact that large-scale climate information relevant for local climate variability is itself not localized in space.

Due to dependencies between different points in space implied by atmospheric dynamics, a spatially extended pattern ("fingerprint") is statistically connected to local climate variability. We will explore this feature and make use of it in the downscaling not only for GDD on the seasonal time scales but also for the daily time scale using daily averaged station temperature as local climate information. This allows for a configuration of the general method not only for questions related to crop productivity, but also for other climate impact applications that need sub-seasonal to daily weather information on a local scale. The method can be applied and possibly merged with other downscaling schemes.

Therefore, this study presents a computationally effective and pragmatic statistical downscaling which is in principle comparable to a weather generator (Dubrovský et al., 2004; Chen et al., 2010; Semenov and Stratonovitch, 2010) conditioned on the large-scale information on daily to seasonal time scales.

1.1.2. Probabilistic wheat phenologic model

"One of the most important questions relating to this research is 'Are there deterministic relations between phenological and climate parameters?' The answer is surely 'No'." Because the climate system is a stochastic system for these main reasons: (1) it is a high dimensionality system with $\sim 10^{31}$ degrees of freedom (2) there are nonlinear interactions between those degrees of freedom (3) a forced system being far away from thermodynamic equilibrium implying large amplitude random fluctuations (Prigogine and Hiebert, 1982; Prigogine, 1997).

This answer motivated us to solve the problem through probabilistic theories. As such we developed a probabilistic phenological model which has the advantage of giving additional information in terms of uncertainty. The statisticians tend to construct the probability models to assess the uncertainty of future quantities as they believe that future lies in uncertainty (Spiegelhalter, 2014).

To that aim, we turned to a statistical analysis named survival analysis. Survival analysis deals with death in biological organisms and failure in mechanical systems. In survival analysis literature, death or failure is considered as an event. By event, in this research we mean ripening date of wheat. We will assume only one event in this special case. By time, we mean the growing duration from sowing to ripening as lifetime for wheat which is a function of GDD. To be more precise we will try to perform the probabilistic forecast for wheat ripening. The probability value will change between 0 and 1. Here, the survivor function gives the probability that the not ripened wheat survives longer than a specific time or will survive to the end of its lifetime as a ripened crop. The survival function at each station is determined by fitting a normal distribution to the GDD as the function of growth duration.

We believe that probabilistic phenological models have the potential to help reduce the vulnerability of agricultural production systems to climate change thereby increasing food security.

1.2. Outline

This dissertation is structured as follows:

Chapter 1 describes an introduction on reviews the literature and gives some information about the study domain.

Chapter 2 explains the data basis, climatic and wheat phenologic observations, ERA-40 reanalysis, CCLM model data.

Chapter 3 presents the statistical methods used for regression and correlation analysis, Fourier analysis for removing the annual and half-annual cycles, survival analysis theory for the aim of probabilistic phenological model, uncertainty handling by the means of cross validation and bootstrapping and verification of probabilistic and deterministic forecasts by continuous ranked probability score (CRPS) and the mean absolute error (MAE).

Chapter 4 depicts the applications of the statistical methods which were used in data preprocessing, statistical downscaling, weather generators and probabilistic phenological model based on explained survival theory.

Chapter 5 describes the results for temperature and GDD separately. We conclude the study in Chapter 6.

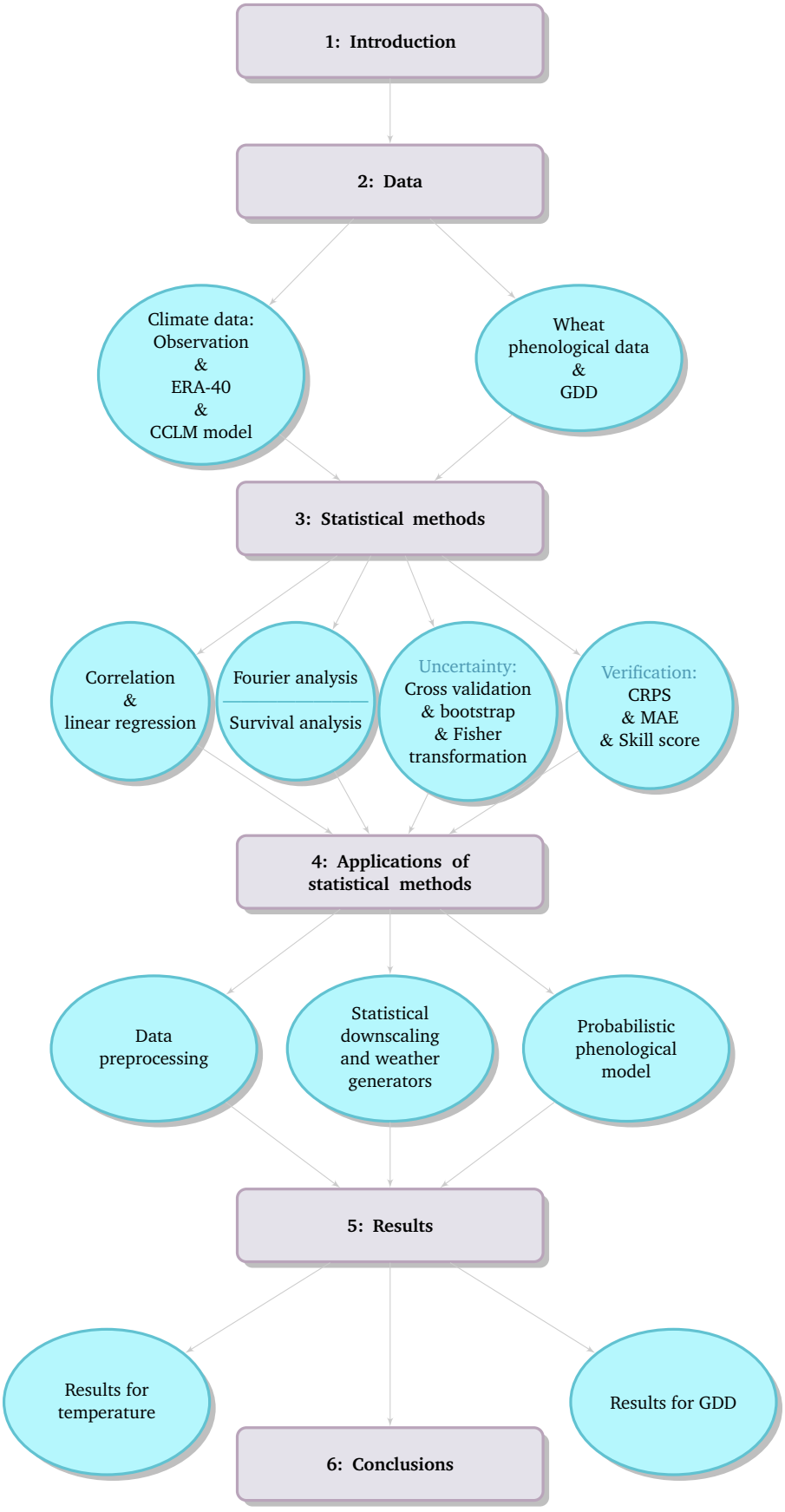
1: Introduction
2: Data
Climate data: Observation & ERA-40 & CCLM model
Wheat phenological data & GDD
3: Statistical methods
Correlation & linear regression
Fourier analysis
Survival analysis
Uncertainty: Cross validation & bootstrap & Fisher transformation
Verification: CRPS & MAE & Skill score
4: Applications of statistical methods
Data preprocessing
Statistical downscaling and weather generators
Probabilistic phenological model
5: Results
Results for temperature
Results for GDD
6: Conclusions

2. Data

2.1. Climate data

2.1.1. Observation

Local information is provided by 3-hourly observations at synoptic stations from the Iranian Meteorological Organization (IRIMO). In our analysis, we used 16 stations with long-term observation records covering a period from January 1961 to December 2005. Figure 1.2 shows the geographical location of the synoptic stations used in this study. Three stations, Tehran-Mehrabad, Mashhad and Shahrekord, are selected for the illustrating the results in Chapter 5.

Table 2.1 shows elevation, latitude and longitude of the weather stations. Ahvaz and Rasht are located at an elevation near sea level. All other stations lie at elevations above 900m.

Table 2.1.: Stations information: elevation, longitude, latitude and distance to the nearest grid point of ERA-40

Station	Elevation(m)	Latitude($^\circ N$)	Longitude($^\circ E$)	Distance(km)
Tabriz	1361	46.28	38.08	31
Ahvaz	22	48.67	31.33	43
Tehran	1190	51.32	35.68	41
Rasht	36	49.65	37.20	41
Shiraz	1481	52.60	29.53	54
Isfahan	1550	51.67	32.62	45
Zanjan	1663	48.48	36.68	58
Mashhad	999	59.63	36.27	43
Kermanshah	1318	47.15	34.35	31
Arak	1708	49.77	34.10	26
Orumieh	1315	45.08	37.53	38
Qazvin	1279	50.05	36.25	18
Yazd	1237	54.28	31.90	31
Sanandaj	1373	47.00	35.33	25
Semnan	1130	53.55	35.58	57
Shahrekord	2048	50.85	32.28	25

2.1.2. ERA-40 reanalysis

In order to provide a global analysis of the atmospheric circulation, the European Centre for Medium Range Weather Forecasts (ECMWF) produced their second generation, 40-yr global ERA-40 reanalysis (Bromwich and Fogt, 2004; S.M. Uppala et al., 2005). Thus, as a global analysis, we used 6-hourly temperature fields at 2-m height above ground from ERA-40 reanalysis.

Due to the complex topography in Iran, a regionalization of ERA-40 temperature is required. Three large water bodies, the Persian Gulf and Gulf of Oman to the South and the Caspian Sea to the North influence the spatial temperature distribution in Iran. Further, local climate is strongly influence by a pronounced orography.

The ERA-40 reanalysis is one of the longest data sets and covers the period from September 1957 until August 2002 at a spatial resolution of $1^\circ \times 1^\circ$. It is the highest quality reanalysis available covering almost completely the period of the observational data, namely the 41 year period from January 1 1961 until December 31 2001. The distance of the stations to the nearest ERA-40 grid point, respectively, is indicated in Table 2.1, and gives a rough estimate of representativeness of ERA-40. The distances are calculated according to the formula of distance between two points in a spherical coordinate system.

We chose the ERA-40 reanalysis data for three reasons. Firstly, this data set covers the period of our local station observations completely in a comparative high resolution in space and time. Secondly, it is the only long-term reanalysis data set, which has corrected some of the biases in the NCEP-1 reanalysis (reanalysis from NCEP-NCAR, The National Centers for Environmental Prediction-National Center for Atmospheric Research)(Marshall, 2002). Thirdly, ERA-40 has used more observations than NCEP, and uses a more advanced data assimilation method. This is particularly important, since it provides not only better statistical dependencies between different regions or grid points in space and time but also guarantees the dynamical dependencies. These important ingredients for the fingerprint assumption are not guaranteed in the often-used re-gridded temperature data sets like the CRU-TS 3.10 data set, which is only available at a monthly resolution (Harris et al., 2013).

Marshall (2002) illustrated some erroneous trends in the stratospheric temperatures in NCEP-1, which demonstrates the inability of NCEP-1 to capture cooling in the stratosphere related to the seasonal ozone destruction.

We did not use the more recent global reanalysis ERA-Interim (Dee et al., 2011), since the ERA-Interim period does not cover the complete station record.

2.1.3. CCLM model data

For the climate model, we used the historical COSMO-CLM data which is operated by the ERA40 reanalysis for time period from 1981 to 2002 at resolution of $0.125^\circ \times 0.154^\circ$ for latitude and longitude respectively. The German Weather Service (DWD) developed a new non-hydrostatic local model LM and CLM as the climate version of LM to answer the demand for higher resolution operational local weather forecasts including the resolution of the convective processes. CLM-Community and LM developers at DWD renamed CLM and LM COSMO model of which the special setup of that for climate simulations is named COSMO-CLM or CCLM (Rockel et al., 2008).

2.2. Wheat phenological and GDD data

Regarding crop parameters, we used wheat phenology data for computing growing degree days (GDD). According to the Food and Agricultural Organization of the United Nations wheat development can be modeled using GDD.

GDD represents the atmospheric energy that a plant physiologically needs to grow over the phenological stages and reach harvesting stage. More precisely, GDD accumulates the average

daily mean temperatures T_i above a certain base temperature T_{base} during the period between date of sowing d1 and harvest d3, which is named as growth duration. We calculated GDD for the period from 1980 to 2001 at 16 observational stations. We also applied an upper threshold of temperature T_{UT}, since many plants do not grow any faster above this limit. We calculate the GDDs as

$$GDD = \sum_{i=d_1}^{d_3} T_i - T_{base} \tag{2.1a}$$

$$T_i = T_{base} \quad \text{if } T_i < T_{base} \tag{2.1b}$$

$$T_i = T_{UT} \quad \text{if } T_i > T_{UT} \tag{2.1c}$$

where T_i is the daily mean temperature. We followed McMaster and Smika (1988) who set $T_{base} = 0°C$ and used an upper threshold of $T_{UT} = 25°C$ for wheat. Before calculating GDD, we applied an interpolation to replace missing daily temperature values. If more than five consecutive days of data are missing, then the complete growing season for wheat is considered as missing, which happened for 21 seasons at all 16 stations during the 40 years study period. The interpolation seems sufficient for our station data, since no peculiar patterns of missing data turned up.

In order to determine the GDD for the growing season of wheat, we analyze the phenological data for wheat for the period from 1980 to 2001 at the 16 synoptic stations. To calculate GDD we use at each station a mean day of sowing and harvest, as displayed in Table 2.2. In

Table 2.2.: Mean value of phenology data for cultivation and harvest during 1980 to 2001 and their variation from the average by standard deviation

	D1(sowing)		D3(harvest)	
Station	Mean	sd(days)	Mean	sd(days)
Tabriz	11 Sep.	6.5	14 June	2.4
Ahvaz	24 Nov.	10.4	25 May	3.3
Tehran	5 Nov.	9.1	28 June	4.2
Rasht	15 Nov.	6.0	22 June	1.4
Shiraz	13 Nov.	10.3	26 June	4.3
Isfahan	16 Nov.	11.5	25 June	4.8
Zanjan	6 Oct.	7.1	16 July	2.2
Mashhad	18 Oct.	9.5	15 July	2.6
Kermanshah	20 Oct.	9.4	3 July	3.6
Arak	20 Oct.	3.2	14 July	3.9
Orumieh	7 Oct.	5.4	16 July	3.5
Qazvin	15 Oct.	8.6	12 July	2.8
Yazd	26 Nov.	9.1	24 June	1.2
Sanandaj	21 Oct.	8.1	10 July	4.1
Semnan	25 Oct.	8.1	10 July	4.2
Shahrekord	8 Oct.	6.5	16 July	2.2

general, the cultivation period of wheat in Iran ranges from mid-September to mid-November. The time of harvest is between the end of May and mid-July of the following year depending on the date of sowing and the weather conditions. The time of harvest shows less variance

compared to the time of sowing. The latter not only depends on the weather conditions but also on management decisions like the date of provision of wheat grain by the ministry of Agriculture, or in some regions on the availability of irrigation water. The same procedure for calculating GDD is used to determine GDDs from the ERA-40 reanalysis with respect to the averaged wheat phenology (as climatology GDD) at the corresponding station.

3. Statistical methods

The statistical approach in this dissertation introduces the exploratory data analysis (EDA) for paired 2m temperature and GDD data with correlation, linear regression and their uncertainties.

In this chapter we describe the statistical relationship between changes in weather patterns and wheat crop phenology by multiple regression analysis including uncertainty assessment. Cross validation and bootstrapping are used (see 3.4) to estimate uncertainties of correlation and regression coefficients, after removing the annual wave cycle (see 3.2) as a deterministic component of all temperature data sets.

Then we explain the first application of the statistical procedure utilizing a classical linear regression forecasting model which is applied for our new pragmatic statistical downscalling method and weather generators. Forecast verification methods are explained including continuous ranked probability score (CRPS), mean absolute error (MAE) and continuous ranked probability skill score (CRPSS).

The second application of the statistical procedure aims to develop a probabilistic phenologic model using survival analysis theory and linear regression models considering the variance of errors. The probabilistic phenologic model has the advantage of giving additional information in terms of uncertainty comparison to common deterministic phenologic models.

Figure 3.1 presents the mind map of our used statistical methods.

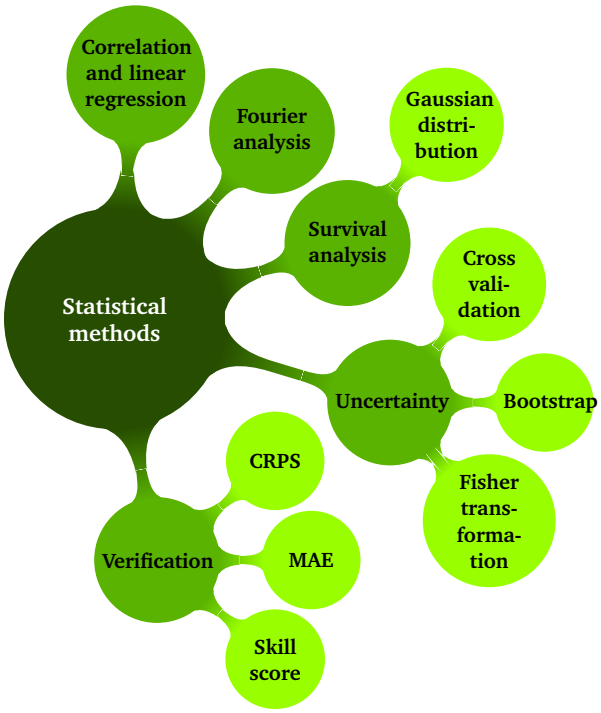

Figure 3.1.: The statistical methods used at a glance

3.1. Correlation and linear regression

In this study, the exploratory correlation approach is applied to pairwise subsets of observed and reanalysis 2m temperature data to provide fingerprints for downscaling purposes and building weather generators.

The relationships between observed 2m temperature data and ERA-40 reanalysis is elucidated by the means of Pearson correlation. For each synoptic station, we thus obtain a field of squared correlation coefficients $(\rho_{yx})^2_{ij}$ on ij, the ERA-40 grid points as fingerprints which are afterward associated by regression analysis and applied to downscaling procedures. The squared correlation coefficient describes the percentage of the variance of one variable explained by the other. The Pearson correlation coefficient is closely associated with regression analysis and is a ratio of covariance of the two variables to the product of two standard deviations (Wilks, 2011). Here, $\vec{y}$ is the 2m temperature data of stations, $\vec{x}$ is the temperature data of ERA-40 reanalysis and m is the time series,

$$\rho_{yx} = \frac{Cov(y,x)}{S_y S_x} = \frac{\sum_{i=1}^{m}[(y_i - \bar{y})(x_i - \bar{x})]}{\left[\sum_{i=1}^{m}(y_i - \bar{y})^2\right]^{1/2}\left[\sum_{i=1}^{m}(x_i - \bar{x})^2\right]^{1/2}} \tag{3.2}$$

For all synoptic stations, the ERA-40 fingerprints are presented as correlation maps (see 5.1). In this case the geographical arrangements of ERA-40 grid points are used to display the correlation information in map form. We identified non-significant values through bootstrapping and illustrated them as gray dots in correlation maps. The squared correlation is bound by 0 and 1 and represents the fraction of variance locally explained by the fingerprint. If $\rho^2_{yx} = 1$, there is a perfect linear association between x and y.

The statistical forecasting approach in this dissertation explores different aspects of classical linear regression models, which describes the linear relationship between two groups of variables, independent or predictors and dependent or predictands which are normally distributed.

The linear regression procedure tries to select the line creating the least error for predicted data given the observed data by minimizing of the sum of the squared errors.

Such we defined our sample data or predictands (observations) as

$$\vec{y} = y_1, ..., y_m \tag{3.3}$$

and predictors (ERA-40 reanalysis) are described as

$$\vec{x} = x_1, ..., x_m. \tag{3.4}$$

The general linear relationship between these two groups of predictands and predictors is

$$\vec{y}_m = \sum_{k=0}^{K} g_k(\vec{x}_m) \cdot a_k + \varepsilon_m \tag{3.5}$$

and the offset terms variables are

$$g_0(x) = 1 \tag{3.6}$$

$$g_1(x) = x \tag{3.7}$$

where in the Eq. (3.5), k is the number of predictors, g_k is the regression function which relates to each predictor, a_k is regression coefficient and ε_m explains the errors of residuals, defined as

$$\varepsilon_m = \vec{y}_m - \hat{y}(x_m) \tag{3.8}$$

where $\hat{y}$ is the predicted value.

We summarize the main linear regression Eq. (3.5) as

$$\vec{y} = G \cdot \vec{a} + \vec{\varepsilon}. \tag{3.9}$$

In this study, G stands for statistical functions for several applications.

Thus, we assume that $\varepsilon \sim \mathcal{N}(\mu, {\sigma_\varepsilon}^2 I)$, which indicates that residuals, $\vec{\varepsilon}$ are normally distributed with the expected value of $\mu = 0$ and σ_ε^2 as variance of residuals.

The standard deviation explains the precision, $\tau_\varepsilon = \frac{1}{\sigma_\varepsilon^2}$. Precision is a term that relates to the standard error of the estimator and indicates how close an estimator is expected to be to the true value of a parameter.[1]

Assuming normally distributed uncertainties, we can use a maximum likelihood approach to estimate the regression model and distribution parameters.

The aim is to compute maximum likelihood estimates (MLE) for the parameters of the model for given sets of data.

To find the maximum likelihood estimates, we need to define a likelihood function as a measure of fit which is a function of unknown parameters for fixed values of observed data (Wilks, 2011).

To be more convenient, we used the logarithm of the likelihood function.

Here we will find the maximum likelihood estimates by minimizing the negative log-likelihood. The negative log-likelihood function corresponding to the likelihood equation, for the Gaussian parameters μ, σ_ε for m samples of observations is

$$NLL(\mu, \sigma_\varepsilon) = -\log\left[\frac{1}{\sqrt{(2\pi\sigma_\varepsilon^2)^m}} exp\left(-(\vec{y} - G\cdot\vec{a})^T \frac{I}{2\sigma_\varepsilon^2}(\vec{y} - G\cdot\vec{a})\right)\right] \tag{3.10}$$

which $\vec{G}\cdot a$ substitute for μ. Then Eq. (3.10) reduces to,

$$NLL = \frac{1}{2\sigma_\varepsilon^2}\left[(\vec{y} - G\cdot\vec{a})^T(\vec{y} - G\cdot\vec{a})\right] + \frac{m}{2}\log(\sigma_\varepsilon^2) + \frac{m}{2}\log(2\pi). \tag{3.11}$$

We solve the above equation by taking partial derivatives with respect to the parameters a, σ_ε. The best estimates of the above model parameters are those which minimize the negative log-likelihood or in another word, minimize the measure of lack of fit.

[1] Statistics Glossary by V. J. Easton and J. H. McColl, http://www.stats.gla.ac.uk/steps/glossary/index.html, checked in February 2014

Solving by setting each derivatives equal to zero gives us,

$$a = (G^T G)^{-1} G^T \vec{y} \tag{3.12}$$

$$\sigma_\varepsilon^2 = (\vec{y} - G \cdot \vec{a})^T (\vec{y} - G \cdot \vec{a}). \tag{3.13}$$

This extremum is indeed a minimum since $(G^T G)$ is positive definite. Note that G varies for different theoretical cases such as annual cycles, cross validation and statistical downscalling.

3.2. Fourier analysis

An important preprocessing for the statistical downscaling of daily or monthly times series is the removal of the annual cycle. Annual and semi-annual (half-annual) cycles are considered as deterministic periodic components in a temperature time-series. They prohibit the stationary assumption which is necessary for the statistical downscaling procedure. We model the annual cycle as a linear combination of periodic temperature variations with periods of 12 months (annual wave cycle) and 6 months (half-annual wave cycle).

In order to estimate the phase and the amplitude of the annual and semi-annual wave cycles, we apply a Fourier analysis to the daily temperatures of ERA-40 reanalysis and station observations, respectively. We filter the wave cycle by using least squares fitting of periodic functions instead of the usual fitting of linear functions.

Here, predictand vector, $\vec{y}$ is the average of daily temperature values during the study period of observations or ERA-40 data with a time series consisting of 365 samples, $t_1 = 1, \ldots t_m = 365$ and the statistical function is G.

$$G = \begin{bmatrix} 1 & \sin(\omega(t_1-1)) & \cos(\omega(t_1-1)) & \sin(2\omega(t_1-1)) & \cos(2\omega(t_1-1)) \\ 1 & \sin(\omega(t_2-1)) & \cos(\omega(t_2-1)) & \sin(2\omega(t_2-1)) & \cos(2\omega(t_2-1)) \\ \vdots & \vdots & \vdots & \vdots & \vdots \\ 1 & \sin(\omega(t_m-1)) & \cos(\omega(t_m-1)) & \sin(2\omega(t_m-1)) & \cos(2\omega(t_m-1)) \end{bmatrix} \tag{3.14}$$

$$\omega = \frac{2\pi}{365.25} \tag{3.15}$$

$$a = (G^T G)^{-1} G^T \vec{y} \tag{3.16}$$

We denote the results of a by

$$a = \begin{bmatrix} T_0 \\ T_1 \\ T_2 \\ T_3 \\ T_4 \end{bmatrix} \tag{3.17}$$

$$\vec{y}_{filter} = G \cdot \vec{a} + \vec{\varepsilon}. \tag{3.18}$$

So $\vec{y}_{filter}$ is calculated by minimizing the residuals, $|\vec{\varepsilon}|^2 \stackrel{!}{=} min$.
$\hat{y}$ is the temperature times series after removal of the annual cycle term.

$$\hat{y} = \vec{y} - \vec{y}_{filter}. \tag{3.19}$$

The annual cycle term (YT) and semi-annual term (HYT) are calculated. Here, $t_i = t_1, ...t_m$ are given by, $t_1 = 1, ...t_m = 365$. Figure 4.2 presents this statistical approach as well.

$$\vec{HYT}_i = T_1 \cdot \sin(\omega(t_i - 1)) + T_2 \cdot \cos(\omega(t_i - 1)) \tag{3.20}$$
$$\vec{YT}_i = T_3 \cdot \sin(2\omega(t_i - 1)) + T_4 \cdot \cos(2\omega(t_i - 1)) \tag{3.21}$$

3.3. Survival analysis

Survival analysis is a statistical method to study the occurrence and timing of events. It deals with death in biological organisms and failure in mechanical systems. In survival analysis literature, death or failure is considered as an event (Kleinbaum, 1998; RP et al., 1950; Cox and Oakes, 1984; Allison, 2012; Woodall et al., 2005).

In this research we define an event as the date of ripening from the random variable of ripening dates of wheat. We will assume only one event in this special case, for instance $4^{th}July$. By time, we mean growth duration (GD) from sowing to ripening of wheat which is a function of GDD. The purpose is to perform a probabilistic forecast of wheat ripening. The probabilities take values in [0,1].

The survivorship function, S(t), gives the probability that a GD value is exceeded, given a value of GDD which is always a number between 0 and 1.

$$GD = d_3 - d_1 = f(GDD) \tag{3.22}$$

$$S(t) = P[GD \geq t] = P[f(GDD) \geq t]. \tag{3.23}$$

By the Gaussian assumption, the survivorship function is in fact the error function or the integral of the Gaussian distribution of predicted GDs. It depends on the expected value μ and variance σ^2, so

$$S(\mu, \sigma^2). \tag{3.24}$$

Fitting the linear function by regression gives us

$$\begin{aligned} GD_i &\sim a \cdot GDD_i + b + \varepsilon_i && (3.25)\\ &\sim \mathcal{N}(a \cdot GDD + b, {\sigma_\varepsilon}^2) && (3.26)\\ \mu &= a \cdot GDD + b && (3.27)\\ \sigma^2 &= \frac{1}{n}\sum_{i=1}^{n}(GD_i - a \cdot GDD_i - b)^2 = {\sigma_\varepsilon}^2. && (3.28) \end{aligned}$$

σ^2 is the residual variance from the regression and is the value of minimizing the function $\frac{1}{n}\sum_{i=1}^{n}(GD_i - a \cdot GDD_i - b)^2$ using the calculated values of a, b.

Instead of the standard method with linear regression, we interpretate the process of growth duration $(d_3 - d_1)$ by a normal distribution with expectation value of $a \cdot GDD + b$ and variances of ${\sigma_\varepsilon}^2$. Thus, the survivorship function is

$$S(d_3 - d_1) = \frac{1}{2}\left[1 + erf\left(\frac{(d_3 - d_1 \mid a \cdot GDD + b) - \mu}{\sqrt{2\sigma^2}}\right)\right] \tag{3.29}$$

3.3.1. The Gaussian Distribution

Gauss was the first person who introduced the distribution about 200 years ago. The Gaussian or normal distribution has many applications in meteorology and climatology. This distribution is encountered frequently in atmospheric sciences. It is determined solely by its mean and variance.

Thus, in this study $(d_3 - d_1 \mid a \cdot GDD + b) \sim \mathcal{N}(\mu, \sigma^2)$ indicates that $(d_3 - d_1 \mid a \cdot GDD + b)$ has a normal distribution with mean μ as location and variance σ^2 as squared scale parameters (Wilks, 2011; Von Storch and Zwiers, 2001). The probability density function or PDF of the Gaussian distribution $(d_3 - d_1 \mid a \cdot GDD + b) \in \mathbf{R}$, is given by

$$f_N((d_3 - d_1 \mid a \cdot GDD + b), \mu, \sigma) = \frac{1}{\sigma\sqrt{2\pi}} exp\left[-\frac{((d_3 - d_1 \mid a \cdot GDD + b) - \mu)^2}{2\sigma^2}\right]. \tag{3.30}$$

The cumulative distribution function is a function of the random variable X, given by the integral of the PDF up to a particular value of x. Thus, the CDF specifies probabilities that the random quantity X will not exceed particular values (Wilks, 2011).

The CDF of the normal distribution is defined by the error function and represents the survivalship in this research. We used CDFs as our survival function of GDD. It can be written as

$$CDF = \frac{1}{2}\left[1 + erf\left(\frac{(d_3 - d_1 \mid a \cdot GDD + b) - \mu}{\sqrt{2\sigma^2}}\right)\right] \quad \mu \in \mathbf{R} \quad \sigma^2 > 0. \tag{3.31}$$

3.4. Uncertainty handling

3.4.1. Cross validation

Cross validation simulates predictions by repeating the entire fitting procedure on data subsets, and then examining the predictions made for the data portions left out of each subset (Wilks, 2011).

Cross validation enables us to derive an estimate for the accuracy of a model and prevents from over fitting by performing the regression on data not involved in the fitting. It is an especially appropriate tool for this purpose (Wilks, 2011).

Here, we used the cross validation technique for testing the regression models on independent samples of data that has been held back during modeling procedure. In cross validation we withheld one year $(\backslash n)$ of data and calculate the regression model with the remaining subset and then examine the predictions for the withheld data. The regression coefficient for the year $(\backslash n)$ is,

$$a^{(\backslash n)} = [(G^{(\backslash n)})^T G^{(\backslash n)}]^{-1} (G^{(\backslash n)})^T \vec{y}^{(\backslash n)}, \tag{3.32}$$

and regression model for the withheld year (n) can be written as,

$$\vec{y_m}^{(n)} = \sum_{k=0}^{K} g_k^{(\backslash n)}(\vec{x}_m) \cdot {a_k}^{(\backslash n)}. \tag{3.33}$$

The predicted survival function in cross validation is given by the regression coefficients, a and b and ${\sigma_\varepsilon}^2$ values from the training data set and the GDD value from the withheld year, $(\backslash n)$. We name it as GD^* and it is calculated by

$$GD^* = GD^{(n)} = a^{(\backslash n)} \cdot GDD^{(n)} + b^{(\backslash n)}. \tag{3.34}$$

3.4.2. Bootstrapping

Sampling uncertainty of the correlation and regression parameters is estimated by the bootstrap method (Tibshirani and Efron, 1993) and cross validation. Instead of relying on theoretical assumptions, the bootstrap procedure creates an empirical sample by resampling the data. Bootstrapping is a nonparametric method of estimating the sampling uncertainty by using the empirical distribution.

Acknowledging the fact that we have sampling errors, it is essential to report the confidence intervals for our results.

In order to preserve the autocorrelations in the daily temperature series, we perform a block-bootstrapping by randomly selecting data blocks with a length of one month(Chernick, 2008). The correlation and regression analysis is repeated for each of the 1000 bootstrap samples, and the 95% confidence interval is estimated. The 95% confidence interval is that part of the interval $[-1,1]$ of possible correlations which contains with a 95% probability the correlation coefficient of the underlying two random variables.

If the value zero for correlation or regression coefficients lies inside this interval, the fingerprint at this grid point is considered non-significant.

3.4.3. Fisher transformation

The Fisher transformation is an easy approach for testing the significance of the correlation coefficients if the underlying data approximately following Gaussian distributions (Wilks, 2011).

Here, in downscaling, 90% (99%) significance of correlations obtained by a Fisher Z transformation of the correlation (Wilks, 2011) considering a five day autocorrelation ($N = \frac{n}{5}$) to determine the degrees of freedom needed in the Z-transform. Under the null hypothesis that the Pearson correlation (3.2), r is zero, the distribution of Z is almost normal distributed with expected value of zero, $\mu = 0$ and $\sigma = \frac{1}{\sqrt{N-3}}$ (Wilks, 2011).

$$Z = \frac{1}{2} ln\Big[\frac{1+r}{1-r}\Big] = tanh^{-1}(r) \tag{3.35}$$

The Fisher transformation yields the confidence interval

$$\Big[tanh(Z - \frac{\phi^{-1}(1-\frac{\alpha}{2})}{\sqrt{N-3}}), tanh(Z + \frac{\phi^{-1}(1-\frac{\alpha}{2})}{\sqrt{N-3}})\Big], \tag{3.36}$$

where ϕ stands for the standard normal cumulative distribution.

3.5. Verification methods

3.5.1. Continuous ranked probability score

For verification of the forecasts, we used the continuous ranked probability score (CRPS). CRPS is a good verification method for probabilistic forecast models. It is a proper score that measures the predictive skill of a model (Gneiting et al., 2005). Here we use the CRPS to

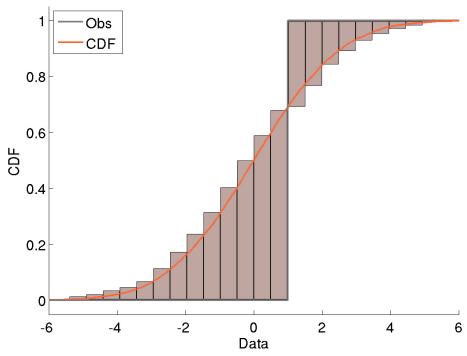

Figure 3.2.: CRPS verification method

compare the cumulative distribution function (CDF) of the predictive conditional probability density function, $S(t)$ with the observation, y (filled area in figure 3.2). In the CRPS formula Eq. (3.37), $H(t-y)$ is the Heaviside function, which takes the value 0 if the argument is negative and 1 if it is positive. CRPS is the integral of the Brier scores at all possible thresholds t for the CDF (Gneiting et al., 2005). It is calculated as follows

$$CRPS = \int_{-\infty}^{\infty} \Big[S(t) - H(t-y)\Big]^2 d_t \tag{3.37}$$

The CRPS for the survival function through cross validation Eq. (3.34) is defined as

$$CRPS = \int_{-\infty}^{\infty} \Big[S(GD^*) - H(GD^* - GD_{obs})\Big]^2 d_{GD^*}. \tag{3.38}$$

When S is the CDF of a normal distribution, $S \sim \mathcal{N}(\mu, \sigma^2)$, then the Eq. (3.37) takes the following form, which we used in this study (Gneiting et al., 2005)

$$crps(\mu, \sigma^2, y) = \sigma\left\{\frac{y-\mu}{\sigma}\left[2\Phi\left(\frac{y-\mu}{\sigma}\right) - 1\right] + 2\varphi\left(\frac{y-\mu}{\sigma}\right) - \frac{1}{\sqrt{\pi}}\right\} \tag{3.39}$$

$$CRPS = \frac{1}{n}\sum_{i=1}^{n} crps(y_i) \tag{3.40}$$

where $\Phi\left(\frac{y-\mu}{\sigma}\right)$ and $\varphi\left(\frac{y-\mu}{\sigma}\right)$ represent the CDF and PDF of the normal distribution with $\mu = 0$ and $\sigma^2 = 1$. Since the *CRPS* is negatively oriented, smaller values indicate better performance.

3.5.2. Mean absolute error

For verification of a deterministic forecast, the mean absolute error (MAE) is a widely used score (Gneiting et al., 2005). It is defined as

$$MAE = \frac{1}{n}\sum_{i=1}^{n}|y_i - \mu_i| \tag{3.41}$$

where μ_i is a deterministic forecast and y_i is the observation. Hersbach (2000) shows that for nonprobabilistic forecasts, *CRPS* reduces to absolute error and the average of *CRPS* (Eq. (3.37)) over n forecasts reduces to the *MAE* (Eq. (3.41)) (Wilks, 2011). For these reasons, *CRPS* can be regarded as a generalized version of the *MAE*.

3.5.3. Continuous ranked probability skill score

Skill score is usually used for measuring the accuracy of forecasts by two forecasting systems which one of them is a reference forecast (Wilks, 2011).

In this research, we use the continuous ranked probability skill score (CRPSS) for comparing the goodness of probabilistic (CRPS) and deterministic (MAE) wheat phenology forecasts and also to compare the deterministic downscaling and the probabilistic weather generator (WG) and evaluate their qualities. As both CRPS and MAE are negatively oriented, then the positive value of the skill score *CRPSS* indicates that the probabilistic model performs better than deterministic model.

$$CRPSS = 1 - \frac{CRPS}{MAE} \tag{3.42}$$

4. Applications of statistical methods

The statistical procedures explained in Chapter 3 are used for three applications in this research: data preprocessing, developing a pragmatic statistical downscaling (DS) method and weather generators (WGs) and innovating a probabilistic phenologic model by the means of survival analysis theory.

Figure 4.1 presents the mind map of the applications of statistical methods in this dissertation. The parts with stars (***) are our innovations in this research.

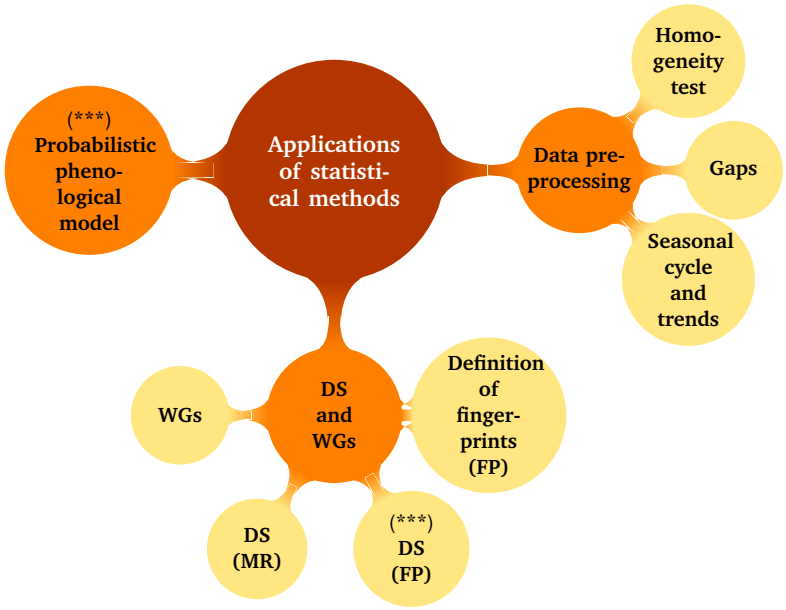

Figure 4.1.: The applications of statistical methods at a glance

4.1. Data preprocessing

4.1.1. Homogeneity test

First, the quality of the station data is assessed visually by searching for obviously erroneous data. The visual inspection did not reveal any obvious inhomogeneities. For investigating in more detail the homogeneity, which is an important issue for climate time series, we applied the Wald-Wolfowitz test as a well-known nonparametric test for investigating the homogeneity or randomness. This was to test that temperature values come in random order and homogeneity existed. It is based on the number of runs of continuous values which exceed or decline from the mean value of temperature series. It tests the null hypothesis for the existence of randomness according to the variation of the number of runs from the mean value divided by the standard deviation when the values are normally distributed.

We conducted the homogeneity test for the anomaly of monthly mean values as adjusting sub-monthly data or low temporal resolution data are not suitable for homogeneity testing

methods (Costa and Soares, 2009).

Overall, through the homogeneity test, the quality of the data is found well except Shiraz from June to December 1966 which has been removed from our data set.

4.1.2. Gaps

In order to fill gaps within the data, we developed a multiple linear regression scheme for the 3-hourly observations. The method used the fewest assumptions and is closely related to the optimal averaging method (Gebhardt et al., 2000). The regression parameters are derived from days with complete observations for each station, month and time of the day, respectively. Note that each day is ideally provided with 8 observations, meaning that we conducted 12 $\times$ 8=96 regression equations for each time in each month from the average of the values. For instance for time 0 in January, we performed the regression M(0-21) = a $\times$ M(3-21) + b, in which M(0-21) is the average of 3 hourly temperatures in complete days and M(3-21) is the average of the temperature in complete days from time 3 to 21 without considering time 0. In this example when the gap exists at time 0 of January, then we use the average value of the existing 7 hours and regression coefficients a, b to predict the mean value for that day. Overall, the regression parameters relate the missing values to the existing ones. If less than 3 observations are missing during one day, the missing value(s) is (are) replaced using the remaining 7, 6 or 5 sub-daily observations based on the multiple linear regression model, respectively. If more than 3 observations are missing for one day, the complete day is removed from the data set and considered as missing. The daily mean temperatures are then calculated from the corrected data set.

Before calculating GDD, we applied an interpolation to replace missing daily temperature values. However, if more than 5 consecutive days of data are missing, then the growing season is considered as missing. This procedure proved to be sufficient for the present station data set because no peculiar patterns of missing data turned up.

4.1.3. Seasonal cycle and trends

Another important preprocessing for the statistical downscaling and probabilistic modeling is the removal of the annual cycle which is explained in Section 3.2.

As a deterministic component of daily and monthly temperature time-series, the annual cycle prohibits the stationary assumption, which is necessary for downscaling analysis. The removal of the annual cycle is performed for ERA-40 as well as for the temperature observations.

The filtering is performed for ERA-40 as well as for the temperature observations. The long-term trends are much smaller (about one order of magnitude) than the derived annual amplitudes which means that the Fourier analysis is hardly affected by the long-term trends. The described Fourier analysis is done by the means of below process, where YT is annual (12 month period) and HYT is semi-annual (six month period):

Figure 4.2 shows the daily averaged temperatures at Tehran averaged over all available years as a function of the number of the day in the year, together with the Fourier components of the annual and semi-annual wave cycle. The same graph for all other stations are shown in Appendix A.1 to A.16. Some more information about temperature variability in the study stations are presented in Tables A.1 to A.16 in Appendix.

Figure 4.3a shows the amplitude of the annual cycle based on ERA-40 data at each grid point. The largest amplitude of the annual wave cycle over Iran amounts to $14^{\circ}C$ and is

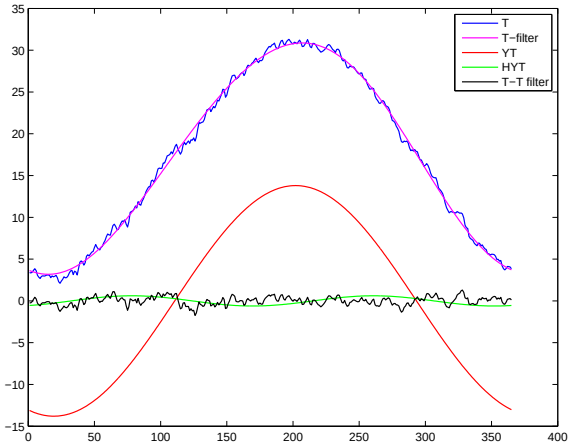

Figure 4.2.: Annual cycle of daily 2m temperature (blue) at Tehran-Mehrabad station, and annual (red line) and semi-annual (green line) wave cycle. The representation of the annual cycle by the annual and semi-annual wave components is given in purple, and the respective anomalies in black.

located over the northern and northeastern part of Iran. It stretches along the southern part of the Alborz Mountains and the northern part of the Dasht-e Kavir desert (Tabari and Talaee, 2011). The smallest amplitude of about $10°C$ is observed along the Caspian Sea coast. The station data as indicated by colored dots and exhibits very similar characteristics.

The amplitude of the semi-annual cycle is displayed in Figure 4.3b. Compared to the annual cycle, it is much weaker with maximum amplitude of about $1°C$ in the West and Southwest. Iranian climate is strongly influenced by the proximity of the Zagros Mountains and by dust storms originating in Sudan, Iraq and Saudi Arabia (Gerivani et al., 2011). They affect Iran during spring and summer along the coast of the Persian Gulf and the Arabian Sea and cause a significant increase in air temperature (Natsagdorj et al., 2003).

Figure 4.4 shows the last dust storm which affected Tehran, on Monday 02 June 2014, at 17:30 with the wind speed of 88.9 (km/h) and the gust speed of 111.1 (km/h).

Another phenomenon that has an influence on the amplitude of the semi-annual cycle is the Asian monsoon circulation. The Asian summer monsoon is defined by seasonally reversed winds and is accompanied by precipitation and heating changes that have a strong impact on the agriculture and economy in the southeastern part of Iran (Gadgil, 2007; Douville and Royer, 1996; Saligheh and Barimani, 2007; Alijani et al., 2007; Fazeli and Zare, 2011).

Another transient change in the climate time series is a potential long-term trend. Kousari et al. (2013) investigated trends of maximum air temperature at 32 synoptic stations in Iran for the period from 1960 to 2005. They show that there are considerable positive trends during the warm season from April to September.

Accordingly, we assess the linear trends in the monthly averaged 2m temperatures and the GDD at our 16 synoptic during the period from 1961 to 2005 for 2m temperatures and from 1961 to 2000 for GDD.

Figure 4.5 shows the linear trends separately for each month of the year. The null hypothesis of “no trend” is rejected at the 5% error level. Seven stations show significant positive trends for more than one month of the year, with a maximum trend encountered at Tabriz of about

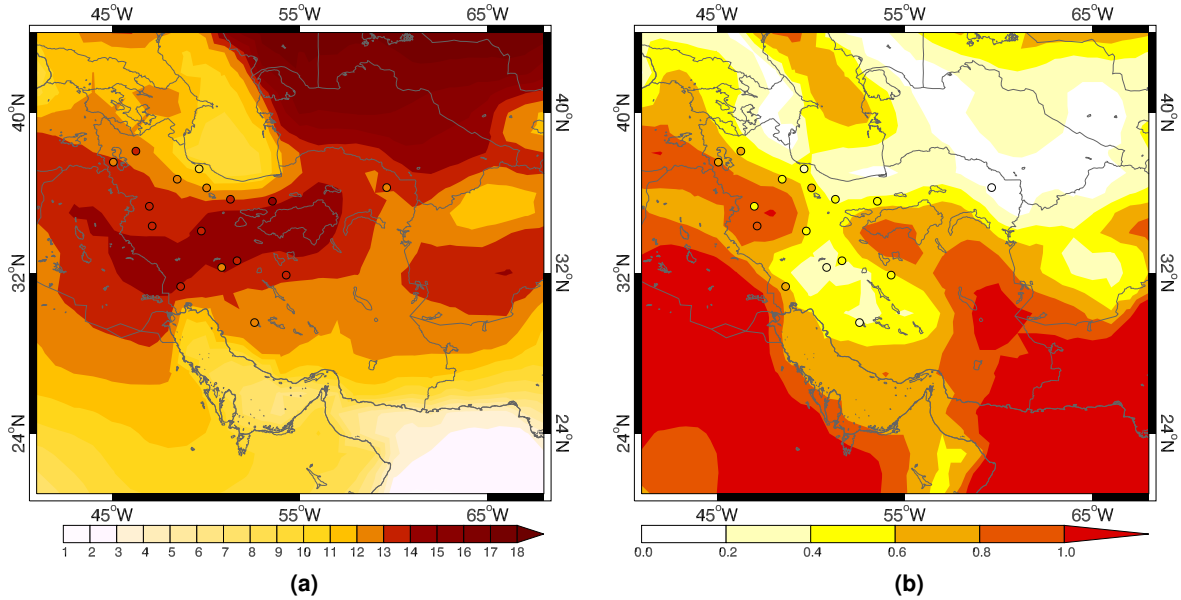

Figure 4.3.: Spectral amplitude of annual (a) and semi-annual (b) wave cycle of daily temperatures from ERA-40 (shading) and weather stations (dots).

Figure 4.4.: Massive dust storm in Tehran, on Monday 02 June 2014, at 17:30

4.5°C in 45 years. The positive temperature trends manifest themselves in significant trends in the GDDs at five stations, namely Tabriz, Tehran, Shiraz, Mashhad and Kermanshah. We observe significant negative trends at six weather stations. However, the negative trends are weaker and significant only for a few months in the year. Hence, for GDD only two stations (Zajan and Shahrekord) show significant negative trends. There is no evidence for a seasonal cycle in the trends, and the spatial variability of the trends is large and without any spatial coherence. For a more detailed discussion of trend signals in Iran the reader is referred to (Kousari et al., 2013). These trends have been removed from the data.

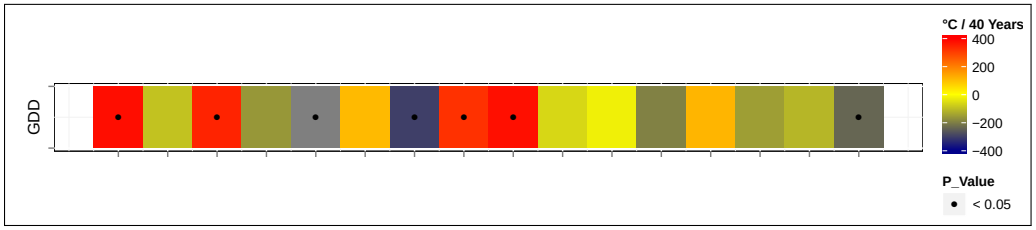

(a)

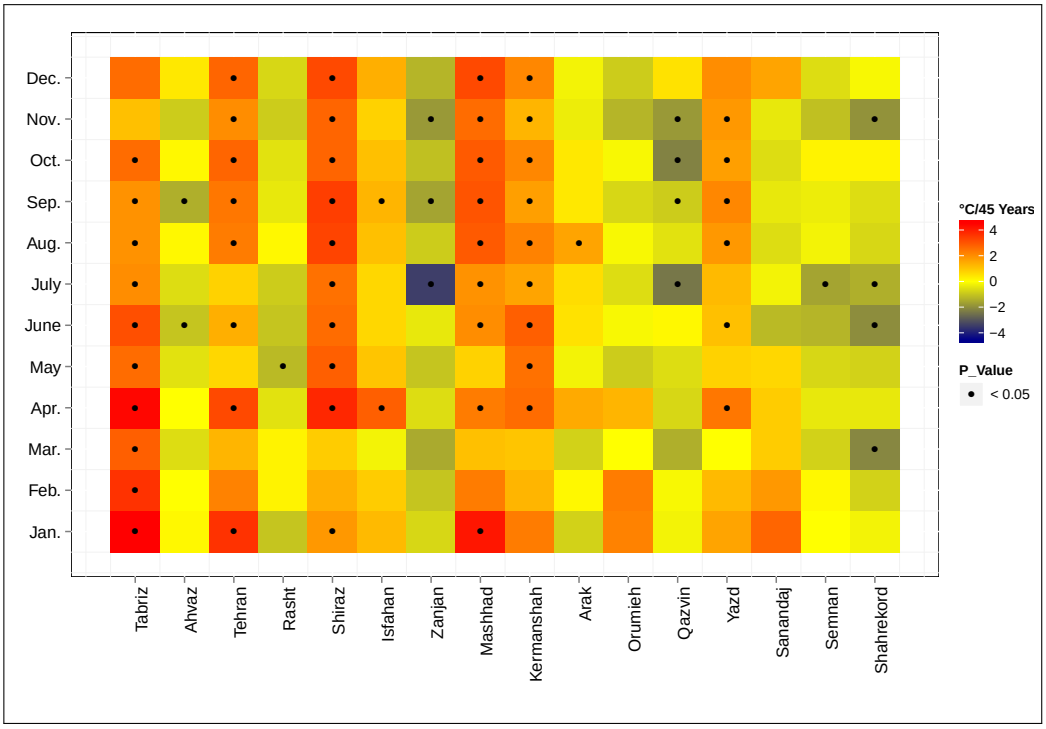

(b)

Figure 4.5.: Linear trend of GGD (a) in $1^{\circ}C/40$ years and monthly mean 2m temperature (b) in $1^{\circ}C/45$ years over the period from 1961 to 2000 and from 1961 to 2005, respectively. Significant trends at the 5% level are marked with black dots.

4.2. Statistical downscaling and weather generators

Downscaling refers to approaches that relate local or regional climate information to large-scale global climate model output (Hewitson and Crane, 1996). One method is the statistical approach. Statistical downscaling involves a statistical model formulation that quantitatively establishes statistical links between the large(r)-scale and the observed local-scale weather (R. Wilby et al., 2004; Maraun et al., 2010; Pielke and R. L. Wilby, 2012).

In this study, statistical downscaling can account for local variability which might influence the crop productivity. We will present two statistical methods of downscaling for the two variables daily temperatures and GDD (see Section 2.2) for the growing season of wheat in Iran.

The aim is to develop statistically sound approaches, which are as simple as possible in the application and as economic in the resources they use. The methods should be applicable to

reanalysis as well as to climate simulations even if these are of different resolution, since in a follow-up study, we intend use this approach for a statistical downscaling of climate simulations. We think that the fingerprint method described below can serve these purposes. The multiple regression method also meet our needs but it is only possible on an a-priori defined small neighborhood, whereas the fingerprint method considers all ERA-40 grid points.

We will present two methods of statistical downscaling for the two variables daily temperatures and annual GDD. One method is based on the definition of so-called fingerprints, which are large-scale regression and correlation pattern of local temperature or GDD in ERA-40. The other approach uses on a linear multiple regression analysis.

We apply both downscaling approaches to daily temperature anomalies, where we subtract the annual and semi-annual wave cycle, as well as the long-term linear trend. We concentrate on daily values during August and February, respectively, as being the warmest and coldest months in Iran. We further apply the same methods to GDD, which consists of annual values. Before we calculate the fingerprints and apply the downscaling, we remove the long-term linear trend from the GDD time series.

Our statistical downscaling approach is based on fingerprints of squared correlation coefficients ${\rho^2}_{ij}$ between observations and ERA-40 reanalysis data on the ERA-40 grid points.

4.2.1. The definition of fingerprints

The general approach of the fingerprint method is to first identify representative large-scale patterns as proxies for local variability. To define the fingerprints, we perform a univariate linear regression between the ERA-40 variable (e.g., daily temperature $T_{ERA,ij}$) at each grid point and the observed variable (e.g., 2m-temperature T_{obs}) such that

$$T_{obs} = a_{ij} + b_{ij} \times T_{ERA,ij} + \varepsilon_{ij} \tag{4.43}$$

where ε_{ij} is the residual error, and the indices i and j denote the ERA-40 grid point. For each synoptic station, the regression analysis is performed independently at each ERA-40 grid point within a region covering Iran and adjacent areas. For each synoptic station, we thus obtain a field of intercepts a_{ij} and regression coefficients b_{ij} on the ERA-40 grid. The corresponding field of squared correlation coefficients ${\rho^2}_{ij}$ represents the ERA-40 fingerprint of the local variable. Sampling uncertainty of the correlation and regression parameters is estimated by the bootstrap method (see 3.4.2), through 1000 bootstrap samples and 95% confidence interval as part of the interval $[-1,1]$.

4.2.2. Statistical downscaling using fingerprints

Statistical downscaling can account for local variability which might influence the crop phenology as well. According to the Food and Agricultural Organization of the United Nations wheat development can be modeled using the growing degree days (GDD) after sowing calculated from daily temperature. Therefore, ERA-40 temperatures are used to estimate local GDD for typical vegetation periods of wheat.

Now we use the fingerprints of local variability as input to a linear regression between the pattern strength and the local anomalies. From each fingerprint, we define a field of weights

W_{ij}

$$W_{ij} = \frac{\rho_{ij}^2}{\sum_{ij} \rho_{ij}^2} \tag{4.44}$$

For each station these weights are used to calculate a weighted spatial average of the ERA-40 anomalies (e.g., $\hat{T}_{ERA}$)

$$\hat{T}_{ERA} = \sum_{ij} W_{ij} T_{ERA,ij} \tag{4.45}$$

In order to relate the weighted average of ERA-40 to the local station variable, we perform another regression analysis but now with the weighted area average as predictor. For temperature this reads $\hat{T}_{obs} = \alpha + \beta \hat{T}_{ERA} + \varepsilon$, where $\hat{T}_{ERA}$ is the weighted average of ERA-40 temperatures, α and β the regression coefficients, and ε the residual error. To prevent overfitting we use cross-validation (see 3.4.1), where we withhold one year of data and calculate the fingerprints ${\rho^2}_{ij}$, the weight fields W_{ij}, the weighted ERA-40 average (e.g.,$\hat{T}_{ERA}$), and the final regression coefficients α and β on the remaining years.

Then the weights W_{ij} are used to estimate $\hat{T}_{ERA}$ for the year, withheld which together with the coefficients α and β provide predictions of the expected value of the local temperature. We tested for an additional quadratic dependence, but it revealed no significant improvements of the downscaling model.

We denote the downscaling based on the complete fingerprints as FP1 (with all points in Finger Prints). We further modify the fingerprint approach by using only those grid points in the fingerprint that are significantly correlated with the observed series, using significance levels of 90% (FP2). The significance levels are obtained from the Fisher Z transformation of the correlation (see 3.4.3).

To determine the effective number of degrees of freedom we assume a five days autocorrelation in the daily temperature series. The autocorrelation in the GDD time series is negligible. In FP3 we only consider a small neighborhood around each station, using the fingerprint at the central grid cell and a neighborhood of eight grid cells.

4.2.3. Statistical downscaling using multiple linear regression

A more standard method for downscaling reanalysis data to point-based observations is multiple regression (MR). As predictors, we use the ERA-40 time series at the central and eight neighboring grid points close to the station. Here, the regression function, $g_k(x)$ in Eq. (3.5) is the temperature time series from ERA-40 grid points and $\vec{y}$ is T_{obs}. The regression coefficient vector for temperature grid points is estimated by maximum likelihood (see Eq. (3.12)).

4.2.4. The weather generator

All downscaling procedures provide estimates of the expected local temperatures. Thereby they miss the remaining uncertainty which results in a loss of variance of the downscaled temperatures. The full solution of the problem is to model the probability density of the residual and take it into account. The assumption is that the residual and therefore also the observed local temperature are realizations from a univariate Gaussian random variable

with expectation $a \cdot \vec{T}_{ERA}$ and variance σ_ε^2. Realizations drawn from that density constitute the weather generator. So, if only the expected value is considered as a downscaled temperature the loss of variance is obvious.

Thus the only statistically correct way to generate time series with realistic variance is to build a weather generator (WG), which draws realizations of the assumed distribution, i.e. adding a normally distributed random number ε_{obs} with expectation zero and the variance σ_ε^2 (Storch, 1999). We estimate the variance σ_ε^2 from the residuals of the local variable, i.e. the difference between the downscaled values and the observations. E.g. a WG based on MR for temperature is obtained by predicting $\hat{\vec{T}}_{obs}$.

A WG provides realizations of the conditional distribution of the local variable. Its predictive skill can be quantified using a proper scoring rule, CRPS. We compared directly the deterministic downscaling and the probabilistic WG and evaluate their quality (see 3.5).

The simplified procedures of the downscalling methods in this dissertation are presented in the flowchart 4.6.

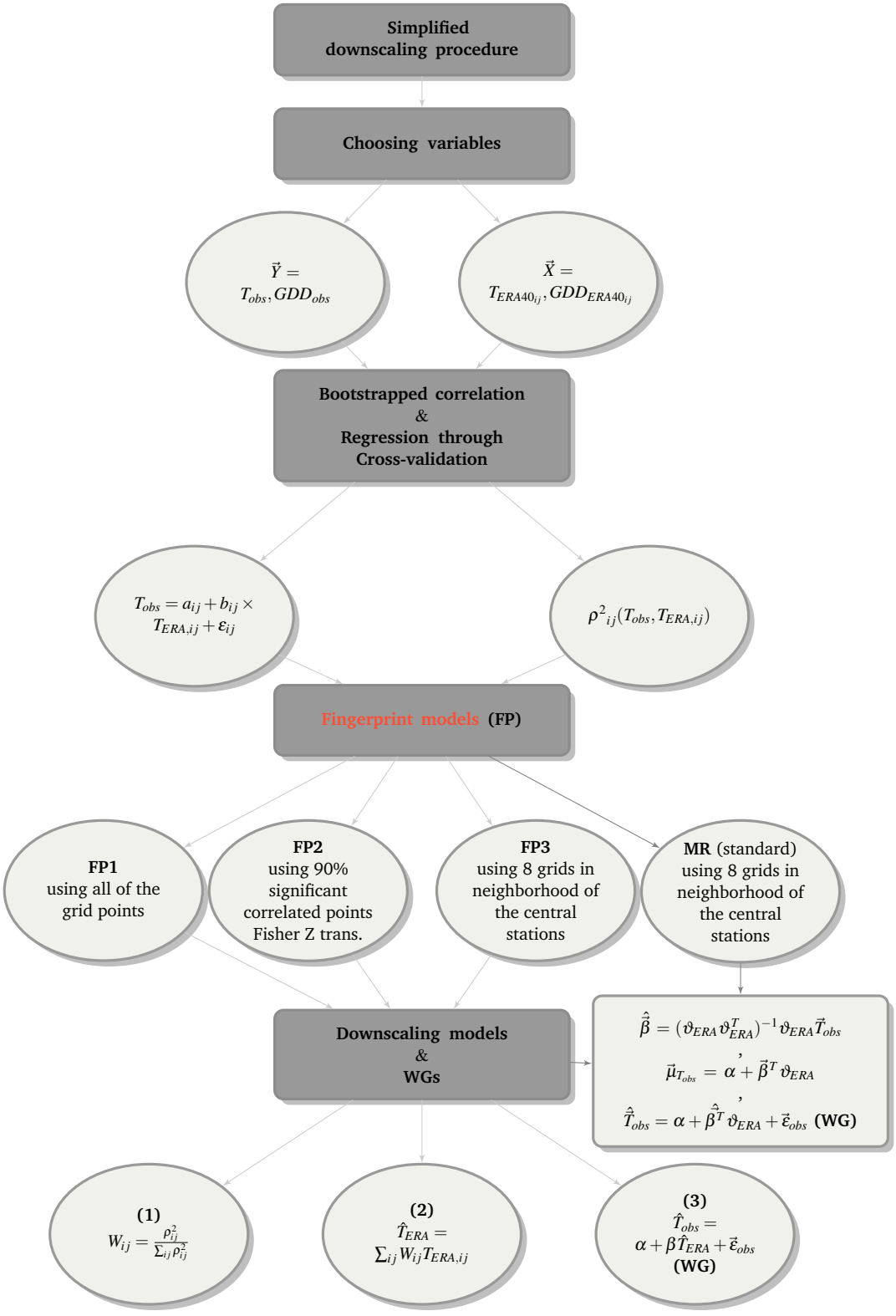

Figure 4.6.: Simplified flowchart for the statistical fingerprint downscaling method

4.3. Probabilistic phenological model

Crops shift their phenology or timing of activities through the variation of the environment. The statistical analysis of phenological stages has a long tradition but as a recent review (Cleland et al., 2007) shows the statistical modeling of phenological stages e.g. first flowering, bud burst and harvest steps are largely treated as implicitly deterministic.

Mean values or trends of mean values have shown to provide essential information on climate variability but still considerable variabilities have not yet been revealed. This may reflect different types of uncertainty such as intraspecies variations of climate sensitivities, soil property variations, unresolved local climate variations, and so on.

Agricultural sciences have almost always focused on phenologic models deterministically, but the question is, is there really a deterministic relation between crop and climatic parameters? To explore the question and respond to the challenges of the effect of climate change on crop phenology and productivity, we developed a probabilistic phenologic model that could have the advantage of reducing the costs of adaptation.

To account for the expected phenological stages and their uncertainty different interpretations of standard statistical analysis, e.g. assuming normal distributed random variables as the basis for the statistics, are proposed. This interpretation is based on the survival analysis method that has been developed by the medical sciences and in insurance mathematics, which provided the basis of our probabilistic wheat model after studying different probabilistic theories such as Binomial distribution, Bernoulli experiments and logistic regression.

The primary idea of this step is to find an appropriate probabilistic wheat model by estimating and interpreting the survival function, on a time scale which is defined by lifetime or growth duration for wheat.

Figure 4.7 presents the difference between the standard and probabilistic methods in phenologic modeling. Two different kinds of interpretation can be seen in red and gray plots in this figure. The red plot shows the deterministic standard phenologic model that almost always has been used in different phenologic modeling research. It represents that in the time A.GDD+B wheat is fully grown with the probability of 1, that means this will happen 100% in that point and 0% before that point.

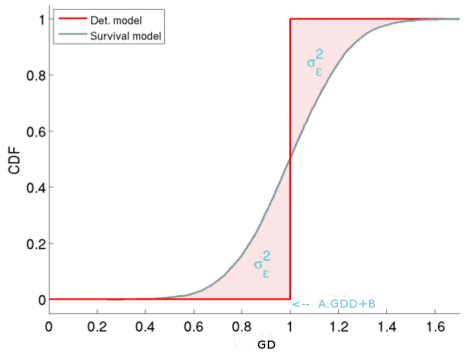

Figure 4.7.: Interpretation of probabilistic phenologic modeling compare with the standard method

We believe that for a reasonable probabilistic phenologic model, the risk or uncertainty range should be factored into the model. In this research we adjusted the probabilistic phenologic model considering the risk in interpretating the maturity time of wheat. We assessed the

survival function based on a normal distribution to demonstrate the overall behavior. The survival function is defined as the error function which depends on the expected value μ and variance σ^2 of the regression between GDD and GD data. To obtain the best estimate for uncertainty, we applied cross-validation through regression modeling. For detailed explanation about applied probabilistic analysis see Section 3.3.

We also conducted the same procedures by applying more predictors rather than GDD such as T_{summer} and T_{spring}. Summer temperature consisted of the average of temperature values for June, July and August. For spring we assumed the averaged temperature of March, April and May. The simplified procedures are presented in the flowchart 4.11.

The relations between GD and different predictors are shown in the Figures 4.8, 4.9 and 4.10. A clear regression relation is visible for T_{summer} and T_{spring} thus we considered one general regression model for all stations together for summer and spring temperature. For GDD, there is not a clear relation between GDD and GD values so we considered the regression models for each station separately.

To compare with a reference condition, we performed all the analysis again with the mean values of the predictors during our study period as the climatology values of the predictors.

We also assessed the survival function with the GDD predictor with historical CCLM model data which is operated by the ERA40 reanalysis. Hence, we considered the nearest neighbor grid points to our stations and calculated the GDD according to the observed phenologic data (GD). Thus, we presented our probabilistic phenologic model for the available CCLM model data in Iran. The available CCLM data for Iran, covered just 10 out of 16 stations. Then we executed survival models based on normal distribution with GDD derived of CCLM data from 1981 to 2002.

We also executed the survival analysis with the GDD predictor for FP1 downscaled ERA40 data, as the best downscaling model for GDD (see Section 5.3).

In the final stage, we assessed the comparison between the results of deterministic and probabilistic models with all predictors and also compared all probabilistic survival models together in Section 5.3.

To compare the results of all deterministic and probabilistic models we applied the CRPS verification skill score (CRPSS) (see 3.5.3).

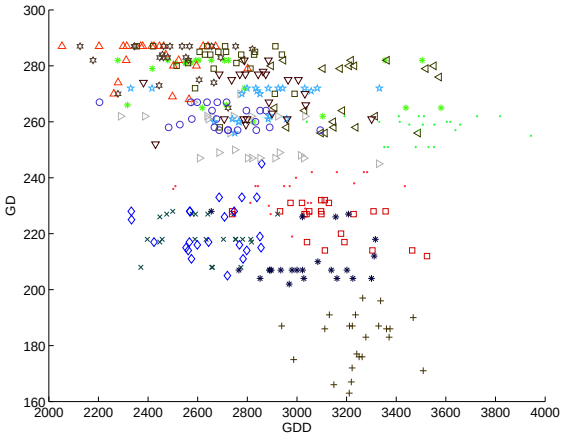

Figure 4.8.: Relation between GDD and GD for all stations

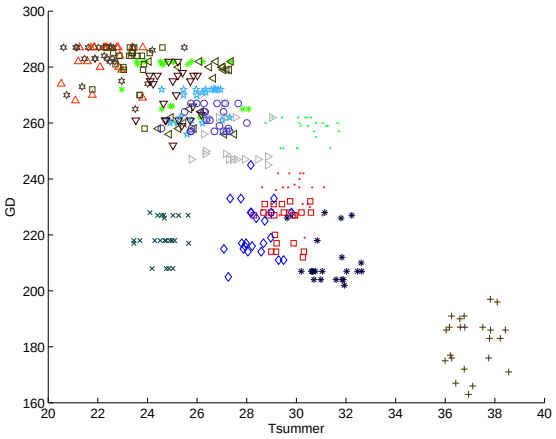

Figure 4.9.: Relation between summer temperatures (JJA) and GD for all stations

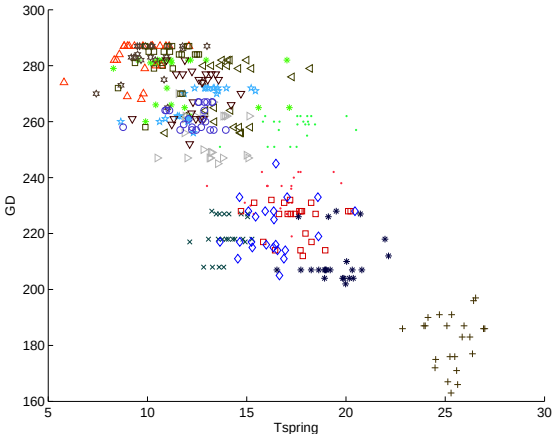

Figure 4.10.: Relation between spring temperatures (MAM) and GD for all stations

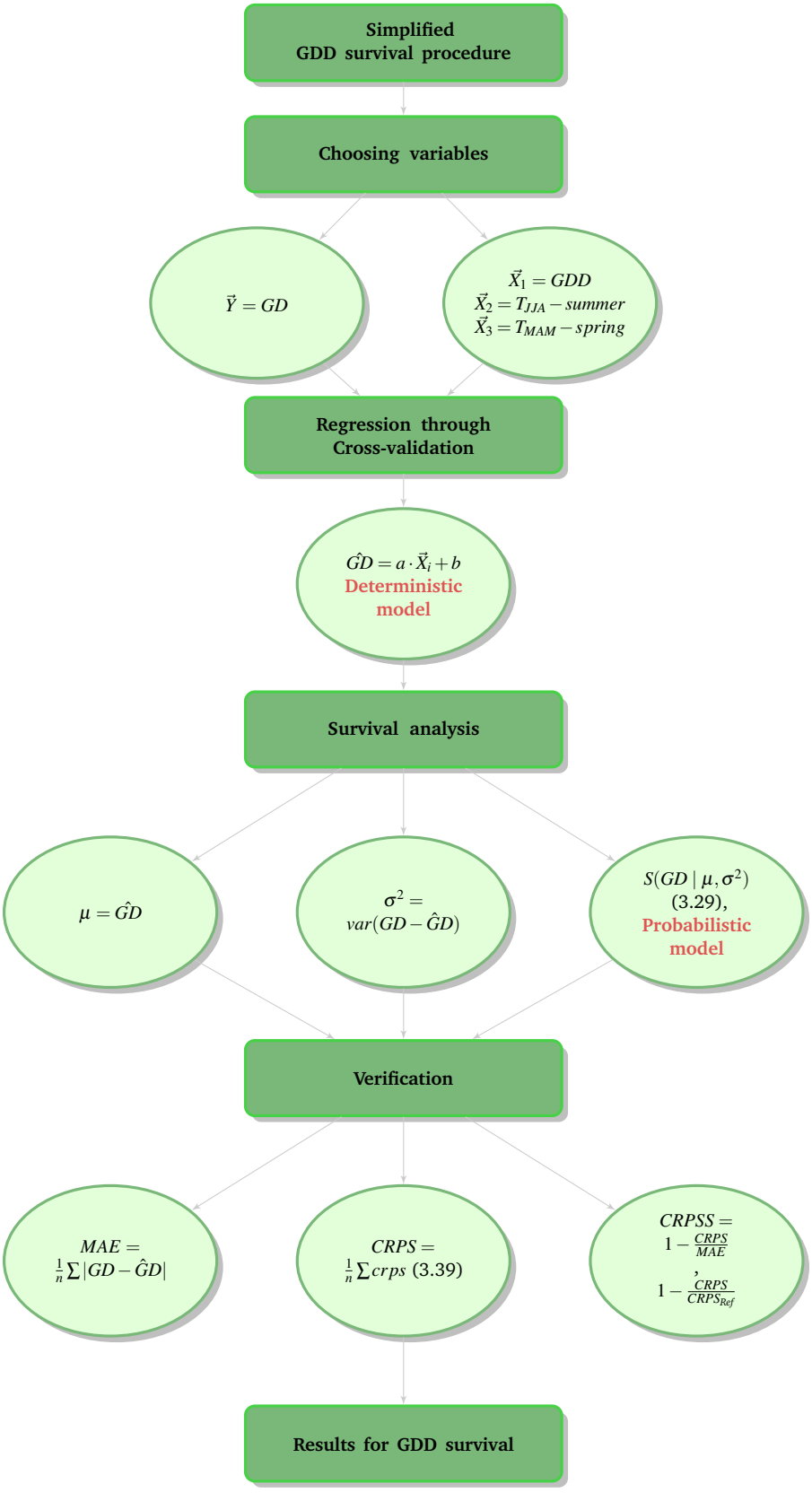

Figure 4.11.: Simplified flowchart for survival procedure with GDD, summer and spring temperatures as predictors

5. Results

5.1. Regression analysis, fingerprints and downscaling for daily temperatures

The amplitudes of patterns of the fingerprints of local temperature variability are considered as input values of a standard regression scheme between local temperature anomalies and the pattern strength. We concentrate on August and February, respectively, as being the warmest and coldest months in Iran.

Note that we used anomalies of temperature values obtained after the removal of the annual cycle. For each synoptic station, the regression is independently performed for all ERA-40 grid points within a region covering Iran and adjacent areas. For each synoptic station, we thus obtain a field of intercepts and regression coefficients on the ERA-40 grid. Further, a field of correlation coefficients is derived as the ERA-40 fingerprints of local temperature (see Section 3.1).

The ERA-40 fingerprints are shown in Figures 5.1, 5.2 and 5.3 for the station Tehran-Mehrabad, Mashhad and Shahrekord, respectively. Non-significant values are marked with gray dots.

For a near perfect reanalysis, one would expect a regression coefficient of $b \approx 1$ near the station. The squared correlation represents the fraction of variance locally explained by the fingerprint. A deviation from the ideal case is expected, since ERA-40 data represent area mean values, whereas the station data are point measurements. Further, ERA-40 provides an analysis that has to fulfill the constraints given by the model.

For Tehran-Mehrabad (Figure 5.1) the maximum squared correlation (regression coefficient) in bootstrap mode amounts to 0.76 (0.93) for February and 0.79 (0.83) for August. The ERA-40 fingerprints for February and August show maxima that follow the Alborz Mountains located north of Tehran. The correlations are largely reduced over the Caspian Sea, where 2m-temperature is strongly influenced by sea surface temperatures.

Although the maximum squared correlations are comparable, Figure 5.1 exhibits significant seasonal variations of the regression fingerprints. The spatial pattern for August is much more localized than that for February. The correspondence between daily temperature series of ERA-40 and the observations at Tehran-Mehrabad is quite good.

The best correspondence is observed for Mashhad (Figure 5.2). The maximum squared correlation amounts to 0.92 (0.84) for February (August) and the maximum regression coefficient is 1.01 (0.89). This indicates that ERA-40 temperatures explain over 90% of the local variance during the cold season even under the bootstrap. As for Tehran-Mehrabad, the correlations are reduced over the Caspian Sea.

However, at some stations the ERA-40 temperature series only weakly corresponds to the local temperatures. The weakest correspondence is observed for Shahrekord (Figure 5.3). Here, maximum squared correlations reach only about 0.6 (0.34) for February (August) with regression coefficients of about 0.91 (0.4). Shahrekord is located in the northern part of the Zagros Mountains, situated at an elevation of 2049 m above sea level. The high elevation is likely to

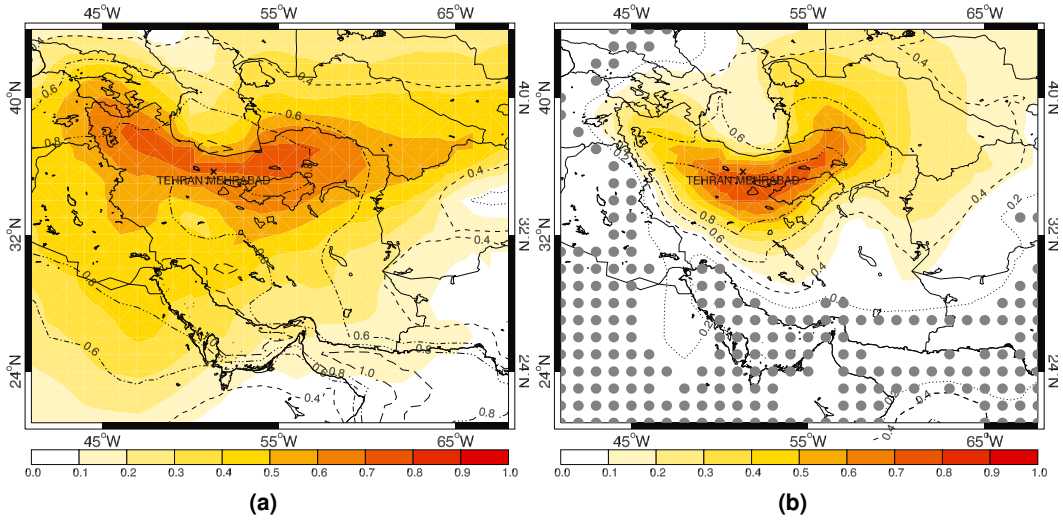

Figure 5.1.: Squared correlation (shading) and regression coefficients (contours) between daily temperature anomalies at the Tehran-Mehrabad station and ERA-40 during February (a) and August (b). Non-significant grid points are marked with gray dots.

be the reason for the reduced representativeness due to the coarse horizontal resolution and the corresponding representativeness errors in surface orography of ERA-40.

We investigated the maximum correlations between T2m for ERA-40 and observations in February and August for each of the 16 stations as a function of longitude, latitude and altitude with the 95% confidence intervals (not shown). A clear relation of the regression coefficients and correlations to the elevation of a station, its latitude or longitude could not be found. However, the analysis confirmed the seasonality in the correspondence, in a sense that the correlation of the observed temperatures to ERA-40 temperatures is larger during February than during August.

The ERA-40 fingerprints for the other stations are shown in Appendix B.1 to B.7.

As explained in Section 4.2, we performed the downscaling by FP1 (with all points of FP), FP2 (with 90% significant points of FP) and FP3 with eight neighboring points around each station and the nearest point to the station as the center point. Moreover, the multivariate regression model (MR) is considered as the standard method for downscaling.

Tables 5.1 and 5.2 summarize the performances of the fingerprint and the standard methods for August and February, respectively. The Tables show ρ_{stat}, the correlation in cross validated mode, between the observations and ERA-40 at the nearest grid point to the station, i.e. no downscaling, and ρ_{max}, the maximum correlation obtained with temperatures at any ERA40 grid point. The correlations vary between 0.52 and 0.91 during August, and between 0.71 and 0.96 during February. Although the fingerprints are more localized, the correlations are highly significant for all stations during all seasons. The best correspondence between downscaled and observed temperatures is obtained for Mashhad. The correlation at Mashhad using FP3 amounts to 0.96 (0.91) for February (August). A small decrease in correlation is expected for the WG (not shown), which for Mashhad is of about 0.06 (0.03) during August (February). The correspondence between (FP3) downscaled and observed temperatures for Shahrekord is weak and amounts to 0.76 (0.48) for February (August). The decrease in correlation for the

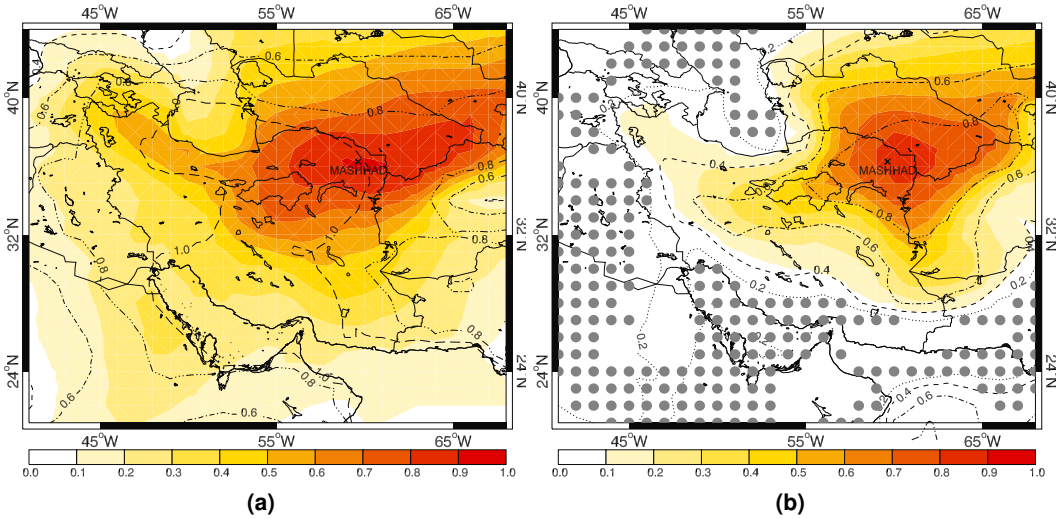

Figure 5.2.: Same as Fig. 5.1 but for Mashhad station, (a) shows February and (b) is for August

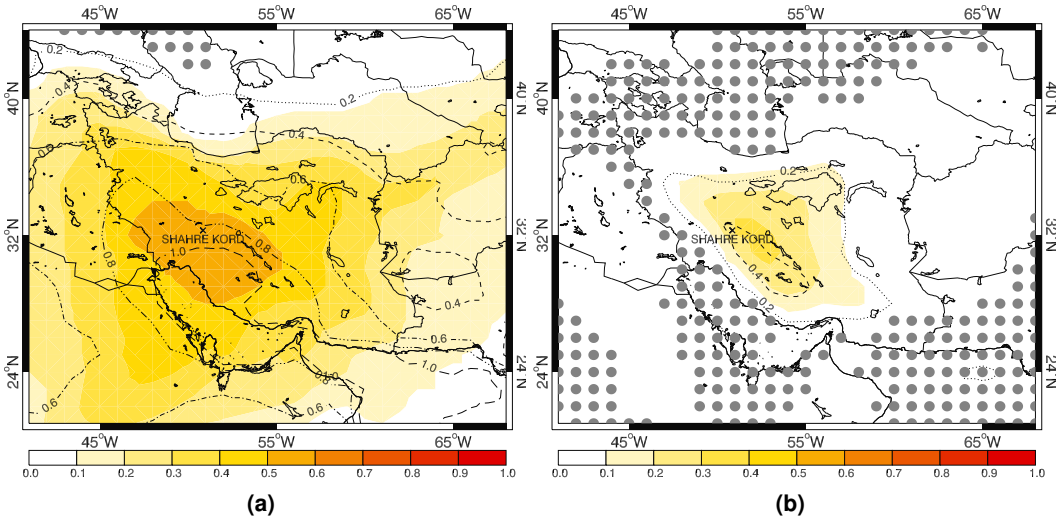

Figure 5.3.: Same as Fig. 5.1 but for Shahrekord station, (a) shows February and (b) is for August

Table 5.1.: Correlation between observed temperatures and ERA-40 temperatures at the closest grid point, maximum correlation with any grid point of ERA40, and correlation between the downscaled and observed temperatures in cross validated mode, using FP1, FP2, FP3 and MR for August.

Station	ρ_{stat}	ρ_{max}	FP1	FP2	FP3	MR
Tabriz	0.85	0.85	0.77	0.77	0.85	**0.86**
Ahvaz	0.55	0.63	0.59	0.62	0.51	**0.67**
Tehran	0.81	0.89	0.78	0.78	0.85	**0.91**
Rasht	0.71	0.78	0.72	0.73	0.71	**0.77**
Shiraz	0.52	0.60	0.22	0.27	0.41	**0.53**
Isfahan	0.75	0.85	0.59	0.68	0.74	**0.84**
Zanjan	0.72	0.72	0.56	0.57	0.70	**0.73**
Mashhad	0.91	0.92	0.88	0.88	0.91	**0.92**
Kermanshah	0.62	0.63	0.40	0.43	0.60	**0.64**
Arak	0.82	0.83	0.63	0.64	0.81	**0.83**
Orumieh	0.76	0.77	0.68	0.68	0.77	**0.80**
Qazvin	0.77	0.77	0.65	0.65	**0.75**	**0.75**
Yazd	0.84	0.87	0.61	0.67	0.85	**0.86**
Sanandaj	0.52	0.62	0.30	0.32	0.45	**0.62**
Semnan	0.72	0.86	0.68	0.70	0.74	**0.84**
Shahrekord	0.55	0.58	0.28	0.39	0.48	**0.53**

WG is stronger than for Mashhad, since more noise has to be added to correct for the loss in variance by the downscaled expected temperatures (not shown).

Both the downscaling methods provide comparable results. However, for some stations the large area fingerprint methods (FP1, FP2) provide smaller correlations compared to MR, whereas the differences between MR and the local fingerprint method (FP3) are generally very small. The advantage of the large area fingerprint methods is that no a-priori decision on the neighborhood is needed, so that data reductions are provided as part of the downscaling method. In the remainder we thus use FP3 if not stated otherwise.

Figure 5.4 summarizes the quality of the different downscaling procedures for all stations in August and February. The correlation ρ_{stat} between the observed and the ERA-40 temperature series at the nearest grid point represents the value which may be obtained without any downscaling and serves as a benchmark. It shows a high variability between the stations with values ranging from 0.52 to 0.91 in August and from 0.71 to 0.96 in February. For most stations MR provides correlations that are slightly better than ρ_{stat}. However, the improvement in correlation obtained by MR downscaling is small. The downscaling based on the fingerprints is less powerful, particularly those that are not restricted to a local neighborhood, namely FP1 and FP2. The best correspondence is obtained between downscaled and observed temperatures for Mashhad, whereas the correlations during August are particularly weak for Ahvaz, Shiraz, Kermanshah, Yazd and Shahrekord.

Table 5.2.: Same as Tab. 5.1 but for February

Station	ρ_{stat}	ρ_{max}	FP1	FP2	FP3	MR
Tabriz	0.87	0.88	0.74	0.75	**0.86**	**0.86**
Ahvaz	0.72	0.74	0.63	0.66	0.73	**0.76**
Tehran	0.86	0.87	0.85	0.84	0.86	**0.88**
Rasht	0.71	0.85	0.73	0.73	0.78	**0.85**
Shiraz	0.87	0.88	0.73	0.74	**0.87**	**0.87**
Isfahan	0.80	0.84	0.83	0.83	0.83	**0.88**
Zanjan	0.81	0.83	0.70	0.72	**0.80**	**0.80**
Mashhad	0.96	0.96	0.91	0.90	**0.96**	**0.96**
Kermanshah	0.83	0.83	0.75	0.78	0.84	**0.85**
Arak	0.76	0.82	0.73	0.74	0.78	**0.80**
Orumieh	0.83	0.84	0.75	0.77	**0.85**	**0.85**
Qazvin	0.80	0.81	0.73	0.72	0.78	**0.79**
Yazd	0.89	0.90	0.82	0.81	0.88	**0.89**
Sanandaj	0.79	0.82	0.68	0.72	0.79	**0.80**
Semnan	0.78	0.85	0.81	0.81	0.83	**0.84**
Shahrekord	0.75	0.77	0.68	0.68	0.76	**0.78**

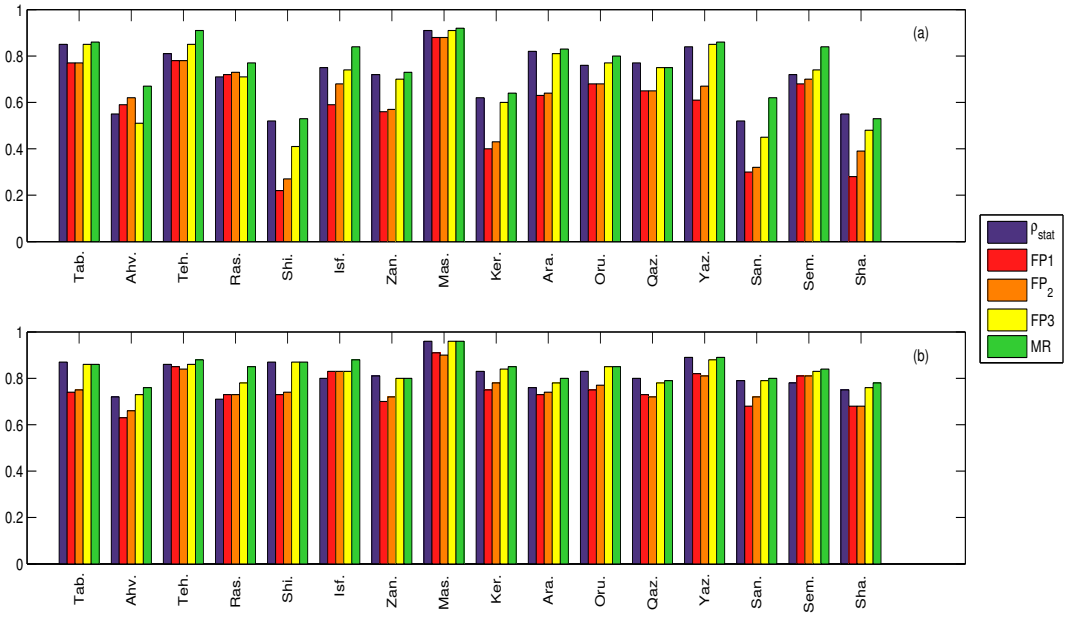

Figure 5.4.: Correlation between observed and ERA-40 daily 2m temperatures at the closest grid point (dark blue), and correlation between downscaled and observed temperatures using FP1 (red), FP2 (orange), FP3 (yellow) and MR (green) for (a) August and (b) February. The x-axis indicates the abbreviated station names. The complete names are given in Fig. 1.2

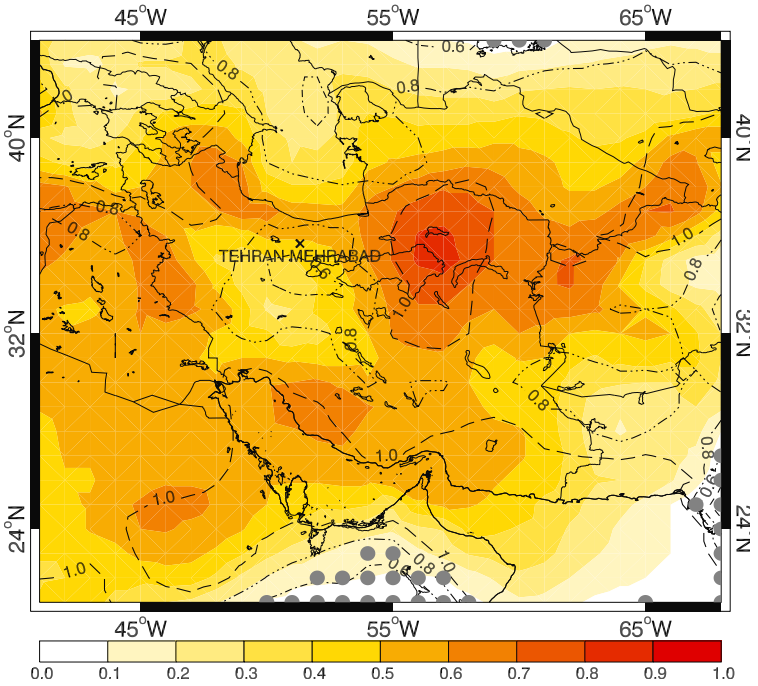

Figure 5.5.: Squared correlation (shading) and regression coefficients (contours) between GDD at Tehran-Mehrabad station and in ERA-40. Non-significant grid points are marked with gray dots.

5.2. Regression analysis, fingerprints, downscaling and weather generator for GDD

We now turn to the downscaling of GDD. For the GDD, we follow the same downscaling procedures as for temperature. We apply the downscaling directly to GDD derived from ERA-40, and then, compare the results to GDD derived from local temperature observations.

The ERA-40 fingerprints for GDD are shown in Figures 5.5, 5.6 and 5.7 for Tehran-Mehrabad, Mashhad and Shahrekord, respectively. Again, we apply bootstrapping to assess the sampling uncertainty, and denote non-significant values with grey dots. The maximum squared correlation (regression coefficient) between Tehran and ERA40 GDD (Figure 5.5) amounts to about 0.84 (1.02) and is located east of Tehran-Mehrabad. Compared to the temperature fingerprint in February (Figure 5.1), the GDD fingerprint is less localized, and the maximum is located further away from Tehran-Mehrabad. For Mashhad, the maximum squared correlation (regression coefficient) for GDD as represented in Figure 5.6 amounts to about 0.79 (1.01). It is located near the station location. The ERA-40 GDD fingerprint for Shahrekord (Figure 5.7) shows a maximum squared correlation (regression coefficient) of about 0.72 (0.75), which is located away from the station to the northwest of Shahrekord. The GDD fingerprints for the other stations are shown in Appendix B.8 to B.11.

Table 5.3 summarizes the results of the downscaling methods. The correlations in cross validated mode, between GDD at the nearest ERA-40 grid point and at the station vary between 0.60 (Isfahan) and 0.90 (Shiraz). The large scale FP methods (FP1, FP2) and MR provide results while are comparable or better, whereas the local FP3 method has weaker predictive

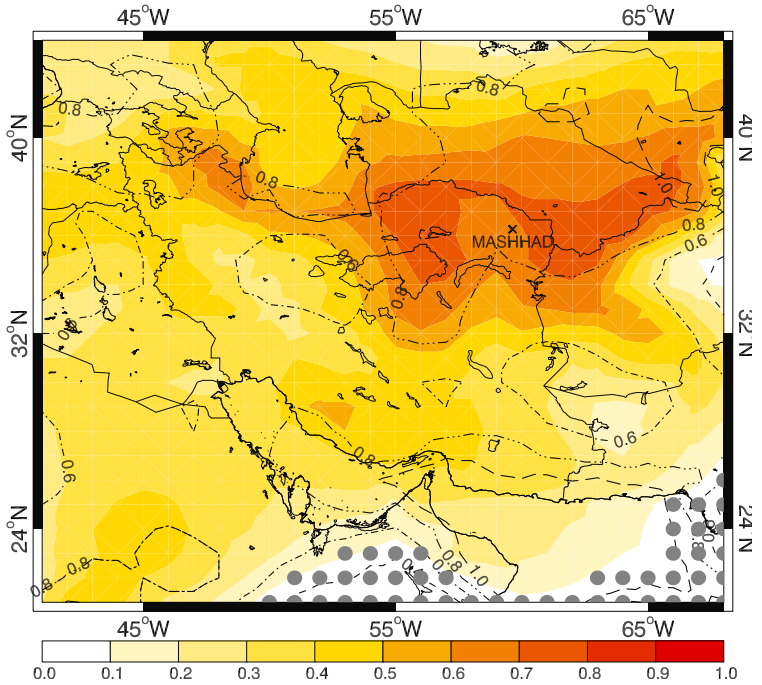

Figure 5.6.: Same as Fig. 5.5 but for Mashhad station.

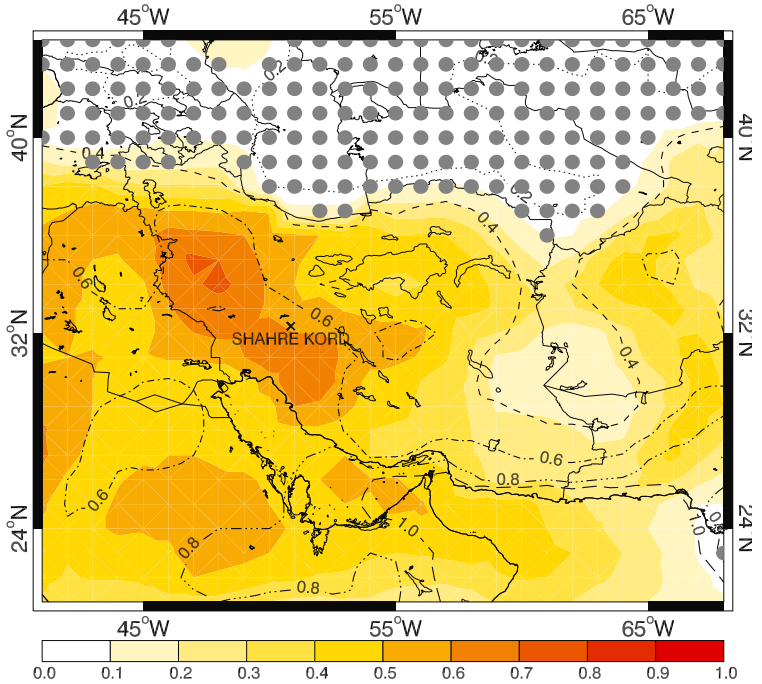

Figure 5.7.: Same as Fig. 5.5 but for Shahrekord station.

Table 5.3.: Same as Tab. 5.1 but for annual GDD

Station	ρ_{stat}	ρ_{max}	FP1	FP2	FP3	MR
Tabriz	0.82	0.86	0.73	0.73	0.54	**0.80**
Ahvaz	0.85	0.85	0.58	0.58	0.78	**0.80**
Tehran	0.72	0.92	0.92	0.92	0.59	**0.89**
Rasht	0.76	0.94	0.84	0.84	0.11	**0.94**
Shiraz	0.90	0.93	0.91	0.91	0.75	**0.92**
Isfahan	0.60	0.89	0.85	0.85	0.58	**0.73**
Zanjan	0.89	0.90	0.75	0.75	0.51	**0.84**
Mashhad	0.83	0.89	0.89	0.89	0.33	**0.81**
Kermanshah	0.86	0.87	0.78	0.78	0.73	**0.82**
Arak	0.72	0.84	0.83	0.83	0.63	**0.70**
Orumieh	0.84	0.87	0.71	0.70	0.30	**0.86**
Qazvin	0.84	0.89	0.84	0.85	0.50	**0.81**
Yazd	0.74	0.83	0.71	0.71	0.56	**0.57**
Sanandaj	0.78	0.84	0.71	0.71	0.63	**0.73**
Semnan	0.88	0.89	0.89	0.89	0.58	**0.82**
Shahrekord	0.77	0.85	0.78	0.79	0.72	**0.80**

power for GDD. For the yearly GDD time series the fingerprints are not very localized and the maximum correlation is often located further away from the station. In the remainder of the section we use FP1 and MR for the downscaling and the weather generator.

For the annual GDD (Figure 5.8 (a)) the correlations between GDD at the nearest ERA-40 grid point and at the station vary between 0.60 at Isfahan and 0.90 at Shiraz. In contrast to daily temperature anomalies, downscaling has the potential to improve local GDD variability. The large-scale FP methods (i.e., FP1 and FP2) and MR provide very comparable results. Since the GDD fingerprints are less localized than the temperature GDD, and the maximum correlation between ERA-40 and observations is often located further away from the station, the local FP3 method has weaker predictive power for GDD. The clear benefit of downscaling, however, is seen in the MAE (Figure 5.8 (b)), which other that correlation also assesses bias and scaling error. It shows that the downscaling is necessary to account for the specific characteristics of local variability (i.e. to correct for calibrated local estimates). Only at two stations, ERA-40 is well calibrated, whereas at all other stations the MAE of the ERA-40 GDD indicates large biases or variance errors. Thus for calibrated local time series, downscaling is indispensable.

We construct WGs for GDD as described in Sec. 4.2.4 and estimate the variance of the noise from the residuals between observed and downscaled GDD. A sample of 1000 realizations is generated as Gaussian random numbers with expectation zero and the estimated noise variance. These random numbers are added to the downscaled value of each year. We concentrate on WGs using FP1 and MR, which have show a comparable performance in results mentioned in this section.

We compared the GDD probabilistic WGs and the deterministic downscaling based on FP1 and MR as mentioned in section 3.5, with CRPS for a deterministic forecast being equivalent to the mean absolute error.

The results are shown in Table 5.4 The correlation between the realizations of the WG and the observations is reduced compared to the downscaled values. However, the CRPS

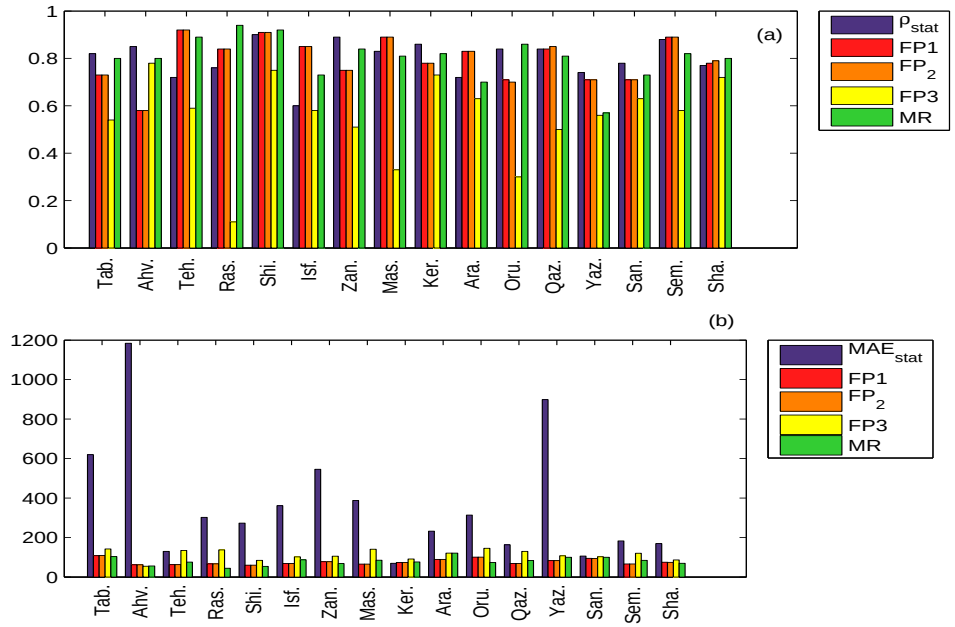

Figure 5.8.: (a) Same as Fig. 5.4 but for GDD. (b) Same as (a) but for MAE. In contrast to correlation,MAE with smaller values indicate better performance.

for the WG improves in relation to the downscaled deterministic values. All CRPS values calculated for the WG are lower, and therefore indicate a better performance, than those for the deterministic FB1 model version. This clearly shows the superiority of a method that accounts for uncertainty in the forecasts.

As is to be expected, the correlations are reduced between the WG and the observed GDD as displayed in Figure 5.9 (a), (b). However, the CRPS is largely improved for the WGs, since the WG accounts for the uncertainty and generates realistic, not too smooth, GDD time series.

The WG for GDD is constructed as described above. The examples of the output of a WG series is displayed in Figures 5.10 (a), 5.11 (a) and 5.12 (a) for Teheran-Mehrabad Mashhad and Shahrekord. The boxes-whiskers represent the uncertainty or the range of the WG based on 1000 realizations. For a calibrated WG, 50% (95%) of the observed values lie within the inner-quartile range (between the 0.025 and 0.975 quantiles). The amount of information provided by a WG is large if the boxes are well separated from one year to another, which is the case at Teheran-Mehrabad indicating a significant discriminative power of the FP1 downscaling model. Similar results are obtained for the other stations as well. Calibration may be visually assessed using quantile plots. Figure 5.10 (b), 5.11 (b) and 5.12 (b) represent the quantile plots for the WG of GDDs with 1000 realization based on FP1 at Tehran-Mehrabad, Mashhad, and Shahrekord. The figures indicates a good calibration without an underestimation of the extreme values which is often found in deterministic downscaling. They also visualize the discriminative power, which is large at Tehran-Mehrabad and Mashhad, and small at Shahrekord. A decomposition of the CRPS (e.g., Hersbach, 2000) gives quantitative estimates of both calibration and discriminative power, and may be used to compare more thoroughly different WGs.

The realizations and calibration of downscaled FP1 for ERA-40 and observed GDD in the

Table 5.4.: Correlation between observed GDD and FP1, MR downscaling models of ERA-40 and the probabilistic WGs and the verification CRPS score for FP1, MR model and WGs, a smaller CRPS is better.

	FP1				MR			
Station	ρ_{FP1}	ρ_{WG}	$CRPS_{FP1}$	$CRPS_{WG}$	ρ_{MR}	ρ_{WG}	$CRPS_{MR}$	$CRPS_{WG}$
Tabriz	0.73	0.69	108.41	83.46	0.80	0.73	103.71	75.88
Ahvaz	0.58	0.51	62.01	47.63	0.80	0.71	55.26	40.18
Tehran	0.92	0.83	62.57	44.10	0.89	0.83	75.69	54.58
Rasht	0.84	0.74	66.82	48.08	0.94	0.94	44.06	31.72
Shiraz	0.91	0.83	60.22	41.72	0.92	0.91	52.58	37.70
Isfahan	0.85	0.67	68.19	47.45	0.73	0.75	88.78	66.28
Zanjan	0.75	0.56	77.70	55.68	0.84	0.78	68.06	48.58
Mashhad	0.89	0.77	65.73	48.49	0.81	0.72	84.82	63.13
Kermanshah	0.78	0.72	73.38	55.85	0.82	0.70	76.48	55.76
Arak	0.83	0.75	88.88	62.99	0.70	0.66	121.12	84.17
Orumieh	0.71	0.64	100.40	72.38	0.86	0.83	81.88	60.24
Qazvin	0.84	0.80	69.16	53.29	0.81	0.77	83.46	62.74
Yazd	0.71	0.52	82.95	61.81	0.57	0.51	98.03	77.88
Sanandaj	0.71	0.47	94.45	67.76	0.73	0.63	98.21	68.00
Semnan	0.89	0.81	66.25	46.89	0.82	0.72	88.32	62.79
Shahrekord	0.78	0.57	74.64	51.74	0.80	0.69	69.40	50.99

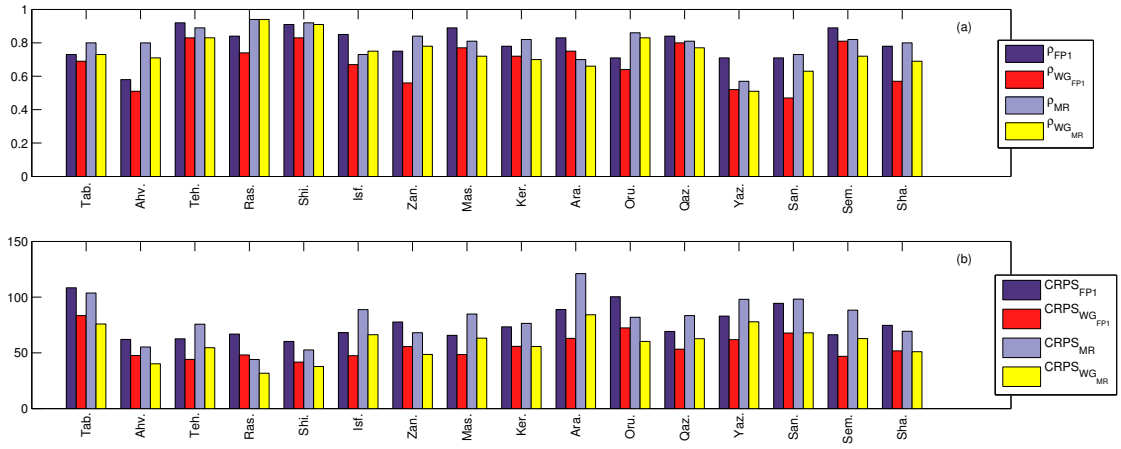

Figure 5.9.: (a) Correlation between observed and downscaled GDD using FP1 (dark blue) and MR (light blue). The respective correlations for the WGs are shown in red for FP1 and yellow for MR. (b) CRPS for the downscaled GDD using FP1 (dark blue) and MR (light blue), and the CRPS for the WGs based on FP1 (red) and MR (yellow). The CRPS, with smaller values indicates better performance.

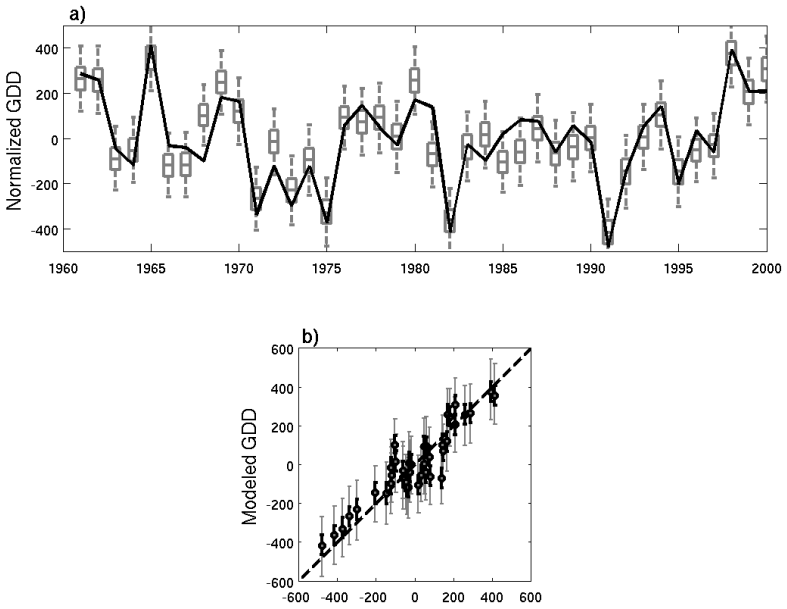

Figure 5.10.: 1000 realizations of the WG using FP1 (box plots), and observed GDD values (black line). The boxes indicate inner-quartile range and median, and the whiskers the 95% interval (a). Modeled GDD from 1000 realizations of WG using FP1 against observed GDD for Tehran-Mehrabad. Black lines and whiskers indicate the inner-quartile range, and gray whiskers the 95% interval (b).

other stations are shown in Appendix C.1 to C.4.

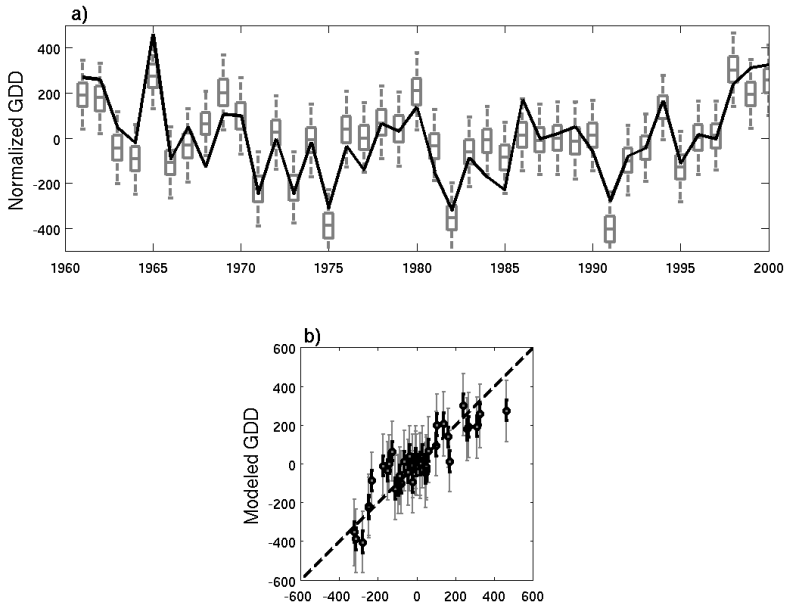

Figure 5.11.: Same as Fig. 5.10 but for Mashhad station

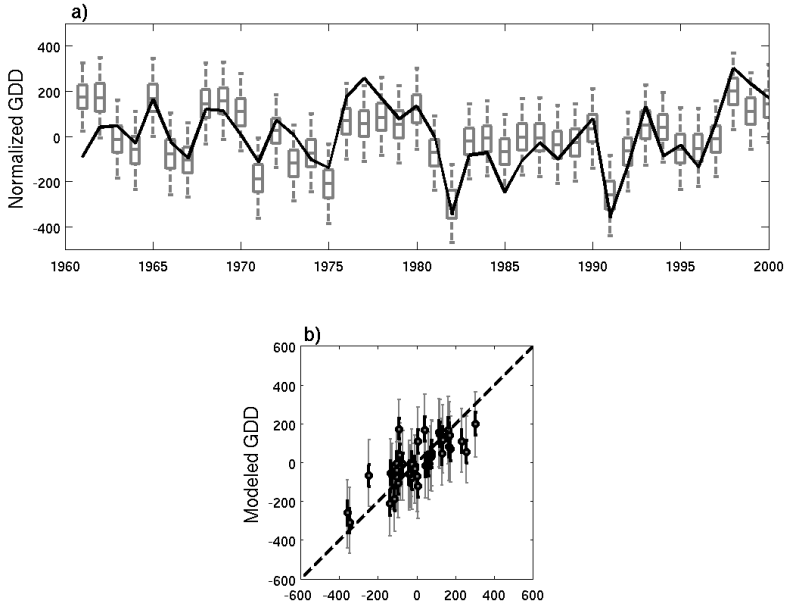

Figure 5.12.: Same as Fig. 5.10 but for Shahrekord station

5.3. Results of probabilistic phenologic model

Results of the probabilistic phenologic models through the survival function for the stations Tehran, Mashhad and Shahrekord are presented in Figures 5.13, 5.14 and 5.15. The figures show the values of the probabilistic survival function which is calculated using the normal CDF with the parameters μ and σ^2 (Section 3.3). The black contour represents the deterministic predicted GD values and gray dots display the normalized observed GDD values. The same figures but for other stations are displayed in Appendix D.1 to D.4.

Years with the peak values of probability contours shifted to the right hand side express the later ripening date with longer and colder growing seasons. In contrast when the probability picks values shifted to the left hand side, it detects an earlier ripening with shorter growing seasons which happens in warmer weather conditions.

If the wheat yield data were available, we could add it to our existing (GD-GDD) model and constitute a multivariate regression model and assess the probabilistic survival functions more effectively.

Forecasting using this probabilistic model could help us to predict a suitable sowing date by shifting it to obtain higher yield through the climatological survival model in each station.

The verification results of the phenologic survival models for comparison between probabilistic and deterministic models are shown in Table 5.5. Here, the larger values of CRPSS are better.

Table 5.5 shows that probabilistic models with all predictors (GDD, T_{summer}, T_{spring}, GDD_{CCLM} and $GDD_{FP1-ERA40}$) are better than deterministic models. These results demonstrate that considering uncertainties in modeling is meaningful and necessary.

Figure 5.16 shows the histograms corresponding to the table and indicates high positive values of CRPSS and a high benefit of probabilistic survival models.

Additionally, we compare the probabilistic models with each other and with reference conditions based on climatological values of GDD, T_{summer} and T_{spring}. Positive values of CRPSS show that the first mentioned predictor in the legend of the figures is more effective than the second. The results are presented in Figures 5.17 and 5.18.

The positive values of CRPSS for the models with T_{summer} and T_{spring} predictors indicate that these temperatures are more effective in growing the crop compared to GDD and the reference condition of GDD. In calculating GDD we considered the temperatures for the whole growth period including positive winter temperatures which is already the dormancy period for the crop. Increasing temperatures in spring and summer causes that crop to reach the greatest mass in its growth duration. Comparing summer and spring predictors together, shows that summer temperature is more effective than spring.

The comparison between the models and their corresponding reference models represent the superiority of the models in some stations with consistently positive CRPSS relative to climatology, except for the stations Tabriz, Shiraz, Kermanshah and Sanandaj.

In contrast when using statistically downscaled FP1-ERA40 (Figure 5.8) and dynamical CCLM, the results consistently show weak negative CRPSS relative to climatology. The validation results are shown in the Figure 5.18. Comparing the validation values between these models did not show a superiority in some stations.

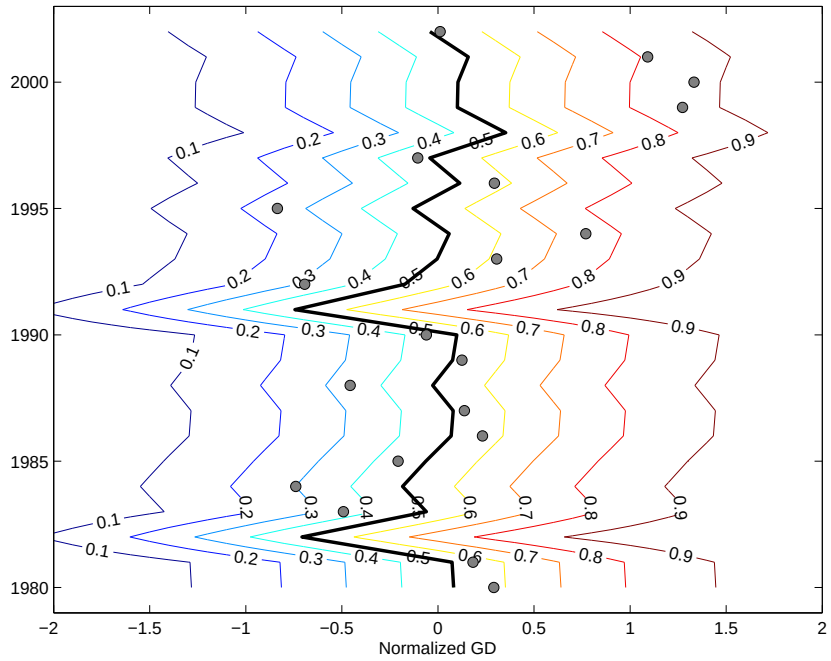

Figure 5.13.: probabilistic phenologic survival model in Teheran-Mehrabad. The black line is deterministic predicted GD and gray dots are observed GDDs.

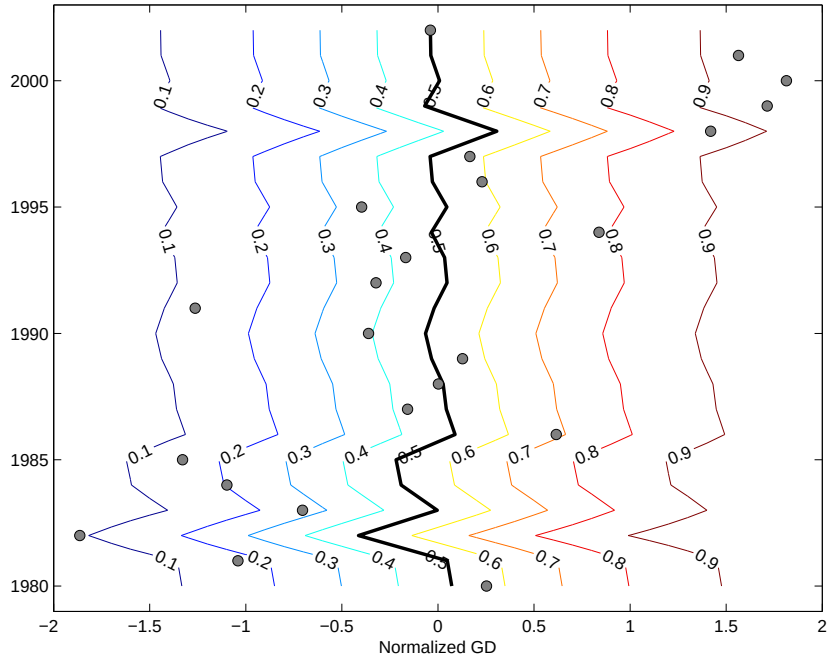

Figure 5.14.: Same as Fig. 5.13 but for Mashhad station

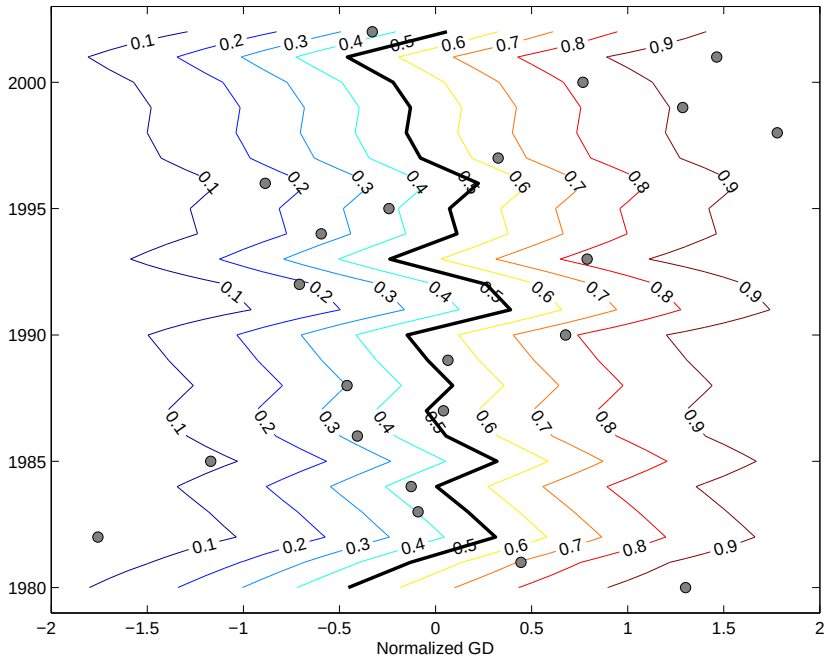

Figure 5.15.: Same as Fig. 5.13 but for Shahrekord station

Table 5.5.: Verification of the deterministic and probabilistic phenologic models (Eq. (3.42)) with different predictors and data resources. Positive and higher CRPSS is better

CRPSS	GDD_{Obs}	$T_{JJA_{Obs}}$	$T_{MAM_{Obs}}$	$CGDD_{CCLM}$	$GDD_{FP1-ERA40}$
Tabriz	0.33	0.36	0.36	0.35	0.33
Ahvaz	0.33	0.33	0.32	—	0.34
Tehran	0.35	0.34	0.34	0.35	0.35
Rasht	0.28	0.29	0.29	0.24	0.31
Shiraz	0.33	0.34	0.32	—	0.34
Isfahan	0.35	0.35	0.34	—	0.35
Zanjan	0.30	0.31	0.31	0.30	0.32
Mashhad	0.38	0.38	0.37	—	0.38
Kermanshah	0.33	0.38	0.38	0.38	0.36
Arak	0.37	0.38	0.37	0.37	0.38
Orumieh	0.28	0.27	0.27	0.28	0.21
Qazvin	0.35	0.36	0.36	0.35	0.36
Yazd	0.29	0.30	0.28	—	0.28
Sanandaj	0.36	0.36	0.36	0.35	0.32
Semnan	0.32	0.32	0.33	0.32	0.33
Shahrekord	0.29	0.27	0.25	—	0.27

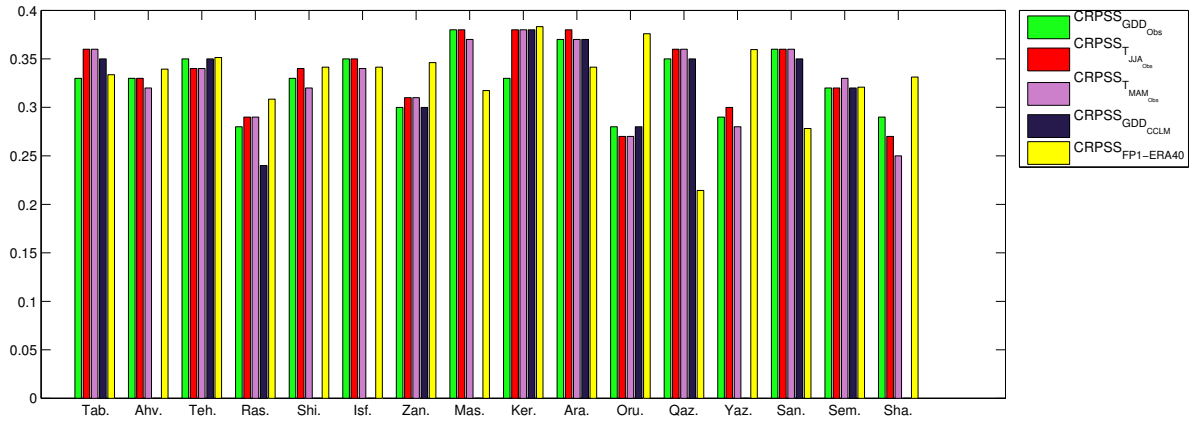

Figure 5.16.: Verifications of probabilistic and deterministic phenologic survival models with different predictors

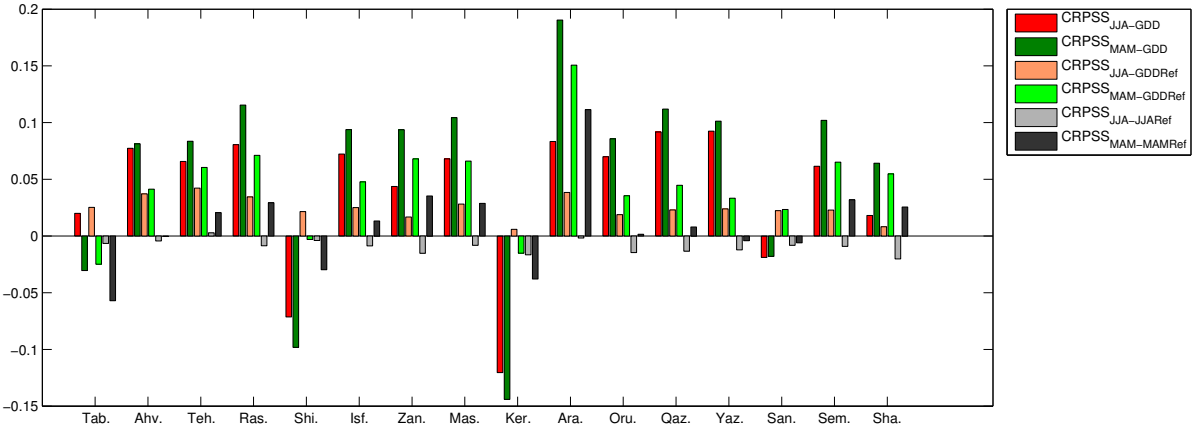

Figure 5.17.: Comparison between the probabilistic survival models with GDD, summer and spring temperatures as predictors

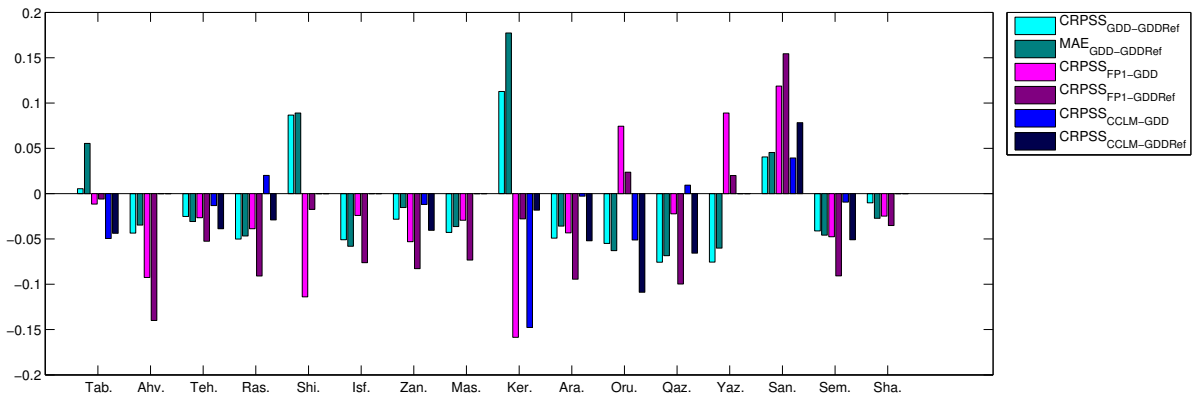

Figure 5.18.: Comparison between the probabilistic survival model with GDD predictor for observations, FP1 downscaled for ERA40 reanalysis and historical data of CCLM

6. Conclusion

This study presents and compares computationally inexpensive and easy to use statistical downscaling approaches for investigating the local effects of climate variability, daily 2m temperature and annual GDD and its impact on wheat cultivation in Iran.

A key factor for phenology is the local daily temperature variability. ERA-40 reanalysis well represent the local daily 2m temperature variability by a spatially well defined fingerprint pattern. The actual representation of the local temperature variability is obtained by a linear regression analysis between the fingerprint amplitude and observations of daily mean temperatures.

The fingerprint shows highly significant correlations with the observed temperature data on a temporal scale as well as different geographical regions with an increase of correlation from west to east and south to north as well. As local variability is dominating during summer, the August fingerprint pattern has a much smaller correlation range than the respective February pattern.

The fingerprint methods use large-scale squared correlations patterns to weight the influence of the large-scale variable for the downscaling. The advantage is that no a-priori selection of a neighborhood is required, the FP downscaling also accounts for remote effects and the dependency on the grid resolution of the large-scale data set is not an issue. This seems to be beneficial for the downscaling of GDD. The alternative approach uses linear multiple regression. For small samples as it is the case for annual GDD, MR has to be restricted to a local neighborhood.

The FP statistical downscaling is restricted to the correction of biases and variance errors for temperature and annual GDD. The potential to improve the correlation with the ERA-40 estimates via downscaling is larger, and the fingerprint method works well in this context. The GDD fingerprints have much larger spatial structures than those of the daily 2m temperature, which seems to favor the fingerprint method over multiple regression. The benefit of downscaling in correcting bias and variance error is larger.

We also demonstrate that the generation of realistic time series should be based on weather generators instead of deterministic downscaling. Although the correlations between the WG time series and the observations are smaller than for the downscaled values, the probabilistic evaluation of the WG using the CRPS shows a clear improvement. The reason is that the weather generator accounts for the uncertainty of the local variability and gives more realistic local time-series. The superiority of the WGs is large for both the daily 2m temperatures and the annual GDD.

To conclude the developed FP statistical downscaling, the fingerprint approach is easy to use and efficient. Since MR relies on the choice of an appropriate neighborhood, it is resolution dependent. If adjusted to a given model, it is not applicable to another model with a different spatial resolution. The fingerprint approach is not restricted by this constraint and in principle applicable to models with different spatial resolution. Given the only minor inferiority of the fingerprint methods compared to the MR approach, we think that the fingerprint approach represents a useful alternative to more common regression methods.

In this research we also developed a probabilistic phenologic model based on survival theory.

For a reasonable phenologic model, the range of uncertainty should be factored in the model. To that aim, we assessed the survival function based on a normal distribution which depends on the expected value and variance of the regression between GDD and GD data under cross-validation.

The survival functions are conducted with different predictors such as observed GDD, calculated GDD with historical CCLM model data, derived GDD from FP1 downscaled ERA40 data and temperatures of summer (JJA) and spring (MAM) and the climatology values derived from the mean values over the study period as the reference conditions of the main predictors. Verification of the models obtained is done using CRPS skill score (CRPSS).

The positive values of CRPSS indicate the large superiority of the probabilistic phenologic survival model to the deterministic models. These results demonstrate that considering uncertainties in modeling are beneficial, meaningful and necessary.

Comparing all probabilistic phenologic models with different predictors show that summer temperature is the most effective predictor of all. It could be expected because during warm season crops growth more effectively and achieve the greatest mass in their growth duration and here, GDD considered the dormancy period which maybe could be an impeding factor.

The probabilistic survival functions also illustrated that with a high probability, in warm weather conditions wheat reached its ripening date earlier. Exteding the survival function based on the normal distribution, other distributions can also be considered (e.g. Weibull or exponential). This would include the uncertainty being dependent on the predictors (Heteroscedasticity).

To summarize, we suggest using the WG fingerprint downscaling method as an easy-to-use statistical method for the downscaling of gridded data to point measurements at a regional scale. We also suggest using probabilistic phenologic modeling rather than deterministic for the agricultural impact studies. We strongly recommend comparative research for the case that precised yield crop and phenological data in different phenological stages are available.

Acknowledgment

This PhD study was funded by the German Academic Exchange Service (Deutscher Akademischer Austauschdienst, DAAD). So I will specially thank DAAD for supporting my research, myself and my family.

I warmly thank my supervisor, Prof. Dr. Andreas Hense from whom I learned so much as one of the best and effective teachers in the whole of my career. I learned from him not only scientifically but also patience and humility through his brilliant personality.

My very special thanks go to my husband, Mohammad who was always beside me in every situation. His love, hopes, help and support always pushed me forward to be success and be able to reach my aims. Thanks so much my love...

I will thank my lovely boys, Mani and Makan for tolerating our difficult student situation. Many thanks my dear children for understanding your Mum when she was very busy and tired. I will repay it for you as I have always promised you ;)

My lovely and kind parents, hereby I will kiss your hands and hearts and respect your valuable patience. I know that you suffered too much parting from your children and your grandchildren. Despite from this suffering separation you always gave me high motivation and too much energy. Respect and many thanks.

Many thanks to my dearest friend, Shahpar who supported and advised me such as a mother with her warm and kind behavior in every time.

Special thanks to my first and the best German friend, Petra who gave me always very good feeling against alienation. Many thanks Petra for your very kind support which I will never forget.

Hereby, I will say my special thanks to Dr. Harry Leach for his splendid and valuable help for checking the English grammar of my dissertation.

I warmly thank my dear teachers and colleagues which supported me scientifically. I will never forget your splendid help and warm working atmosphere that you made for me. It was my best experience in studying and working in whole my student career. So many thanks to,

- Liselotte Bach
- Annemarie Debus
- PD. Dr. Petra Friederichs
- Lucia Halas
- Dr. Jan Keller
- Ehsan Khorsandi
- Dr. Volker Küll
- Marc Mertes
- Kaleem Muhammad

- Ingeborg Rassow
- Dr. Jehan Rihani
- Dr. Vanya Romanova
- Elke Rustemeier
- Dr. Pablo Saavedra Garfias
- Dr. Thorsten Simon
- Sophie Stolzenberger
- Insa Thiele-Eich
- Benno Thoma
- Sabrina Wahl
- Chris Weijenborg
- Dr. Michael Weniger

The last but not least, many thanks to Prof. Dr. Sahar Sodoudi for providing the available CCLM data for Iran. Also I will thank very much Jamil Roohani, director of JAME IRAN consulting engineers in Tehran and the Iran Meteorological Organization (IRIMO) for providing the data.

Bibliography

Alijani, B. et al. (2007). "Circulation Patterns Of The Monsoon Rains During July 1994 Of Iran." In: *Journal Of Geographical Sciences* 7.10, pp. 7–38.

Allison, Paul David (2012). *Survival analysis using SAS: a practical guide*. Sas Institute.

Badripour, H (2004). "Islamic Republic of Iran. Country Pasture/Forage Resource Profiles. Rangeland Management Expert in the Technical Bureau of Rangeland–grown at three environments." In: *Crop Science* 16, pp. 347–349.

Batts, GR et al. (1997). "Effects of CO2 and temperature on growth and yield of crops of winter wheat over four seasons." In: *European Journal of Agronomy* 7, pp. 43–52.

Bromwich, David H and Ryan L Fogt (2004). "Strong Trends in the Skill of the ERA-40 and NCEP-NCAR Reanalyses in the High and Midlatitudes of the Southern Hemisphere, 1958-2001*." In: *Journal of Climate* 17, pp. 4603–4619.

Brown, Robert A and Norman J Rosenberg (1999). "Climate change impacts on the potential productivity of corn and winter wheat in their primary United States growing regions." In: *Climatic Change* 41, pp. 73–107.

Challinor, AJ et al. (2005). "Simulation of the impact of high temperature stress on annual crop yields." In: *Agricultural and Forest Meteorology* 135, pp. 180–189.

Chavas, Daniel R et al. (2009). "Long-term climate change impacts on agricultural productivity in eastern China." In: *Agricultural and Forest Meteorology* 149, pp. 1118–1128.

Chen, Jie et al. (2010). "A daily stochastic weather generator for preserving low-frequency of climate variability." In: *Journal of hydrology* 388.3, pp. 480–490.

Chernick, M. R. (2008). *Bootstrap methods: A guide for practitioners and researchers*. Vol. 619. John Wiley & Sons.

Cleland, Elsa E et al. (2007). "Shifting plant phenology in response to global change." In: *Trends in ecology & evolution* 22.7, pp. 357–365.

Costa, Ana Cristina and Amílcar Soares (2009). "Homogenization of climate data: review and new perspectives using geostatistics." In: *Mathematical geosciences* 41, pp. 291–305.

Cox, David Roxbee and David Oakes (1984). *Analysis of survival data*. Vol. 21. CRC Press.

Dee, DP et al. (2011). "The ERA-Interim reanalysis: Configuration and performance of the data assimilation system." In: *Quarterly Journal of the Royal Meteorological Society* 137.656, pp. 553–597.

Deihimfard, R. et al. (2007). "Herbicide risk assessment during the Wheat Self-sufficiency Project in Iran." In: *Pest Management Science* 63.10, pp. 1036–1045.

Douville, H. and J. F. Royer (1996). "Sensitivity of the Asian summer monsoon to an anomalous Eurasian snow cover within the Meteo-France GCM." In: *Climate Dynamics* 12.7, pp. 449–466.

Dubrovský, Martin et al. (2004). "High-frequency and low-frequency variability in stochastic daily weather generator and its effect on agricultural and hydrologic modelling." In: *Climatic Change* 63.1-2, pp. 145–179.

Fazeli, N. and R. Zare (2011). "Effect of Seasonal Monsoons on Calanoid Copepod in Chabahar Bay-Gulf of Oman." In: *Jordan Journal of Biological Sciences* 4.1, pp. 55–62.

Gadgil, S. (2007). "The Indian Monsoon." In: *Resonance* 12.5, pp. 4–20.

Gebhardt, C. et al. (2000). "Optimal averaging of incomplete climatological data." In: *Theoretical and applied climatology* 65, pp. 137–155.

Gerivani, H. et al. (2011). "The Source of Dust Storm in Iran: A Case Study Based On Geological Information And Rainfall Data." In: *Carpathian Journal of Earth and Environmental Sciences* 6.1, pp. 297–308.

Gneiting, Tilmann et al. (2005). "Calibrated probabilistic forecasting using ensemble model output statistics and minimum CRPS estimation." In: *Monthly Weather Review* 133, pp. 1098–1118.

Gohari, Alireza et al. (2013). "Climate change impacts on crop production in Iran's Zayandeh-Rud River Basin." In: *Science of The Total Environment* 442, pp. 405–419.

Haim, David et al. (2008). "Assessing the impact of climate change on representative field crops in Israeli agriculture: a case study of wheat and cotton." In: *Climatic Change* 86, pp. 425–440.

Harris, I et al. (2013). "Updated high-resolution grids of monthly climatic observations–the CRU TS3. 10 Dataset." In: *International Journal of Climatology —*,

Hersbach, Hans (2000). "Decomposition of the continuous ranked probability score for ensemble prediction systems." In: *Weather and Forecasting* 15, pp. 559–570.

Hewitson, BC and RG Crane (1996). "Climate downscaling: techniques and application." In: *Climate Research* 7.2, pp. 85–95.

Huth, Radan (2002). "Statistical downscaling of daily temperature in central Europe." In: *Journal of Climate* 15.13, pp. 1731–1742.

Jeong, DI et al. (2012). "Comparison of transfer functions in statistical downscaling models for daily temperature and precipitation over Canada." In: *Stochastic Environmental Research and Risk Assessment* 26.5, pp. 633–653.

Kleinbaum, David G (1998). "Survival Analysis, a Self-Learning Text." In: *Biometrical Journal* 40, pp. 107–108.

Kousari, Mohammad Reza et al. (2013). "Temporal and spatial trend detection of maximum air temperature in Iran during 1960–2005." In: *Global and Planetary Change* 111, pp. 97–110.

Luo, Qunying et al. (2013). "A comparison of downscaling techniques in the projection of local climate change and wheat yields." In: *Climatic change* 120.1-2, pp. 249–261.

Maraun, D. et al. (2010). "Precipitation downscaling under climate change: Recent developments to bridge the gap between dynamical models and the end user." In: *Reviews of Geophysics* 48.3, RG3003.

Marshall, Gareth J (2002). "Trends in Antarctic geopotential height and temperature: A comparison between radiosonde and NCEP-NCAR reanalysis data." In: *Journal of Climate* 15, pp. 659–674.

McMaster, Gregory S. and D.E. Smika (1988). "Estimation and evaluation of winter wheat phenology in the central Great Plains." In: *Agricultural and Forest Meteorology* 43.1, pp. 1–18.

McMaster, Gregory S. and Wallace W. Wilhelm (1998). "Is soil temperature better than air temperature for predicting winter wheat phenology?" In: *Agronomy journal* 90, pp. 602–607.

Modarres, R. and A. Sarhadi (2011). "Statistically-based regionalization of rainfall climates of Iran." In: *Global and Planetary Change* 75.1, pp. 67–75.

Mozny, Martin et al. (2009). "The impact of climate change on the yield and quality of Saaz hops in the Czech Republic." In: *Agricultural and Forest Meteorology* 149, pp. 913–919.

Murphy, J. (1999). "An evaluation of statistical and dynamical techniques for downscaling local climate." In: *Journal of Climate* 12.8, pp. 2256–2284.

Natsagdorj, L. et al. (2003). "Analysis of dust storms observed in Mongolia during 1937-1999." In: *Atmospheric Environment* 37.9-10, pp. 1401–1411.

Niu, Xianzeng et al. (2009). "Reliability and input-data induced uncertainty of the EPIC model to estimate climate change impact on sorghum yields in the US Great Plains." In: *Agriculture, Ecosystems & Environment* 129, pp. 268–276.

Özgen, M. et al. (1998). "Efficient callus induction and plant regeneration from mature embryo culture of winter wheat (Triticum aestivum L.) genotypes." In: *Plant Cell Reports* 18.3, pp. 331–335.

Pielke, Roger A and Robert L Wilby (2012). "Regional climate downscaling: What's the point?" In: *Eos, Transactions American Geophysical Union* 93.5, pp. 52–53.

Prigogine, Ilya (1997). *The End of Certainty*.

Prigogine, Ilya and Erwin N Hiebert (1982). "From being to becoming: Time and complexity in the physical sciences." In: *Physics Today* 35, p. 69.

Rockel, B. et al. (2008). "The regional climate model COSMO-CLM (CCLM)." In: *Meteorologische Zeitschrift* 17, pp. 347–348.

Röder, M. S. et al. (1998). "A microsatellite map of wheat." In: *Genetics* 149.4, pp. 2007–2023.

RP, GAGE et al. (1950). "Calculation of survival rates for cancer." In: *Proceedings of the staff meetings of the Mayo Clinic* 25, pp. 270–286.

Saligheh, M. and F. Barimani (2007). "Effects Of Climatic Systems Of Seasonal In Balouchestan's Agriculture." In: *Geography And Development* 9.5, pp. 25–38.

Schär, Christoph et al. (2004). "The role of increasing temperature variability in European summer heatwaves." In: *Nature* 427, pp. 332–336.

Semenov, Mikhail A and Pierre Stratonovitch (2010). "Use of multi-model ensembles from global climate models for assessment of climate change impacts." In: *Climate research (Open Access for articles 4 years old and older)* 41.1, p. 1.

Spiegelhalter, DJ (2014). "The future lies in uncertainty." In: *Science* 345.6194, pp. 264–265.

Storch, Hans von (1999). "On the use of "inflation" in statistical downscaling." In: *Journal of Climate* 12, pp. 3505–3506.

Tabari, H. and P. H. Talaee (2011). "Analysis of trends in temperature data in arid and semi-arid regions of Iran." In: *Global and Planetary Change* 79, pp. 1–10.

Teutschbein, C. et al. (2011). "Evaluation of different downscaling techniques for hydrological climate-change impact studies at the catchment scale." In: *Climate dynamics* 37.9, pp. 2087–2105.

Tibshirani, R. J. and B. Efron (1993). "An introduction to the bootstrap." In: *Monographs on Statistics and Applied Probability* 57, pp. 1–436.

Tsvetsinskaya, EA et al. (2003). *Issues in the Impacts of Climate Variability and Change on Agriculture, The effect of spatial scale of climatic change scenarios on simulated maize, winter wheat, and rice production in the Southeastern United States*. Springer, pp. 37–71.

Uppala, S.M. et al. (2005). "The ERA-40 re-analysis." In: *Quarterly Journal of the Royal Meteorological Society* 131.612, pp. 2961–3012.

Valizadeh, J et al. (2013). "Assessing climate change impacts on wheat production (a case study)." In: *Journal of the Saudi Society of Agricultural Sciences* —,

Van Ittersum, MK et al. (2003). "Sensitivity of productivity and deep drainage of wheat cropping systems in a Mediterranean environment to changes in CO2, temperature and precipitation." In: *Agriculture, ecosystems & environment* 97, pp. 255–273.

Von Storch, Hans and Francis W Zwiers (2001). *Statistical Analysis in Climate Research*. Cambridge University Press.

Wilby, RL et al. (2004). "Guidelines for use of climate scenarios developed from statistical downscaling methods." In: *IPCC Task Group on Data and Scenario Support for Impacts and Climate Analysis —*,

Wilby, Robert L and Hayley J Fowler (2010). "3 Regional Climate Downscaling." In: *Modelling the Impact of Climate Change on Water Resources*, p. 34.

Wilks, Daniel S (2011). *Statistical Methods in the Atmospheric Sciences*. Access Online via Elsevier.

Woodall, CW et al. (2005). "Applying survival analysis to a large-scale forest inventory for assessment of tree mortality in Minnesota." In: *Ecological Modelling* 189, pp. 199–208.

Zand, E. et al. (2007). "Broadleaved weed control in winter wheat (Triticum aestivum L.) with post-emergence herbicides in Iran." In: *Crop Protection* 26.5, pp. 746–752.

Appendix

Table of appendices

A. Appendix of seasonal cycle and trends

Figures A.1 to A.16 shows the daily averaged temperatures for all other stations averaged over all available years as a function of the number of the day of the year. As a continuous line, we added the 12 month and six month periodic component determined by the Fourier analysis.

The tables in Appendix A.1 to A.16 present some information about temperature variability is assessed with 5% significant linear trend ($^{\circ}C$ per 45 years) of monthly average temperature data from 1961 to 2005, intraseasonal interannual average of temperature and its standard deviation, amplitude of daily temperature (difference between the maximum and minimum temperatures) and average of synoptic temperature variable or average of intramonthly variability. All trends are tested against the Null hypothesis "no trend" which was rejected for all months at the 5% significance level.

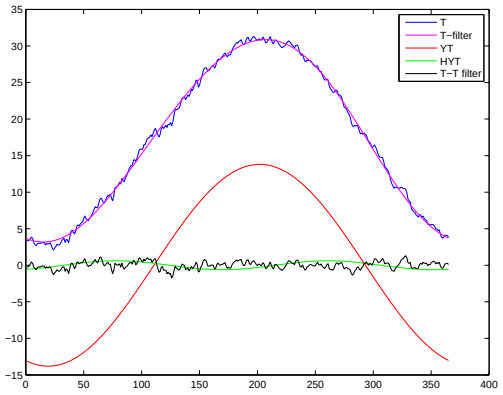

Figure A.1.: Long term mean daily temperature (blue), annual (YT, 12 month period, red) and half annual (HYT, six month period, green) Fourier component, sum of annual mean and periodic components T_{filter} (purple) and residual, $T - T_{filter}$ (black) at Tehran station

Table A.1.: Monthly average of temperature and its standard deviation, amplitude of daily temperature, 5% significant linear regression trend in monthly from 1961 to 2005 and average of synoptic temperature variable for Tehran station

Month	T_{mean} $^{\circ}C$	T_{min} $^{\circ}C$	T_{max} $^{\circ}C$	T_{sd} $^{\circ}C$
January	3.23	-9.45	13.95	3.90
February	5.47	-6.55	14.93	4.01
March	10.37	-3.00	21.18	4.26
April	16.78	1.13	27.75	4.06
May	22.26	6.85	31.40	3.68
June	28.03	16.3	36.00	2.95
July	30.85	22.08	37.55	2.46
August	29.89	19.98	36.33	2.45
September	25.66	13.18	32.13	2.99
October	18.74	5.63	27.13	3.57
November	11.40	0.18	19.95	3.62
December	5.55	-7.95	14.7	3.58

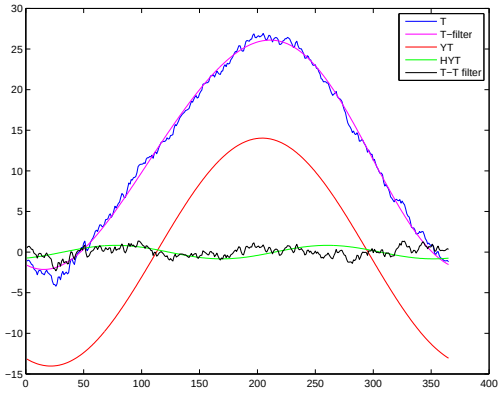

Figure A.2.: Same as Fig. A.1 but for Tabriz station

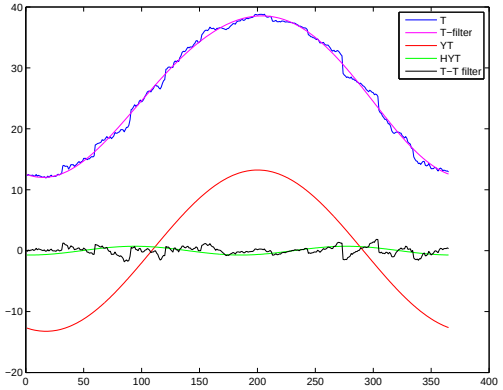

Figure A.3.: Same as Fig. A.1 but for Ahvaz station

Table A.2.: Temperature variability as Tab. A.1 but for Tabriz station

Month	T_{mean} $^{\circ}C$	T_{min} $^{\circ}C$	T_{max} $^{\circ}C$	T_{sd} $^{\circ}C$
January	-2.23	-20.05	10.50	4.71
February	-0.03	-15.93	11.55	4.66
March	5.45	-12.45	18.20	4.26
April	11.62	-3.48	23.41	3.96
May	16.99	5.13	27.13	3.62
June	22.47	10.23	31.68	3.32
July	26.26	14.28	34.10	2.87
August	25.76	15.98	33.15	2.69
September	21.25	8.83	29.45	3.01
October	14.11	-1.15	22.73	3.50
November	6.70	-4.93	17.00	3.62
December	0.92	-14.98	13.55	4.13

Table A.3.: Temperature variability as Tab. A.1 but for Ahvaz station

Month	T_{mean} $^{\circ}C$	T_{min} $^{\circ}C$	T_{max} $^{\circ}C$	T_{sd} $^{\circ}C$
January	12.36	4.68	21.28	2.01
February	14.57	6.43	22.38	1.99
March	19.05	8.80	27.03	2.50
April	25.60	14.65	33.23	2.76
May	32.25	22.15	39.50	2.52
June	36.49	30.48	41.93	1.60
July	38.32	34.20	43.15	1.30
August	37.31	31.03	42.00	1.30
September	33.76	26.93	39.48	1.78
October	27.35	16.33	33.83	2.16
November	19.76	9.20	27.50	2.87
December	13.87	5.95	22.15	2.35

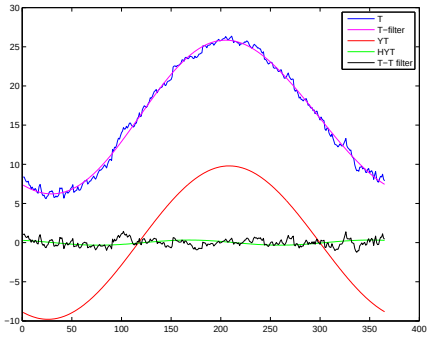

Figure A.4.: Same as Fig. A.1 but for Rasht station

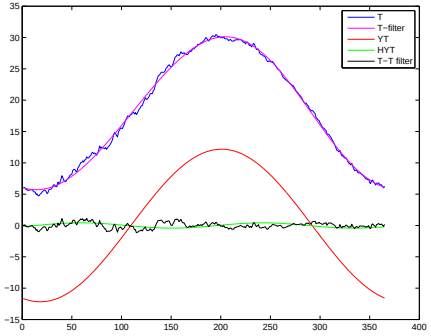

Figure A.5.: Same as Fig. A.1 but for Shiraz station

Table A.4.: Temperature variability as Tab. A.1 but for Rasht station

Month	T_{mean} $^{\circ}C$	T_{min} $^{\circ}C$	T_{max} $^{\circ}C$	T_{sd} $^{\circ}C$
January	6.95	-3.78	24.38	3.64
February	6.59	-2.68	22.23	3.24
March	8.90	-0.43	26.83	2.85
April	14.24	4.18	28.80	2.94
May	19.13	8.30	25.93	2.51
June	23.29	14.73	28.88	2.08
July	25.64	17.15	28.95	1.75
August	25.23	17.60	29.43	1.72
September	22.04	13.48	27.80	2.04
October	17.62	8.08	26.23	2.81
November	12.79	2.13	26.28	2.82
December	8.84	0.25	25.05	3.26

Table A.5.: Temperature variability as Tab. A.1 but for Shiraz station

Month	T_{mean} $^{\circ}C$	T_{min} $^{\circ}C$	T_{max} $^{\circ}C$	T_{sd} $^{\circ}C$
January	5.61	-5.80	13.40	2.74
February	7.94	-3.40	16.03	2.82
March	11.83	3.03	19.40	2.72
April	16.72	6.05	24.13	3.21
May	22.89	12.48	30.48	3.13
June	27.84	19.03	33.05	2.01
July	29.96	21.40	35.53	1.95
August	28.92	19.93	34.33	2.12
September	24.79	15.86	30.80	2.61
October	18.91	9.28	25.53	2.61
November	12.07	2.44	19.13	2.78
December	7.41	-3.33	14.38	2.78

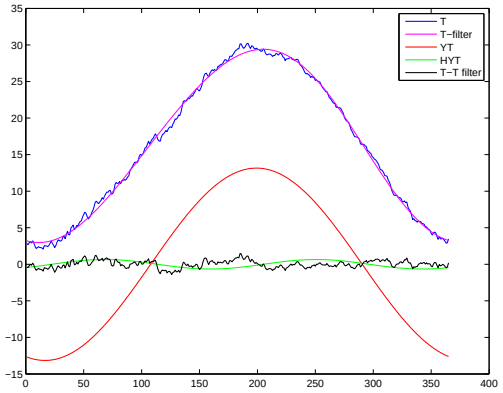

Figure A.6.: Same as Fig. A.1 but for Isfahan station

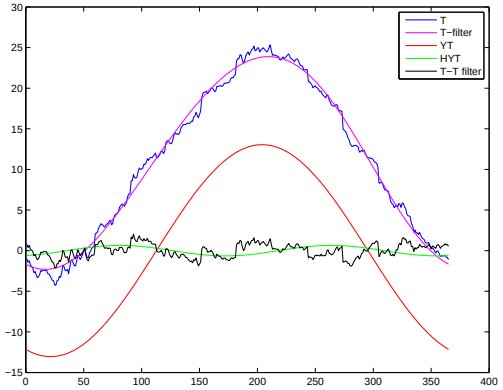

Figure A.7.: Same as Fig. A.1 but for Zanjan station

Table A.6.: Temperature variability as Tab. A.1 but for Isfahan station

Month	T_{mean} $^{\circ}C$	T_{min} $^{\circ}C$	T_{max} $^{\circ}C$	T_{sd} $^{\circ}C$
January	2.79	-12.05	12.81	3.41
February	5.71	-7.40	15.43	3.52
March	10.43	-1.00	20.68	3.55
April	16.02	0.63	24.35	3.42
May	21.39	10.25	29.30	3.18
June	27.15	17.08	32.05	2.23
July	29.53	21.15	34.75	2.06
August	28.00	19.23	33.23	2.00
September	23.71	14.84	29.58	2.53
October	17.06	8.03	24.55	2.93
November	9.92	-0.28	17.65	3.22
December	4.58	-8.85	13.00	3.19

Table A.7.: Temperature variability as Tab. A.1 but for Zanjan station

Month	T_{mean} $^{\circ}C$	T_{min} $^{\circ}C$	T_{max} $^{\circ}C$	T_{sd} $^{\circ}C$
January	-2.68	-18.80	8.69	4.95
February	-0.94	-18.83	8.95	3.99
March	4.37	-12.55	17.73	3.74
April	10.73	-1.40	20.15	3.21
May	15.03	3.05	23.88	2.65
June	20.22	9.18	28.10	2.23
July	24.31	14.48	32.10	2.80
August	23.45	14.48	30.45	2.03
September	18.99	9.58	25.55	2.25
October	12.59	0.45	19.90	2.75
November	5.92	-7.03	14.05	3.18
December	0.53	-16.95	11.65	4.25

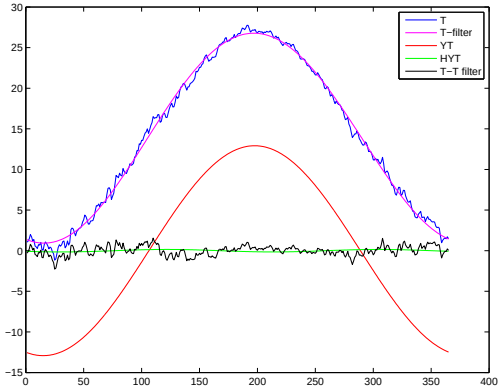

Figure A.8.: Same as Fig. A.1 but for Mashhad station

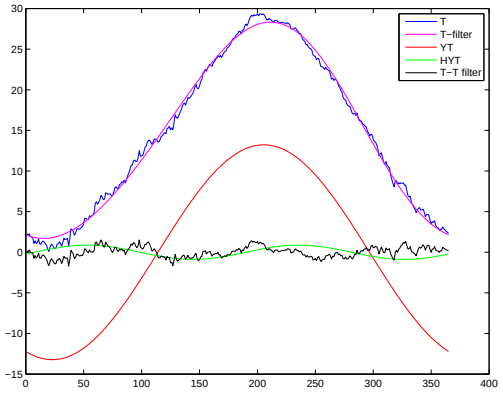

Figure A.9.: Same as Fig. A.1 but for Kermanshah station

Table A.8.: Temperature variability as Tab. A.1 but for Mashhad station

Month	T_{mean} $^{\circ}C$	T_{min} $^{\circ}C$	T_{max} $^{\circ}C$	T_{sd} $^{\circ}C$
January	0.86	-18.50	14.98	4.98
February	2.88	-17.98	19.28	5.21
March	7.98	-6.38	22.08	4.87
April	14.43	-0.10	25.98	4.56
May	19.71	4.78	30.39	3.74
June	24.92	11.53	32.25	2.82
July	27.14	17.35	34.13	2.13
August	25.18	15.83	31.78	2.54
September	20.40	7.58	30.28	3.35
October	13.98	-1.98	24.88	4.15
November	8.18	-6.75	19.00	4.17
December	3.28	-15.43	16.55	4.55

Table A.9.: Temperature variability as Tab. A.1 but for Kermanshah station

Month	T_{mean} $^{\circ}C$	T_{min} $^{\circ}C$	T_{max} $^{\circ}C$	T_{sd} $^{\circ}C$
January	1.31	-17.38	11.98	4.36
February	3.10	-14.78	14.11	4.08
March	7.82	-4.10	19.78	3.43
April	12.95	1.20	21.73	3.26
May	17.90	6.85	28.58	3.18
June	24.14	15.55	31.18	2.60
July	28.49	5.79	34.75	2.20
August	27.67	21.60	33.38	2.07
September	22.69	12.70	30.28	2.28
October	16.30	5.23	24.09	2.94
November	9.13	-2.15	20.28	3.18
December	4.02	-10.08	14.60	3.51

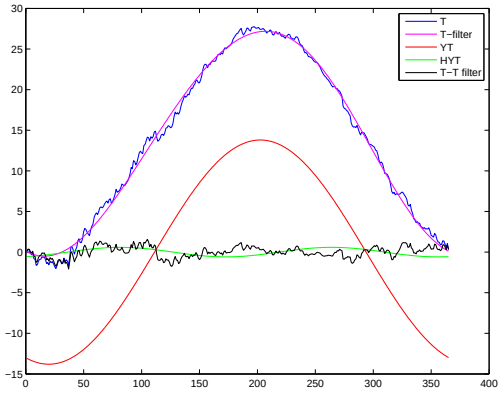

Figure A.10.: Same as Fig. A.1 but for Arak station

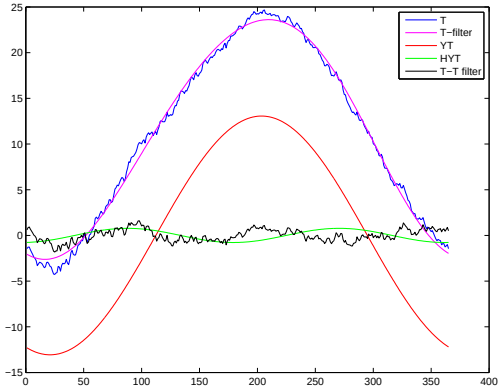

Figure A.11.: Same as Fig. A.1 but for Orumieh station

Table A.10.: Temperature variability as Tab. A.1 but for Arak station

Month	T_{mean} $\circ C$	T_{min} $\circ C$	T_{max} $\circ C$	T_{sd} $\circ C$
January	-0.97	-21.70	11.38	5.43
February	1.26	-22.24	13.32	5.32
March	7.00	-12.62	19.22	4.08
April	13.09	0.12	21.20	3.57
May	18.30	5.70	26.64	3.44
June	24.26	12.74	30.58	2.43
July	27.38	20.20	33.04	1.87
August	26.30	17.78	32.02	1.93
September	21.83	12.08	27.50	2.48
October	15.08	3.18	22.92	3.05
November	7.88	-3.24	17.04	3.38
December	2.32	-17.78	13.04	4.30

Table A.11.: Temperature variability as Tab. A.1 but for Orumieh station

Month	T_{mean} $\circ C$	T_{min} $\circ C$	T_{max} $\circ C$	T_{sd} $\circ C$
January	-2.82	-17.05	10.48	4.12
February	-1.07	-14.50	8.93	4.05
March	4.62	-10.43	18.58	3.94
April	10.73	-1.88	20.63	3.30
May	15.47	4.33	23.10	3.05
June	20.26	9.83	27.08	2.65
July	23.80	14.35	30.00	2.03
August	23.21	15.75	29.03	2.09
September	18.95	9.90	26.78	2.48
October	12.60	0.65	21.46	3.07
November	5.87	-9.00	16.03	3.35
December	0.37	-11.75	11.03	3.80

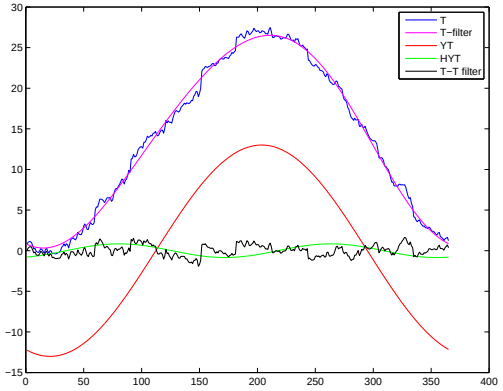

Figure A.12.: Same as Fig. A.1 but for Qazvin station

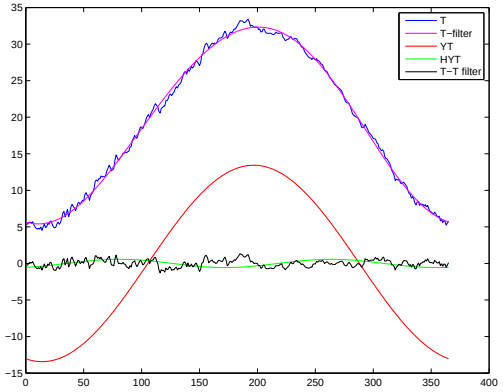

Figure A.13.: Same as Fig. A.1 but for Yazd station

Table A.12.: Temperature variability as Tab. A.1 but for Qazvin station

Month	T_{mean} $^{\circ}C$	T_{min} $^{\circ}C$	T_{max} $^{\circ}C$	T_{sd} $^{\circ}C$
January	0.24	-13.73	10.55	3.74
February	2.08	-11.73	11.18	3.51
March	7.33	-5.28	17.85	3.60
April	13.37	0.03	22.23	3.06
May	17.63	4.38	26.75	2.61
June	23.31	15.80	30.83	2.01
July	26.75	17.13	32.00	2.04
August	25.92	17.40	31.60	1.94
September	21.70	12.18	28.20	2.22
October	15.68	3.23	25.28	3.52
November	8.60	-2.98	17.13	3.23
December	2.55	-12.13	13.05	3.45

Table A.13.: Temperature variability as Tab. A.1 but for Yazd station

Month	T_{mean} $^{\circ}C$	T_{min} $^{\circ}C$	T_{max} $^{\circ}C$	T_{sd} $^{\circ}C$
January	5.42	-6.28	17.65	3.58
February	8.37	-1.60	21.75	3.85
March	13.59	0.23	23.93	4.21
April	19.64	4.75	29.33	3.75
May	25.26	13.35	32.38	3.16
June	30.65	21.23	36.68	2.20
July	32.49	25.23	38.33	2.29
August	30.73	21.28	39.00	2.45
September	26.38	14.13	33.55	2.77
October	19.63	7.18	27.88	3.20
November	12.33	-0.09	21.00	3.59
December	7.13	-9.68	17.43	3.80

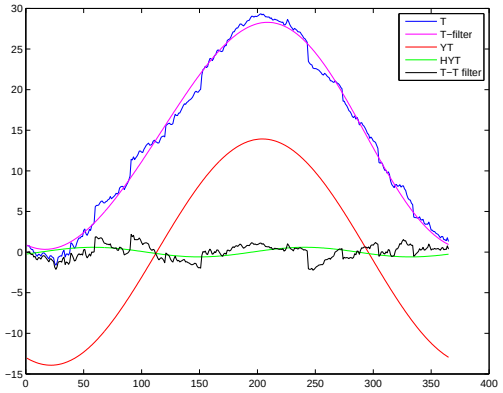

Figure A.14.: Same as Fig. A.1 but for Sanandaj station

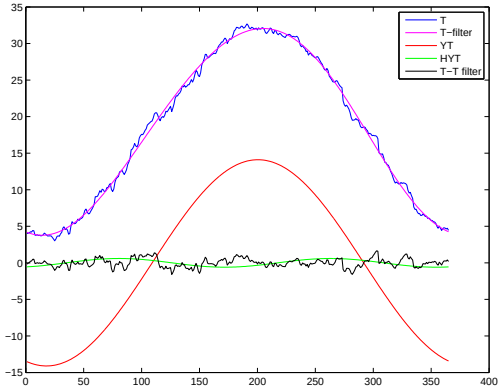

Figure A.15.: Same as Fig. A.1 but for Semnan station

Table A.14.: Temperature variability as Tab. A.1 but for Sanandaj station

Month	T_{mean} °C	T_{min} °C	T_{max} °C	T_{sd} °C
January	0.05	-16.50	16.80	4.52
February	1.76	-21.00	19.88	4.35
March	7.32	-5.93	22.70	3.11
April	13.11	1.08	26.93	2.84
May	18.04	7.60	32.73	3.06
June	24.84	15.08	36.85	3.16
July	28.79	20.80	39.05	1.99
August	27.78	19.50	36.48	2.04
September	21.94	15.20	33.98	2.02
October	16.02	6.13	30.13	2.97
November	8.70	-2.05	24.23	3.19
December	3.12	-14.80	14.38	3.45

Table A.15.: Temperature variability as Tab. A.1 but for Semnan station

Month	T_{mean} °C	T_{min} °C	T_{max} °C	T_{sd} °C
January	3.86	-3.73	11.53	2.61
February	5.99	-3.48	15.03	3.23
March	11.17	-2.08	21.23	3.85
April	18.24	5.15	26.98	3.71
May	23.49	10.00	32.30	3.42
June	29.45	19.33	36.98	2.90
July	32.06	20.50	38.20	2.55
August	30.76	20.58	35.93	2.21
September	26.52	16.53	32.73	2.75
October	19.26	7.03	27.00	3.05
November	11.78	1.35	19.68	3.17
December	5.70	-2.70	14.20	2.79

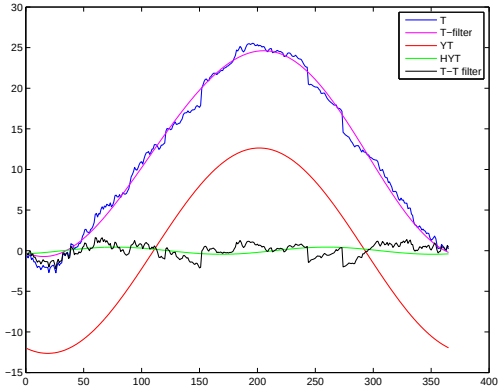

Figure A.16.: Same as Fig. A.1 but for Shahrekord station

Table A.16.: Temperature variability as Tab. A.1 but for Shahrekord station

Month	T_{mean} $^{\circ}C$	T_{min} $^{\circ}C$	T_{max} $^{\circ}C$	T_{sd} $^{\circ}C$
January	-1.79	-22.15	9.84	4.37
February	1.12	-14.65	11.45	3.93
March	6.08	-4.33	14.38	2.94
April	11.58	1.08	19.89	2.74
May	16.30	7.85	21.83	2.05
June	21.91	13.70	28.07	2.00
July	24.96	17.33	30.70	1.57
August	23.87	16.68	29.73	1.46
September	19.00	9.38	24.20	1.88
October	12.63	3.30	19.58	1.93
November	7.21	-3.23	16.39	2.95
December	1.57	-21.75	9.88	3.58

B. Appendix of fingerprints

The ERA-40 fingerprints are displayed in Figs. B.1 to B.7 for all other stations. Figs.(A, C) show the fingerprints in the coldest month in Iran (February) and Figs.(B, D) show the fingerprints in the warmest month in Iran (August). Non-significant values are marked with gray dots. For an almost perfect reanalysis, one would expect a regression coefficient of $b \approx 1$ near the station. The squared correlation (shading) represents the fraction of variance locally explained by the fingerprint. The contours explain the regression coefficients.

The ERA-40 fingerprints for GDD are displayed in Figs B.8 to B.11 for all stations. Squared correlation between GDD at station and ERA-40 grids are shown with shading areas and contours represent the regression coefficients. Non- significant grid points are also marked with gray dots.

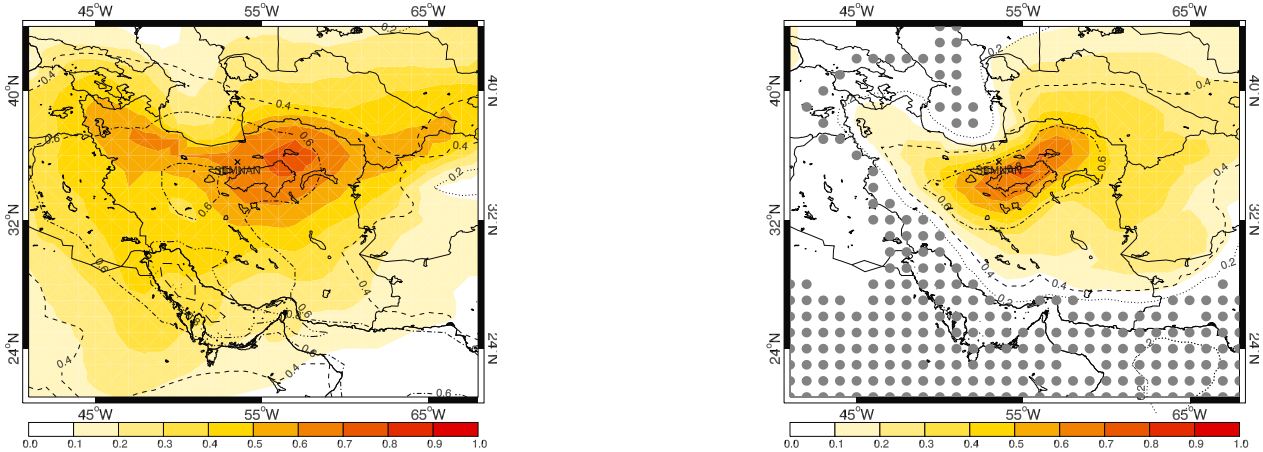

Figure B.1.: Squared correlation (shading) and regression coefficients (contours) between daily temperature anomalies at the Tabriz station and in ERA-40 during February (A) and August (B) for Semnan station. Non-significant grid points are marked with gray dots.

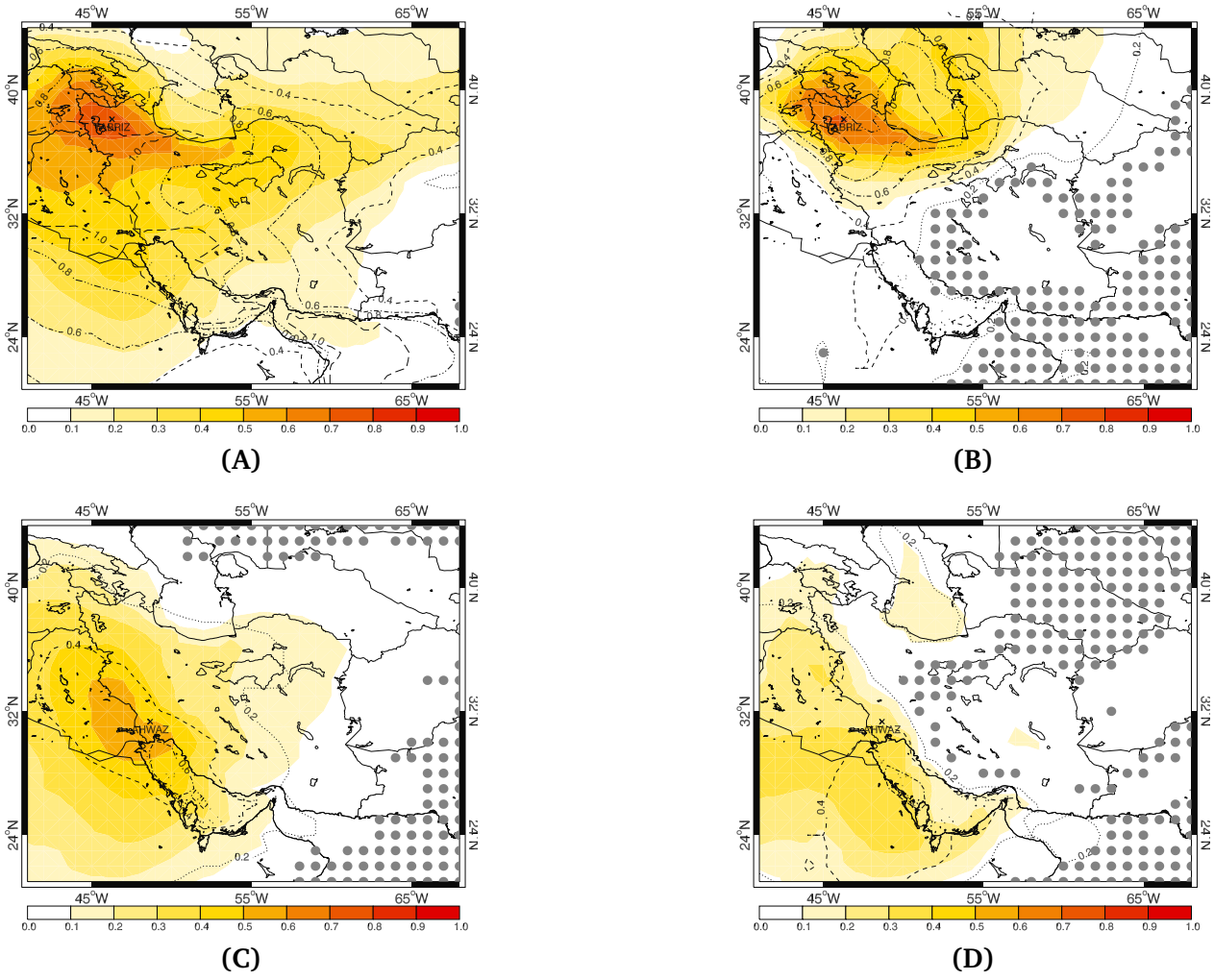

Figure B.2.: Same as Fig. B.1 but (A, B) for Tabriz station and (C, D) for Ahvaz station

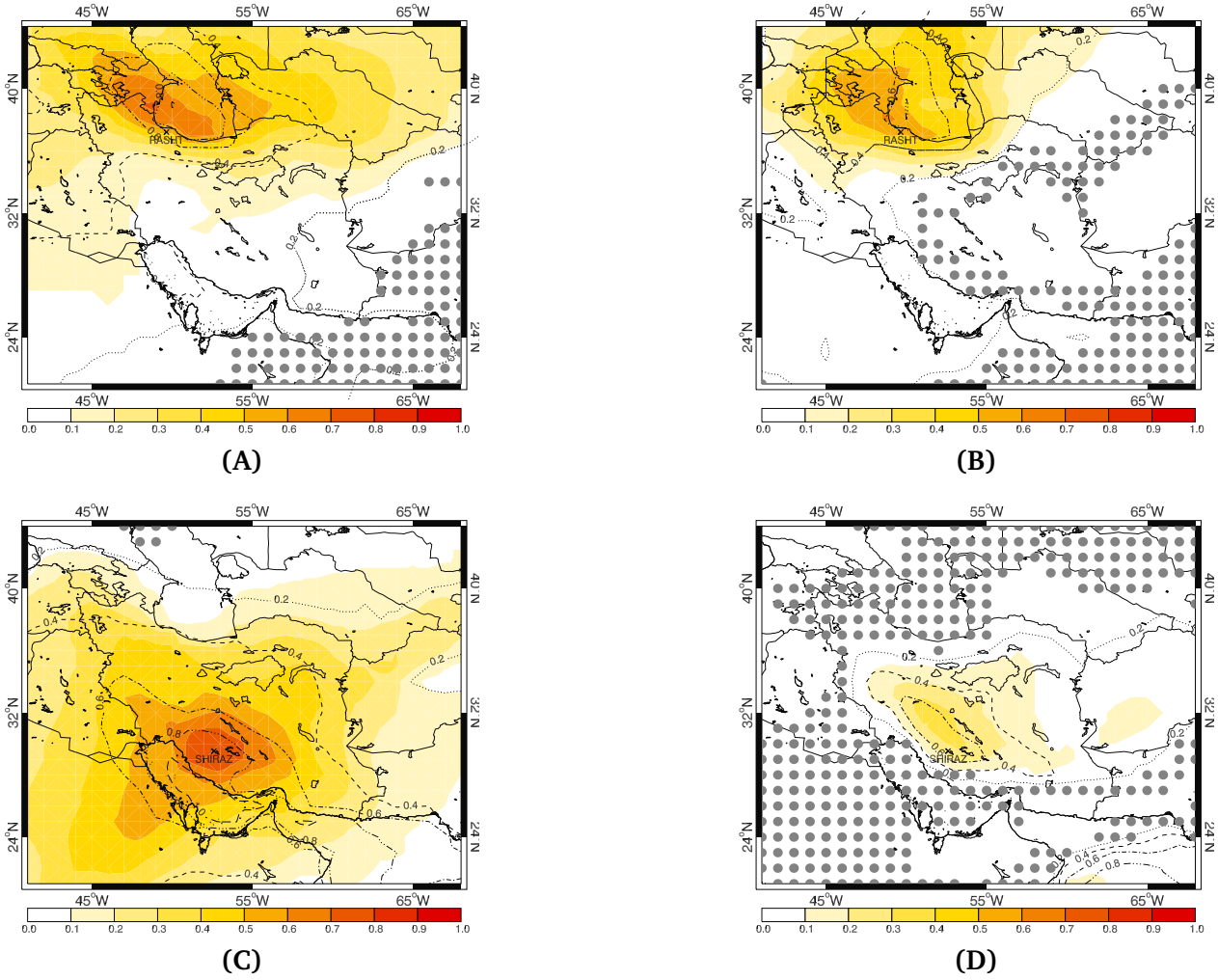

Figure B.3.: Same as Fig. B.1 but (A, B) for Rasht station and (C, D) for Shiraz station

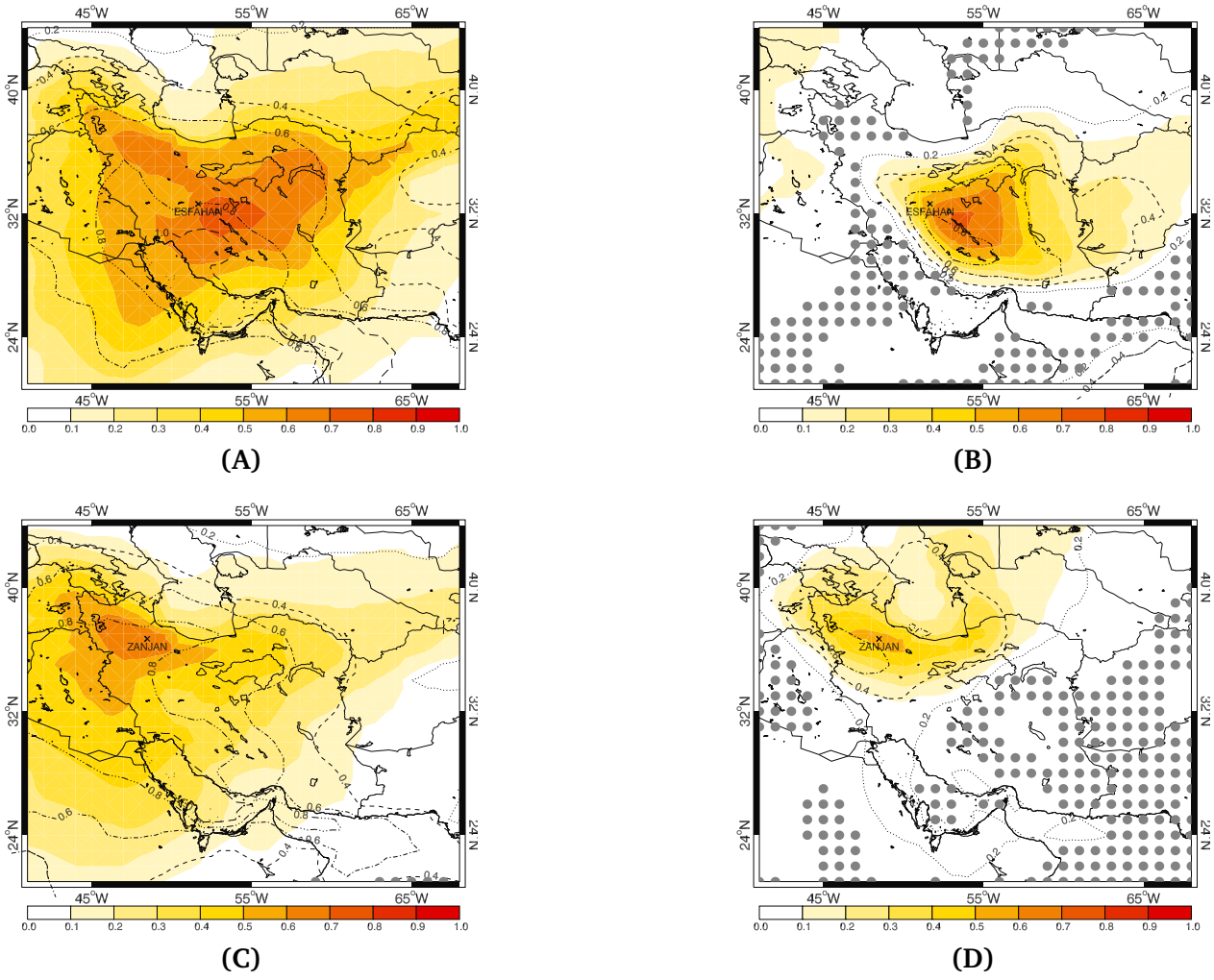

Figure B.4.: Same as Fig. B.1 but (A, B) for Isfahan station and (C, D) for Zanjan station

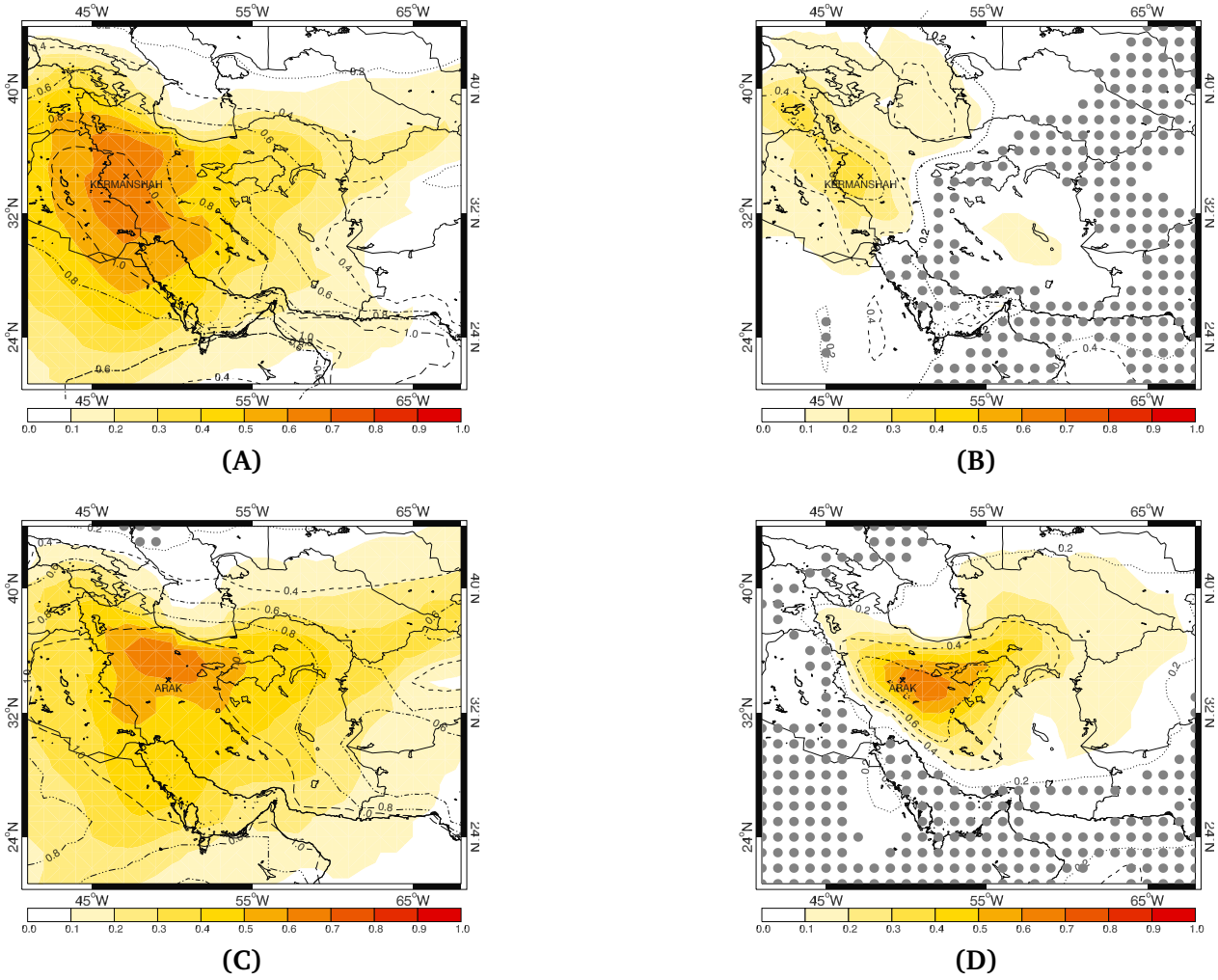

Figure B.5.: Same as Fig. B.1 but (A, B) for Kermanshah station and (C, D) for Arak station

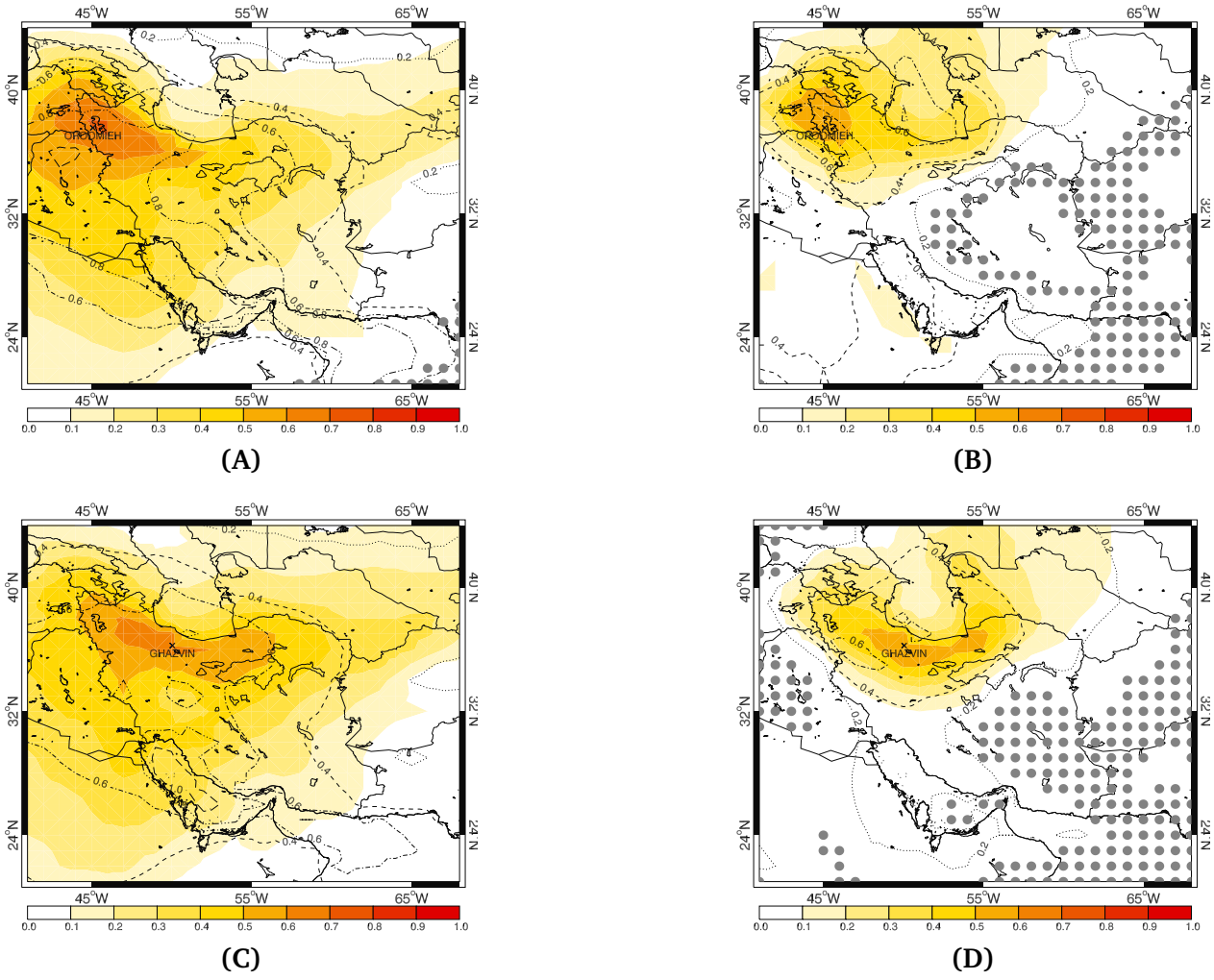

Figure B.6.: Same as Fig. B.1 but (A, B) for Orumieh station and (C, D) for Qazvin station

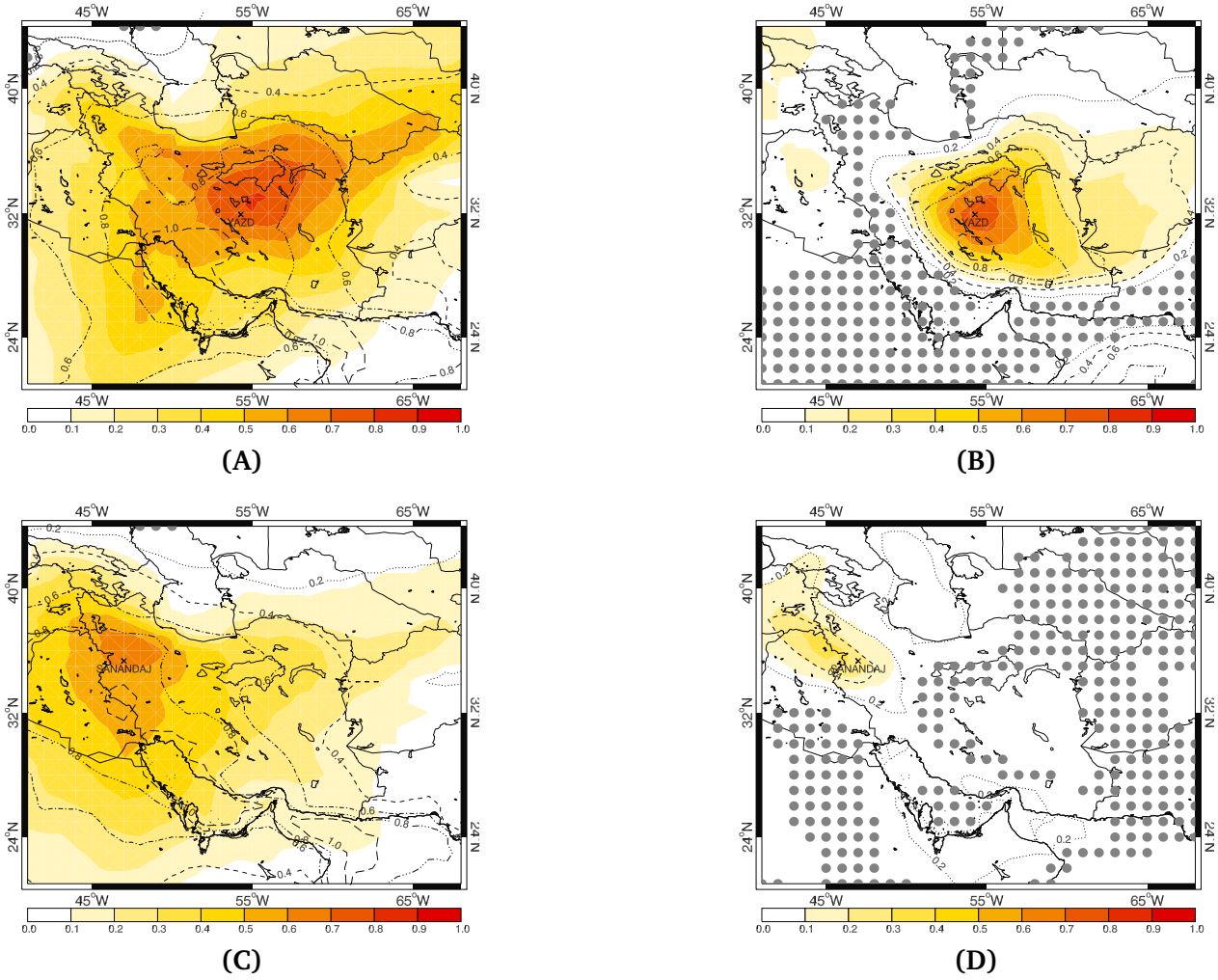

Figure B.7.: Same as Fig. B.1 but (A, B) for Yazd station and (C, D) for Sanandaj station

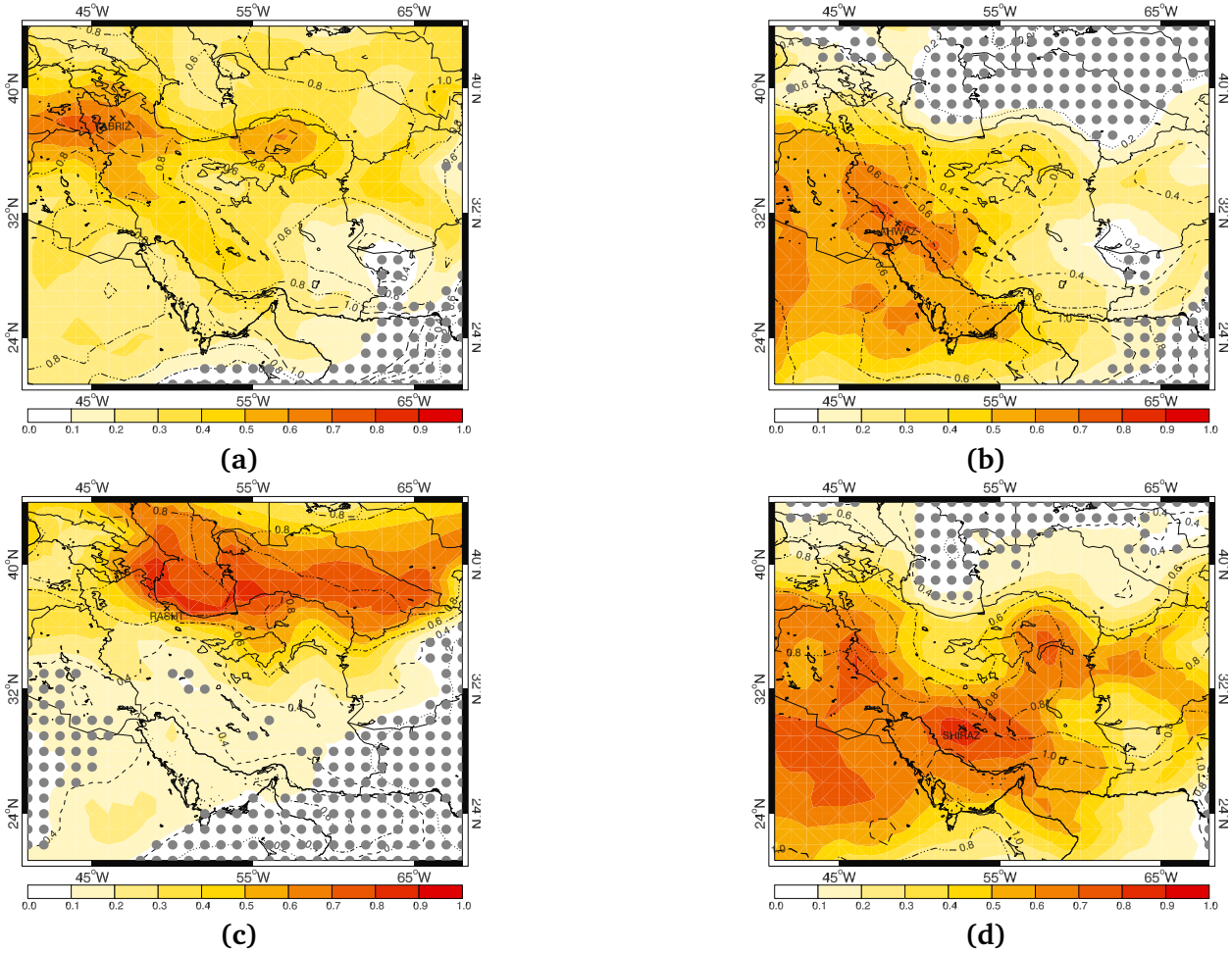

Figure B.8.: Squared correlation (shading) and regression coefficients (contours) between GDD at stations and in ERA-40. Non-significant grid points are marked with gray dots. Stations are (a) Tabriz, (b) Ahvaz, (c) Rasht and (d) Shiraz.

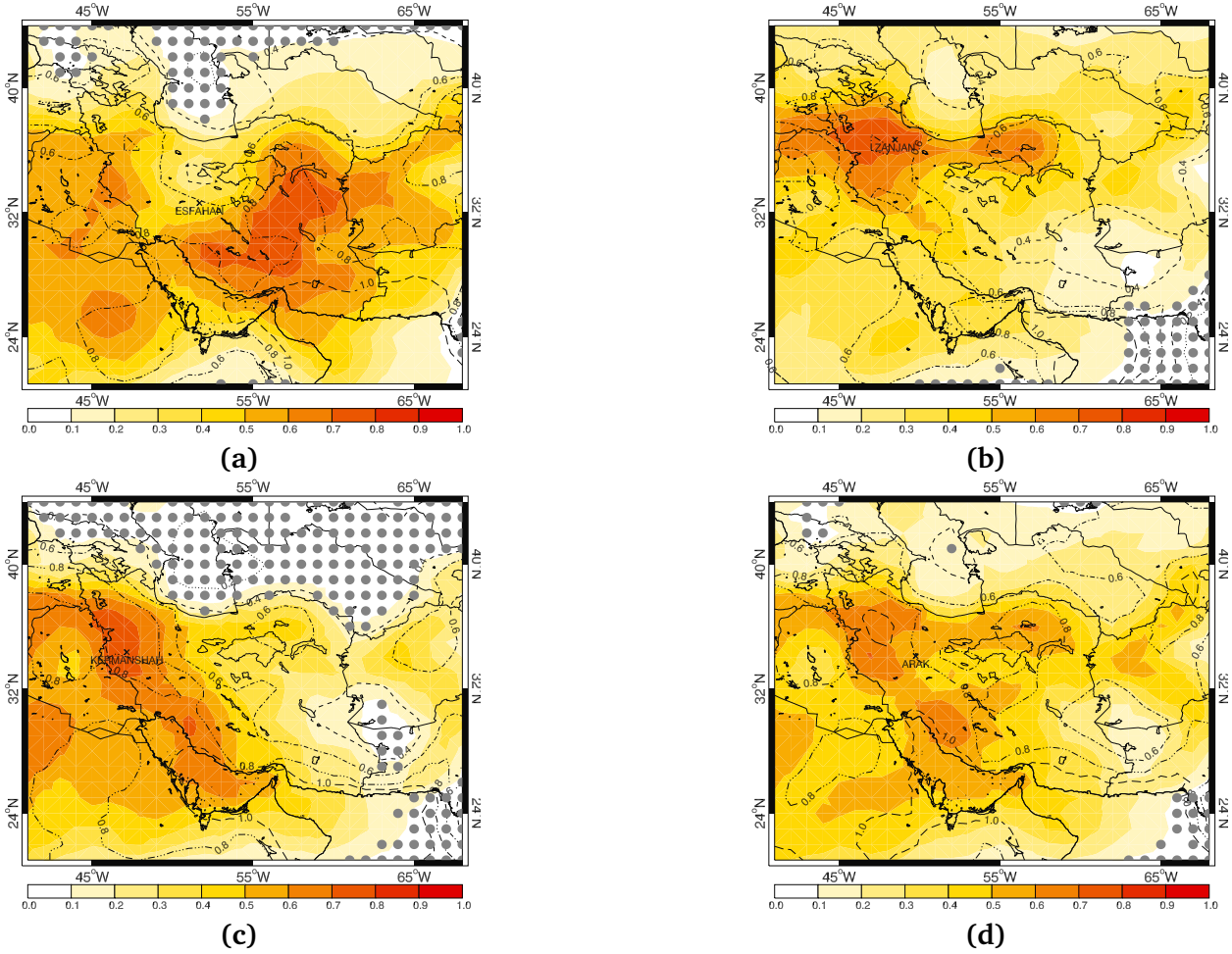

Figure B.9.: Same as Fig. B.8 but for stations: (a) Isfahan, (b) Zanjan, (c) Kermanshah and (d) Arak

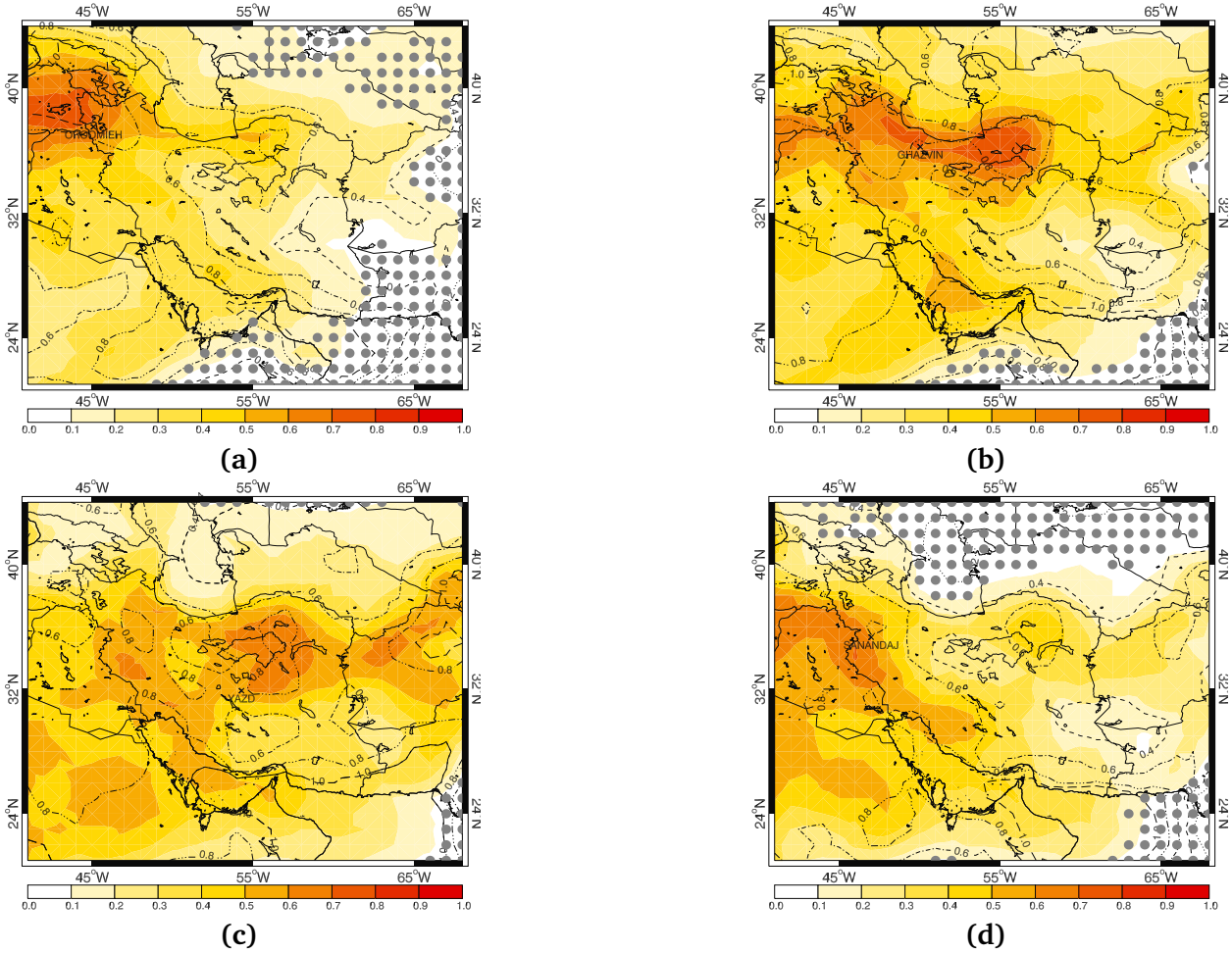

Figure B.10.: Same as Fig. B.8 but for stations: (a) Orumieh, (b) Qazvin, (c) Yazd and (d) Sanandaj

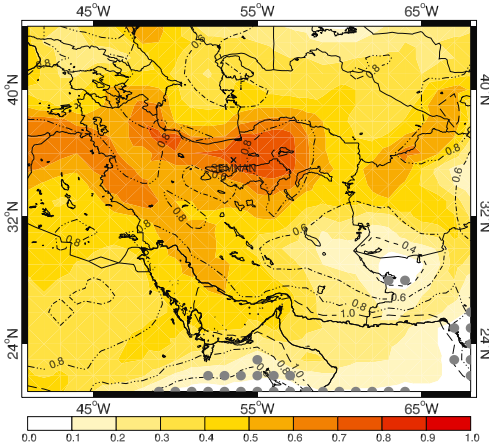

Figure B.11.: Same as Fig. B.8 but for Semnan station

C. Appendix of weather generator (WG) for GDD

The realizations of the WG are displayed in Figs. C.1(a) to C.4(a) for all other stations. The boxes represent the inner-quartile range of the realizations, and the whiskers the 0.025 and the 0.975 quantiles. Figs. C.1(b) to C.4(b) presents the quantile plots between the WG of downscaled FP1 for ERA-40 and observed GDD (black dots) in all stations. The box plot of the probability of WGs shows the 95% confidence interval.

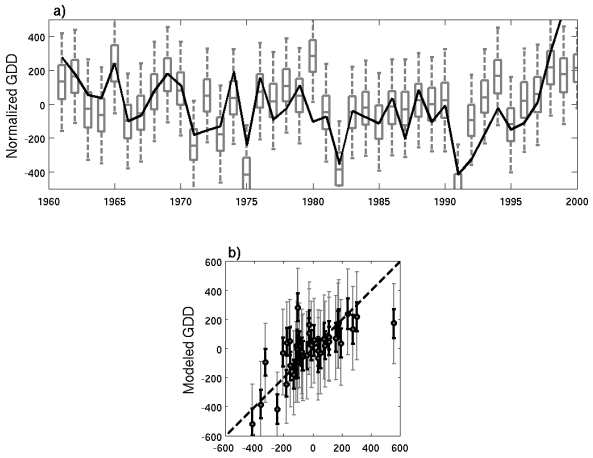

Figure C.1.: 1000 realizations of the WG using FP1 (box plots), and observed GDD values (black line). The boxes indicate inner-quartile range and median, and the whiskers the 95% interval (a). Modeled GDD from 1000 realizations of WG using FP1 against observed GDD at Tabriz station. Black lines and whiskers indicate the inner-quartile range, and gray whiskers the 95% interval (b)

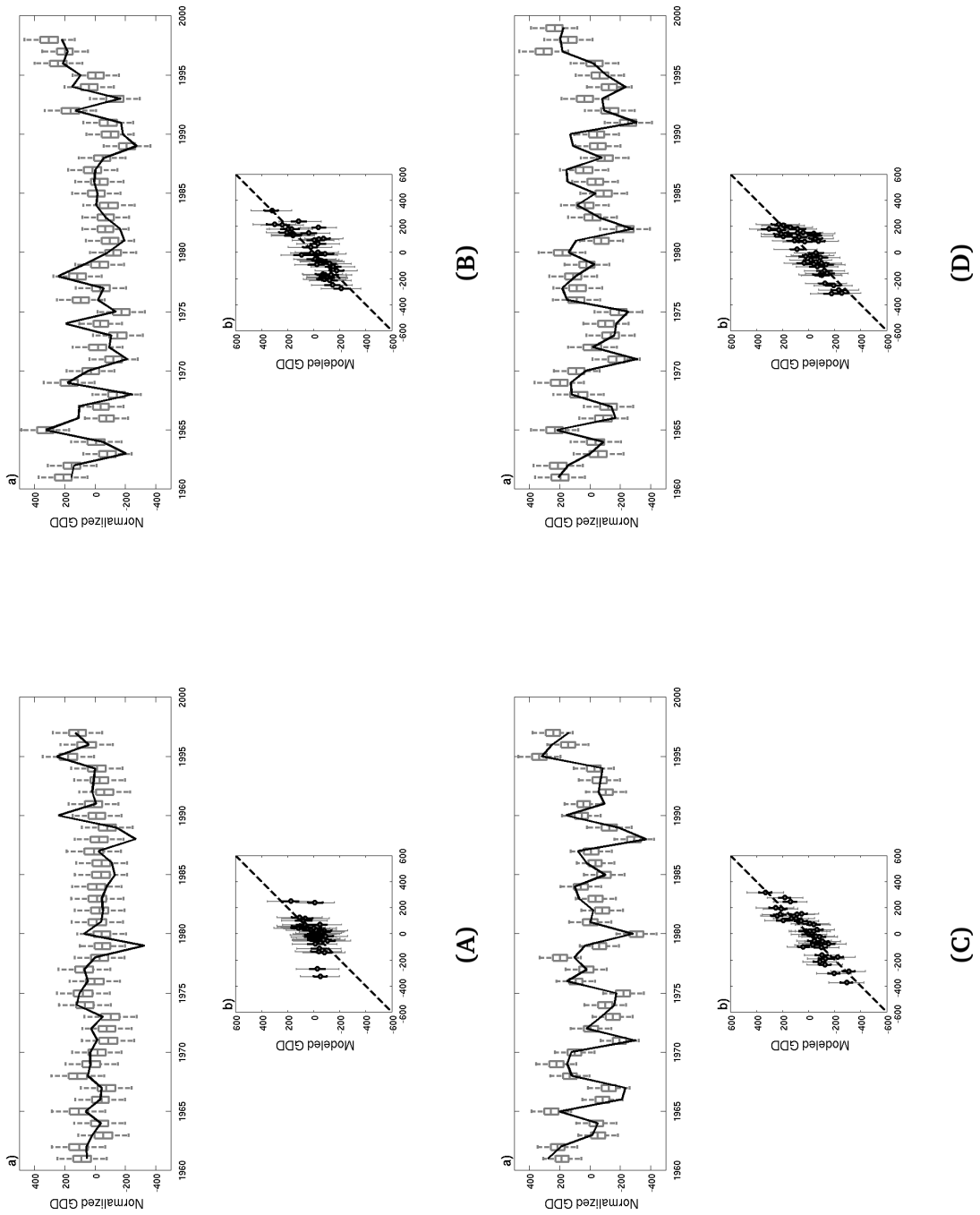

Figure C.2.: Same as Fig. C.1 but for stations: (A) Ahvaz, (B) Rasht, (C) Shiraz and (D) Isfahan

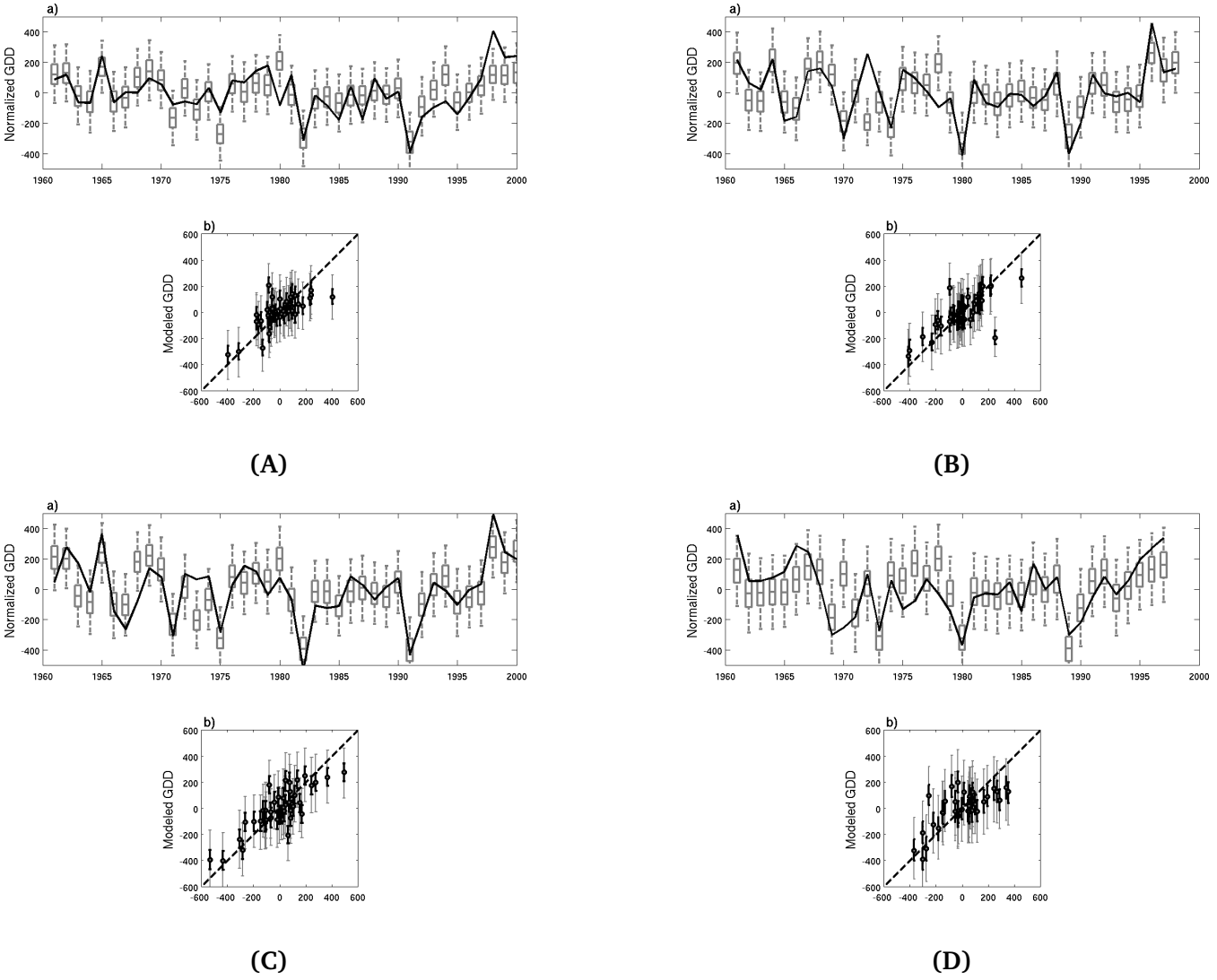

Figure C.3.: Same as Fig. C.1 but for stations: (A) Zanjan, (B) Kermanshah, (C) Arak and (D) Orumieh

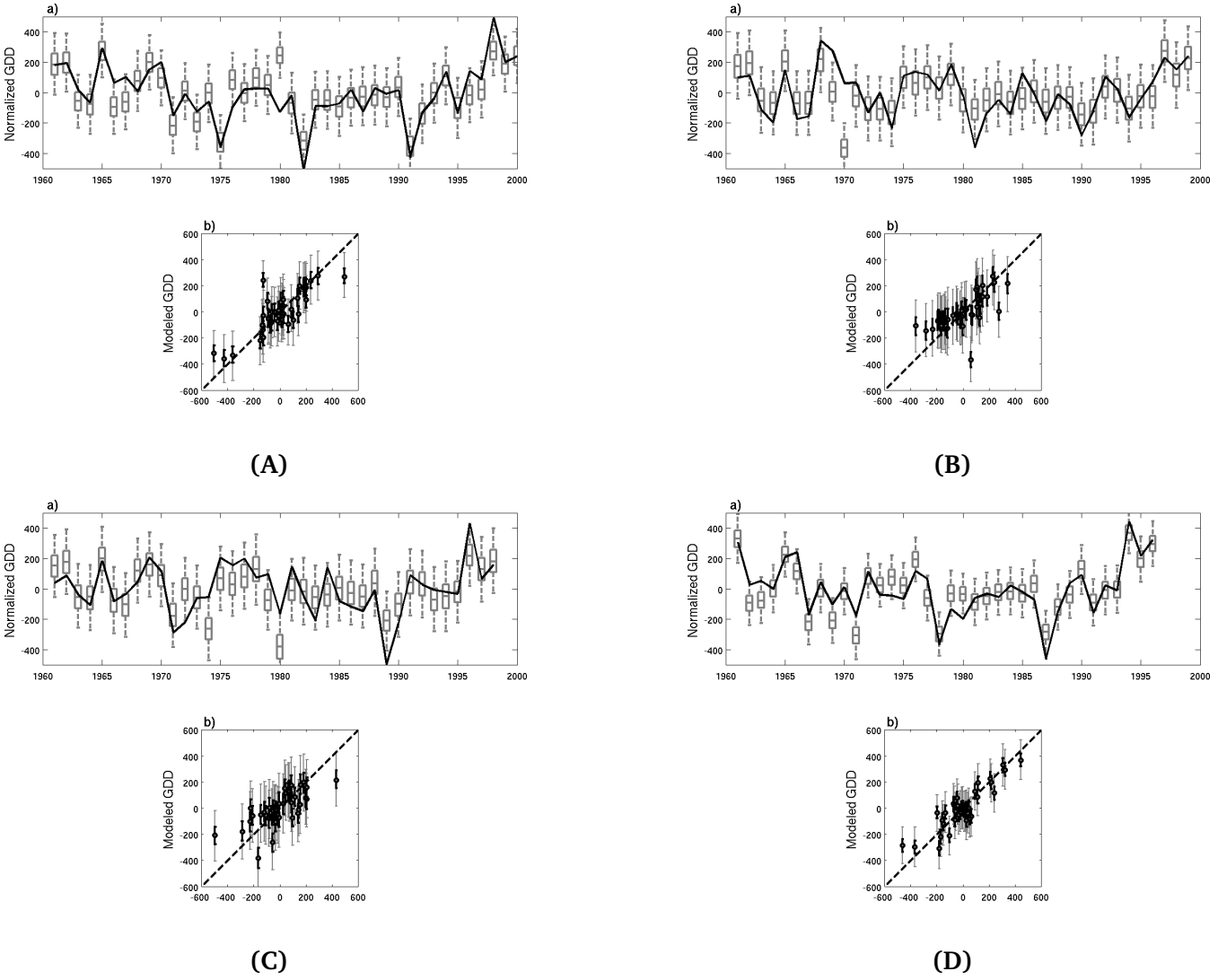

Figure C.4.: Same as Fig. C.1 but for stations: (A) Qazvin, (B) Yazd , (C) Sanandaj and (D) Semnan

D. Appendix of phenologic model analysis

Probabilistic phenologic models through the survival analysis are displayed in Figs. D.1 to D.4 for all other stations. In these figures, the probabilistic and deterministic phenologic models for normalized growth duration are presented through linear regression analysis. The black contour represents the deterministic predicted GD values and gray dots display the normalized observed GD values. The probabilistic predicted GD values are shown by color contours.

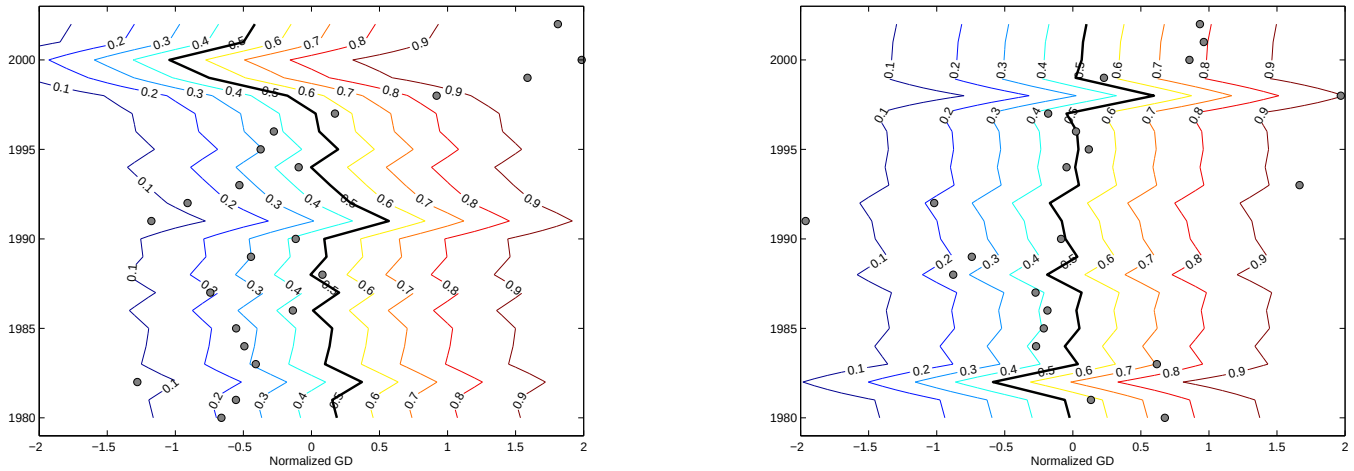

Figure D.1.: phenologic model analysis at (A) Tabriz and (B) Ahvaz stations. The black line indicates the deterministic forecasting of GD and gray dots show the observed values of GD. Color contour lines presents the probabilistic phenologic forecasting model

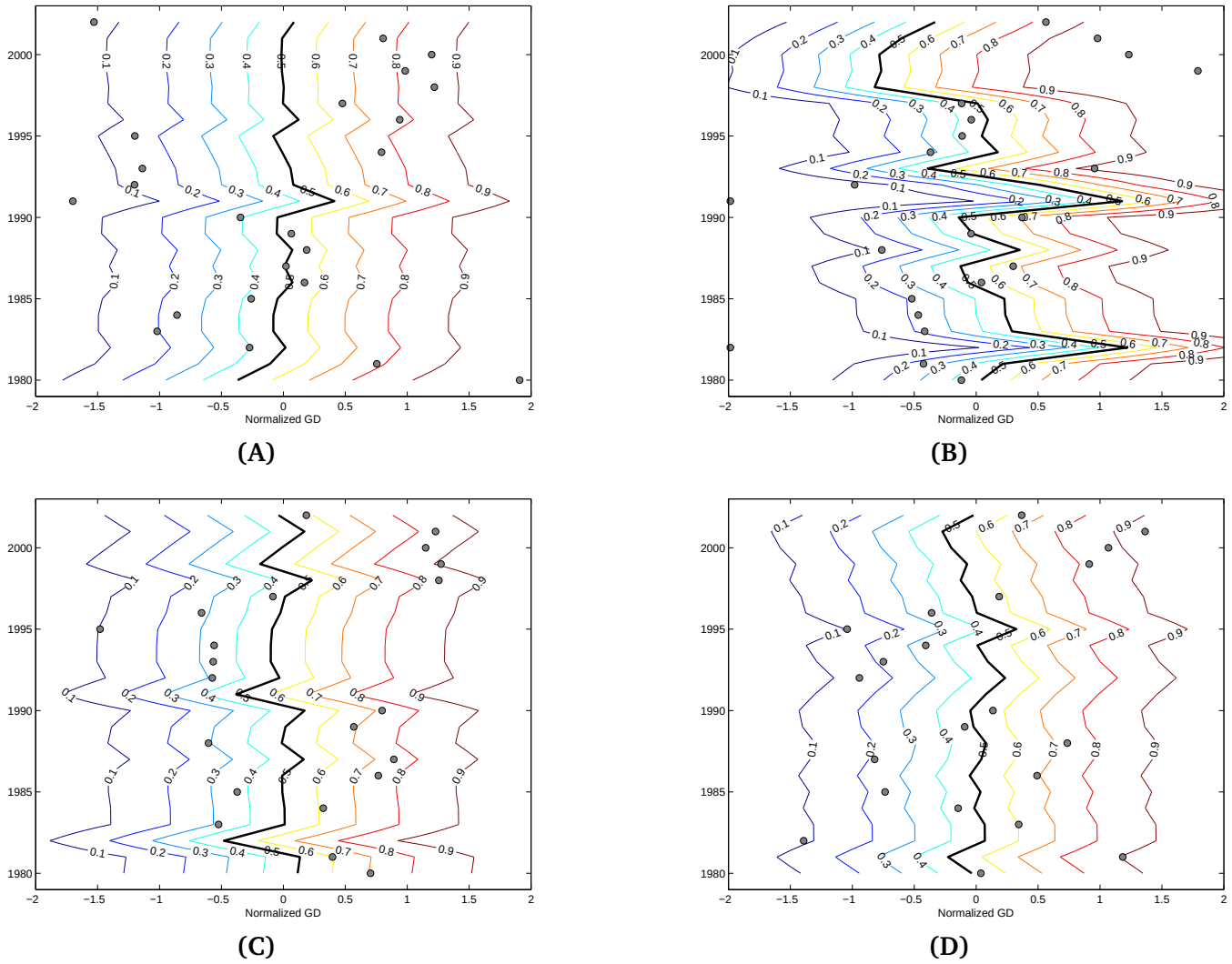

Figure D.2.: Same as Fig. D.1 but for stations: (A) Rasht, (B) Shiraz, (C) Isfahan and (D) Zanjan

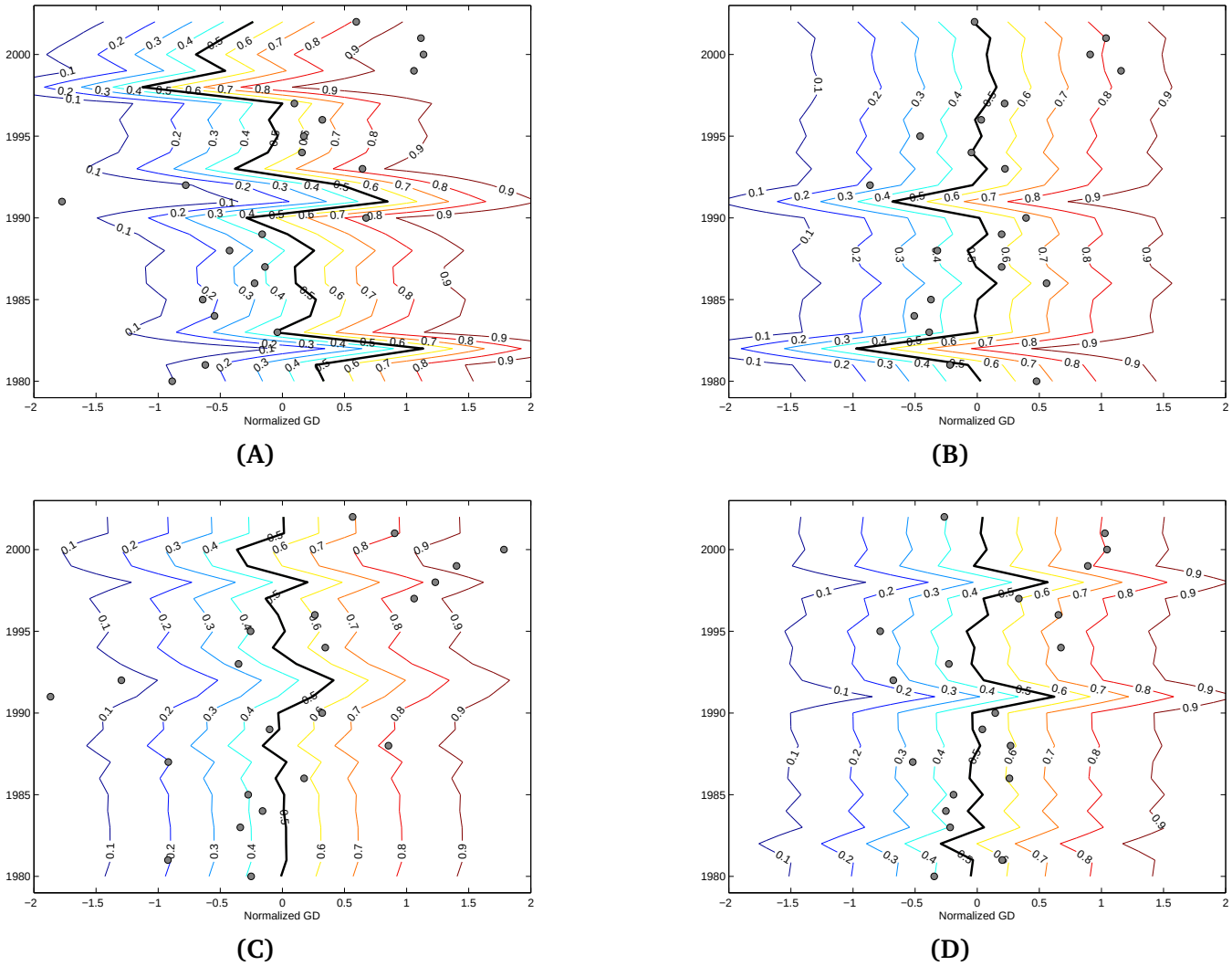

Figure D.3.: Same as Fig. D.1 but for stations: (A) Kermanshah, (B) Arak, (C) Orumieh and (D) Qazvin

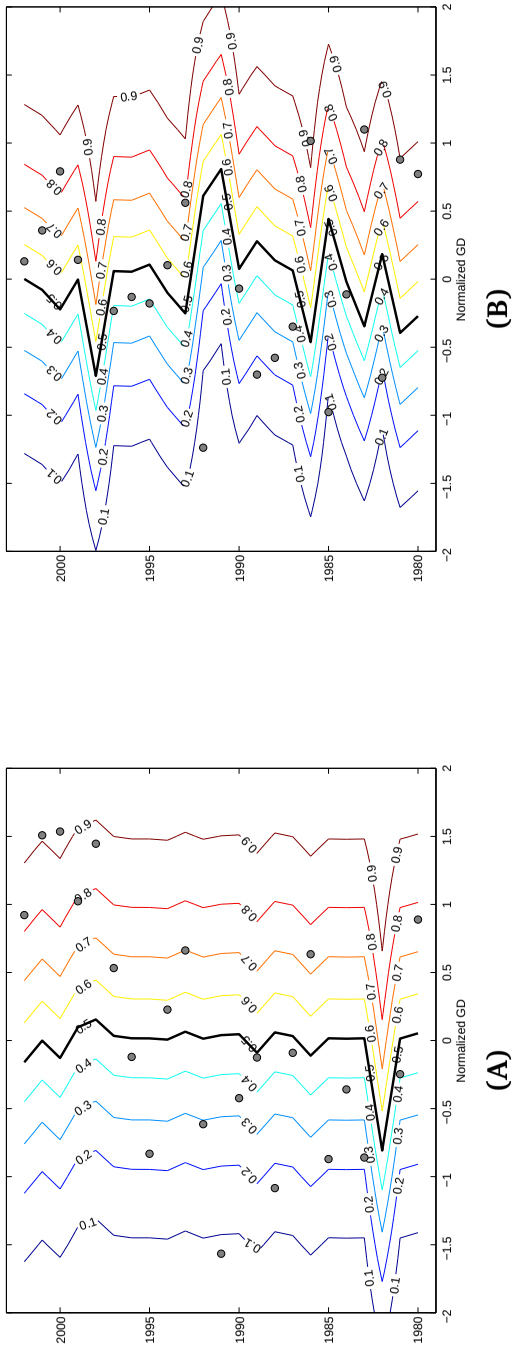

Figure D.4.: Same as Fig. D.1 but for stations: (A) Yazd, (B) Sanandaj and (C) Semnan

BONNER METEOROLOGISCHE ABHANDLUNGEN

Herausgegeben vom Meteorologischen Institut der Universität Bonn durch Prof. Dr. H. FLOHN (Hefte 1-25), Prof. Dr. M. HANTEL (Hefte 26-35), Prof. Dr. H.-D. SCHILLING (Hefte 36-39), Prof. Dr. H. KRAUS (Hefte 40-49), ab Heft 50 durch Prof. Dr. A. HENSE.

Heft 1-39: siehe `http://www2.meteo.uni-bonn.de/bibliothek/bma.html`

Heft 40: ***Hermann Flohn***: Meteorologie im Übergang Erfahrungen und Erinnerungen (1931-1991). 1992, 81 S. + XII. € 23

Heft 41: ***Adnan Alkhalaf and Helmut Kraus***: Energy Balance Equivalents to the Köppen-Geiger Climatic Regions. 1993, 69 S. + IX. € 19

Heft 42: ***Axel Gabriel***: Analyse stark nichtlinearer Dynamik am Beispiel einer rei- bungsfreien 2D-Bodenkaltfront. 1993, 127 S. + XIV. € 30

Heft 43: ***Annette Münzenberg-St.Denis***: Quasilineare Instabilitätsanalyse und ihre Anwendung auf die Strukturaufklärung von Mesozyklonen im östlichen Weddellmeergebiet. 1994, 131 S. + XIII. € 33

Heft 44: ***Hermann Mächel***: Variabilität der Aktionszentren der bodennahen Zirkulation über dem Atlantik im Zeitraum 1881-1989. 1995, 188 S. + XX. € 48

Heft 45: ***Günther Heinemann***: Polare Mesozyklonen. 1995, 157 S. + XVI. € 46

Heft 46: ***Joachim Klaßen:*** Wechselwirkung der Klima-Subsysteme Atmosphäre, Meereis und Ozean im Bereich einer Weddellmeer-Polynia. 1996, 146 S. + XVI. € 43

Heft 47: ***Kai Born***: Seewindzirkulationen: Numerische Simulationen der Seewind- front. 1996, 170 S. + XVI. € 48

Heft 48: ***Michael Lambrecht***: Numerische Untersuchungen zur tropischen 30-60-tägigen Oszillation mit einem konzeptionellen Modell. 1996, 48 S. + XII. € 15

Heft 49: ***Cäcilia Ewenz***: Seewindfronten in Australien: flugzeuggestützte Messungen und Modellergebnisse. 1999, 93 S. + X. € 30

Heft 50: ***Petra Friederichs***: Interannuelle und dekadische Variabilität der atmosphärischen Zirkulation in gekoppelten und SST-getriebenen GCM-Experimenten. 2000, 133 S. + VIII. € 25

Heft 51: ***Heiko Paeth***: Anthropogene Klimaänderungen auf der Nordhemisphäre und die Rolle der Nordatlantik-Oszillation. 2000, 168 S.+ XVIII. € 28

Heft 52: ***Hildegard Steinhorst***: Statistisch-dynamische Verbundsanalyse von zeitlich und räumlich hoch aufgelösten Niederschlagsmustern: eine Untersuchung am Beispiel der Gebiete von Köln und Bonn. 2000, 146 S. + XIV. € 25

Heft 53: ***Thomas Klein***: Katabatic winds over Greenland and Antartica and their interaction with mesoscale and synoptic-scale weather systems: three-dimensional numerical models. 2000, 146 S. + XIV. € 25

Heft 54: ***Clemens Drüe***: Experimentelle Untersuchung arktischer Grenzschichtfronten an der Meereisgrenze in der Davis-Straße. 2001, 165 S. + VIII. € 28

Heft 55: ***Gisela Seuffert***: Two approaches to improve the simulation of near surface processes in numerical weather prediction models. 2001, 128 S. + VI. € 25

Heft 56: ***Jochen Stuck***: Die simulierte axiale atmosphärische Drehimpulsbilanz des ECHAM3-T21 GCM. 2002, 202 S. + VII. € 30

Heft 57: ***Günther Haase***: A physical initialization algorithm for non-hydrostatic weather prediction models using radar derived rain rates. 2002, 106S. + IV. € 25

Heft 58: ***Judith Berner***: Detection and Stochastic Modeling of Nonlinear Signatures in the Geopotential Height Field of an Atmospheric General Circulation Model. 2003, 157 S. + VIII. € 28

Heft 59: ***Bernd Maurer***: Messungen in der atmosphärischen Grenzschicht und Validation eines mesoskaligen Atmosphärenmodells über heterogenen Landoberflächen. 2003, 182 S. + IX. € 30

Heft 60: ***Christoph Gebhardt***: Variational reconstruction of Quaternary temperature fields using mixture models as botanical – climatological transfer functions. 2003, 204 S. + VIII. € 30

Heft 61: ***Heiko Paeth***: The climate of tropical and northern Africa – A statistical-dynamical analysis of the key factors in climate variability and the role of human activity in future climate change. 2005, 316 S. + XVI. € 15

Heft 62: ***Christian Schölzel***: Palaeoenvironmental transfer functions in a Bayesian framework with application to Holocene climate variability in the Near East. 2006, 104 S. + VI. € 15

Heft 63: ***Susanne Bachner***: Daily precipitation characteristics simulated by a regional climate model, including their sensitivity to model physics, 2008, 161 S. € 15

Heft 64: ***Michael Weniger***: Stochastic parameterization: a rigorous approach to stochastic three-dimensional primitive equations, 2014, 148 S. + XV. open access[1]

Heft 65: ***Andreas Röpnack***: Bayesian model verification: predictability of convective conditions based on EPS forecasts and observations, 2014, 152 S. + VI. open access[1]

Heft 66: ***Thorsten Simon***: Statistical and Dynamical Downscaling of Numerical Climate Simulations: Enhancement and Evaluation for East Asia, 2014, 48 S. + LXXVII. open access[1]

Heft 67: ***Elham Rahmani***: The effect of climate variability on wheat in Iran, 2015, 96 S. + XIII open access[1]

[1]Available at `http://hss.ulb.uni-bonn.de/fakultaet/math-nat/`

METEOROLOGISCHES INSTITUT
MATHEMATISCH NATURWISSENSCHAFTLICHE FAKULTÄT
UNIVERSITÄT BONN

Meteorologisches Institut
Universität Bonn